

ABSTRACT

Title of Thesis: THE EFFECTS OF UNMITIGATED IDLE TIME ON THE PERFORMANCE OF MAGNETORHEOLOGICAL DAMPERS AS A STRUCTURAL PROTECTIVE SYSTEM.

Sami Ur-Rahman Khan
Master of Science
Civil and Environmental Engineering
2018

Thesis Directed By: Dr. Brian Phillips, Assistant Professor. Civil and Environmental Engineering

This thesis discusses the long-term performance degradation of seismic protective systems due to age and inactivity (termed “idle time effects”). Over the lifetime of a structures there is the potential for a significant reduction in ability for the structural control systems to mitigate earthquakes. This can affect the resilience of the structure and lead to uncertainty in engineering judgement when designing seismic protective systems. Further research into these idle time effects could help to create solutions to mitigate age-dependent performance loss. This paper will use magneto-rheological (MR) dampers, which serve as a good analog for other semi-active control devices, to study idle time effects on seismic protection. MR dampers provide controllable damping through the magnetization of small MR particles in a carrier fluid. These particles can settle over time, influencing their performance. Using a model MR fluid, accelerated testing was performed to analyze the consequences of idle time.

THE EFFECTS OF UNMITIGATED IDLE TIME ON THE PERFORMANCE OF
MAGNETORHEOLOGICAL DAMPERS AS A STRUCTURAL PROTECTIVE
SYSTEM.

by

Sami Ur-Rahman Khan

Thesis submitted to the Faculty of the Graduate School of the
University of Maryland, College Park, in partial fulfillment
of the requirements for the degree of
Master of Science
2018

Advisory Committee:
Dr. Brian M. Phillips, Chair
Dr. M. Sherif Aggour
Dr. Norman M. Wereley

© Copyright by
Sami Ur-Rahman Khan
2018

Acknowledgements

This thesis would not have been able to be completed without the help, advice, motivation, and continual support of Dr. Brian Phillips. I am grateful and appreciative for every meeting, email, and conversation that we have shared. Thank you so much, I would not be in the place I am today if I had not met you during my undergraduate academic career.

Thank you also to the other graduate students in the UMD structures lab, for the support and laughs that were ever present in the company of Ashkan, Jingzhe, and Ruiyang. Thank you for three full years of memories of researching together, of obstacles that were overcome, and of the effort that was put into setting up the equipment that has made this and other research possible. Thank you also to Professor Richard E. Christenson at the University of Connecticut for providing the large-scale MR damper on loan to our research group at the University of Maryland.

Finally, thank you to my friends, family, housemates, and loved ones for your unconditional support. Thank you for supporting me throughout these years and especially over this last hurdle. Raza, Zohaib, Nyssa, Brian and Cheryl, I could not have done this without all of you.

Table of Contents

Acknowledgements.....	ii
Table of Contents.....	iii
List of Tables.....	iv
List of Figures.....	v
Chapter 1: Introduction.....	1
Chapter 2: Literature Review.....	6
2.1 Structural Control Systems.....	6
2.2 Passive Control Systems.....	8
2.3 Active Control Systems.....	11
2.4 Semi-Active Control Systems.....	13
2.5 Hybrid Control Systems.....	14
2.6 Time-varying performance of structural control systems.....	16
2.7 Magnetorheological (MR) Fluids.....	18
2.8 Magnetorheological (MR) Dampers.....	20
2.9 Bingham Plastic Model.....	23
Chapter 3: Experimental Setup.....	25
3.1 Physical Substructure.....	25
3.2 Numerical User Interface and Control Equipment.....	28
3.3 Real-Time Hybrid Simulation Setup.....	31
Chapter 4: Bingham Plastic Damper Model Creation.....	33
Chapter 5: Idle-Time Behavior of MR Fluids.....	39
5.1 Idle Time Factors Affecting Performance.....	40
5.1.1 Particle Settlement.....	41
5.1.2 Mixing Behavior & Participant Ratio.....	43
5.2 Idle-Time Sine Wave Testing Results.....	45
5.3 Generalized Idle Time Model.....	51
Chapter 6: Impact of Idle Time on Seismic Performance of Structures.....	64
6.1 Structural Model.....	64
6.2 Earthquake Ground Motion Records.....	67
6.3 Semi-Active Controller.....	68
6.4 Experimental Testing.....	69
6.5 Numerical Simulations for Long-Term Performance.....	77
Chapter 7: Conclusion and Future Studies.....	84
References.....	88

List of Tables

Table 3.1: MR Damper Properties.....	26
Table 4.1: Bingham Plastic Fitted Parameters.....	35
Table 5.1: Idle Time Sine Wave Test Parameters.....	45
Table 5.2 (a): Idle Time Sine Wave Test Data Summary Table (S.I. Units).....	50
Table 5.2 (b): Idle Time Sine Wave Test Data Summary Table (U.S. Units).....	51
Table 5.3: Assumed MR Fluid Parameters.....	53
Table 5.4: Calculation of Total MR Fluid Volume in Large-Scale 200 kN Damper....	55
Table 5.5: Calculation of Maximum Height of Settled Particle Layer.....	56
Table 5.6: Parameters for Participant Ratio Formula.....	58
Table 6.1: 5-story Base Isolation Structural Parameters.....	64
Table 6.2: Earthquake Ground Motion Records Details.....	67
Table 6.3: Earthquake Ground Motion PGA Scaling.....	74

List of Figures

Fig. 1.1: General Earthquake Ground Motion Record.....	4
Fig. 2.1: Types of Passive Structural Control Systems (Murty, 2005).....	9
Fig. 2.2: Effects of Seismic Base Isolation (Bridgestone, 2017).....	10
Fig. 2.3: Tuned Mass Damper on Taipei-101 (Taipei-101, 2014).....	11
Fig. 2.4: Active Control System Component Block Diagram.....	12
Fig. 2.5: Sendagaya INTES Building with HMDs (Spencer, 2008).....	15
Fig. 2.6: MR Fluids Under Magnetic Field (Kciuk & Turczyn, 2006).....	19
Fig. 2.7: Basic Operational Modes of MR Fluid Devices.....	21
Fig. 2.8: Illustrations of Pinch Mode Action (Goncalves & Carlson, 2009).....	22
Fig. 2.9: Generic Bingham Plastic Model.....	23
Fig. 3.1: Lord Corporation MR Damper (Jiang et. al., 2010; Phillips et. al., 2010).....	26
Fig. 3.2: Schematic of Actuator and MR Damper Setup on Top of I-beam.....	27
Fig. 3.3: Actuator and MR Damper Setup.....	27
Fig. 3.4: Schematic of PWM Setup.....	29
Fig. 3.5: Picture of PWM Setup.....	30
Fig. 3.6: RTHS Block Diagram.....	32
Fig. 4.1: Bingham Plastic Model.....	33
Fig. 4.2: Force-Time Plots for Calibrated Model and Sine Wave Test Data.....	34
Fig. 4.3: Force-Displacement Plot from Experimental Data (a) and Numerical Model (b).....	34
Fig. 4.4: Force versus Velocity Plot from Experimental Data (a) and Numerical Model (b).....	35
Fig. 4.5: Variation of Bingham Plastic Parameters.....	36
Fig. 4.6: Effect of Transition Function on Bingham Plastic Model.....	37

Fig. 5.1: Relationship of the Three Factors Which Create the Participant Ratio.....	41
Fig. 5.2: Sine Wave (1 inch, 0.5 Hz, & 2.5 A) Test Data – Fully Mixed.....	45
Fig. 5.3 (a): Force-Time Plot for 0 – 10 Seconds of 3 Month Idle Time Data.....	46
Fig. 5.3 (b): 3 Month Idle Time Sinusoidal Test Data – UMD Structures Lab.....	46
Fig. 5.4: 6 Month Idle Time Sinusoidal Test Data Stitched.....	47
Fig. 5.5 (a): Force-Time Plot for 0 – 10 Seconds of 6 Month Idle Time Data.....	47
Fig. 5.5 (b): 6 Month Idle Time Sinusoidal Test Data.....	48
Fig. 5.6 (a): Force-Time Plot for 0 – 40 seconds of 2.5 Year Idle Time Data	49
Fig. 5.6 (b): 2.5 Year Idle Time Sinusoidal Test Data – UMD Structures Lab.....	49
Fig. 5.7: Block Diagram of Generalized Idle Time Model.....	52
Fig. 5.8: (a) Horizontal Cylindrical Segment Volume Calculation, (b) Example of Settling Particles Visualized as Layers Sinking.....	54
Fig. 5.9: Variation of Participant Ratio Model Parameters.....	57
Fig. 5.10: Variation of Participant Ratio Model.....	60
Fig. 5.11: Example of Bingham Plastic Coulomb Friction Component Calculation Including Idle Time Effects.....	61
Fig. 5.12: Simulink Model of Bingham Plastic With Idle Time Effects Affecting the Parameters.....	62
Fig. 5.13: Case 1–0.25 Year Idle Time Sine Wave Displacement.....	62
Fig. 5.14: Case 2 – 0.5 Year Idle Time Sine Wave Displacement.....	63
Fig. 5.15: Case 3 – 2.5 Year Idle Time Sine Wave Displacement.....	63
Fig. 6.1: 5-story Base Isolated Structure with MR Damper.....	65
Fig. 6.2: Matrices Used to Represent Numerical 6DOF Structure.....	65
Fig. 6.3: Mode Shapes and Frequencies for 6DOF Lumped Mass Structure.....	66
Fig. 6.4: Idle Time RTHS Test 1 Data and Tracking Performance.....	71
Fig. 6.5: Idle Time RTHS Comparison with “Fully-Mixed” Case.....	71

Fig. 6.6: Idle Time RTHS Comparison Plots from 0 – 10 Seconds.....	72
Fig. 6.7: Comparison of Numerical Simulation and RTHS Testing.....	73
Fig. 6.8: Comparison of 0 – 10 sec Numerical Simulation and RTHS Testing.....	73
Fig. 6.9: 2.5 Year Idle Time with Passive-off Control Under Hachinohe (Case a), Northridge (Case b), Kobe (Case c), and Elcentro (Case d) Ground Motion.....	75
Fig. 6.10: 2.5 Year Idle Time with Semi-Active Control Under Hachinohe (Case a), Northridge (Case b), Kobe (Case c), and Elcentro (Case d) Ground Motion.....	76
Fig. 6.11: 2.5 Year Idle Time with Passive-On Control Under Hachinohe (Case a), Northridge (Case b), Kobe (Case c), and Elcentro (Case d) Ground Motion.....	77
Fig. 6.12: Max. Displacement of Base Isolation Under EQ Ground Motion with Causal Semi-Active Controller.....	79
Fig. 6.13: Max. Damping Force Under EQ Ground Motion with Causal Semi-Active Controller.....	79
Fig. 6.14: Max. Acceleration of Superstructure Under EQ Ground Motion with Causal Semi-Active Controller.....	80
Fig. 6.15: Max. Displacement of Base Isolation Under EQ Ground Motion with Passive-Off Controller.....	80
Fig. 6.16: Max. Damping Force Under EQ Ground Motion with Passive-Off Controller.....	81
Fig. 6.17: Max. Acceleration of Superstructure Under EQ Ground Motion with Passive-Off Controller.....	81
Fig. 6.18: Max. Displacement of Base Isolation Under EQ Ground Motion with Passive-On Controller.....	82
Fig. 6.19: Max. Damping Force Under EQ Ground Motion with Passive-On Controller.....	82
Fig. 6.20: Max. Acceleration of Superstructure Under EQ Ground Motion with Passive-On Controller.....	83

Chapter 1: Introduction

With the recent occurrences of severe earthquakes, hurricanes, and other natural disasters around the world it has become ever more important for improvement in the field of structural dynamics and structural control systems. The 2017 Central Mexico earthquake with a magnitude of 8.2 caused the collapse of 40 buildings which in turn led to the death of 300 and injuries of over 6000 people (BBC, 2017; Chavez, 2017; Ellis, 2017; Weaver, 2017). The 2005 Kashmir earthquake had a magnitude of 7.6 and killed more than 80,000 people while leaving 4 million others displaced in parts of northern Pakistan, India and Afghanistan (History, 2009). Even more recently, on November 13th, 2017 a magnitude 7.3 earthquake hit Iran and Iraq which, according to the New York Times, led to the deaths of at least 400 people and the injuries of more than 6000 people (Erdbrink, 2017). The structural and soil failures are reported to be the main reasons behind these terrible incidents. Properly designed infrastructure is a critical part of ensuring the safety of the world's populations and cities

Megacities are very susceptible to these high cost damages caused by natural disasters due to the density of the infrastructure within the cities (Sullivan, 2017). These natural disasters not only cause immense damage to people and buildings, but to other resources and civil works, such as transportation infrastructure, which can cripple affected areas for years. Our society requires better, more resilient infrastructure to protect their citizens and cities from the drastic effects of dynamic excitation. Although structures are designed to withstand natural hazards, they are only able to absorb seismic energy through their own deformation. This can lead to

major structural failures, which in turn result in increased difficulty in the evacuation of people, more lives lost, and high damage costs. Using structural control systems, these deformations can be limited to safe levels thereby better protecting people and cities. Major seismic activity can also lead to massive devastation, particularly in less developed rural areas. By implementing cost effective structural protection systems, such as recycled rubber base isolators (STPs) or sliding type isolators using stone rather than metal for friction (Yamaguchi et al., 2008; Taywade & Savale, 2015), better damage mitigation and protection for non-engineered structures in these regions can be achieved.

Although these systems can provide sufficient protection to the structures when designed and implemented properly, all structures and structural control systems undergo performance degradation over time. This can occur through fatigue, creep of concrete, cracking of concrete, moisture effects on building materials, wearing of friction elements and connections, corrosion in steel elements, and foundation settlement, among others. All these sources of performance loss have a possibility to occur over the life of the structure, although how quickly this happens will depend on the construction quality, use of the building, and the surrounding environment. Seismic protective systems can be affected by these same sources and partially lose their effectiveness over time to protect the building against natural hazards. These sources of performance degradation and their affects will be discussed in further detail in the literature review in Chapter 2.

This thesis will focus on the long-term performance of seismic protective systems, in particular, the performance degradation due to age and inactivity (henceforth also termed “idle time effects”). Over the long lifetimes of structures between earthquake occurrences, there is the potential for a significant reduction in ability for the structural control systems to mitigate earthquakes. This reduction can affect the resilience of the structure and lead to uncertainty in engineering judgement when designing seismic protective systems. As such, further research into these idle time effects, would allow for the creation of improvements in maintenance and device design to mitigate the age-related performance loss. This paper will use magnetorheological (MR) dampers, which serve as a good analog for other semi-active control devices, to study these idle time effects on seismic protection.

Magnetorheological (MR) fluids are tiny magnetizable particles, often carbonyl iron particles, suspended within a viscous carrier fluid. When the MR fluid is exposed to a magnetic field, the fluid particles can increase the yield strength and viscosity of the fluid which provides added resistance to any external force (Carlson 1996; Jolly, 1996; Jolly, 1998; Yang, 2001; Goncalves, 2005; Peng et. al., 2013; Spaggiari, 2013). By absorbing the energy of vibrations, earthquake damage may be mitigated or damped. Furthermore, as MR dampers work using magnetic fields, the magnetic field strength can be varied to output controllable damper forces (Goncalves, 2005; Christenson et al. 2008; Jiang et. al., 2010; Phillips et. al., 2010; Keivan et. al., 2017). This aspect of variable strength is key in how MR dampers can be used to control structural responses. Using semi-active control algorithms, measurements of the structural response and the ground motion can be used to modify

the current supplied to the MR damper, hence modifying its dampening capabilities to best respond to the loading (Spencer et. al., 1997; Spencer et. al., 1998; Yang, 2001; Christenson et al. 2008; Phillips et. al., 2010). This allows the MR damper to effectively dissipate the energy of structure when under the effects of seismic ground motion, thereby reducing the structural displacements and accelerations and mitigating seismic damage. As MR dampers work through the magnetization of small MR particles in a viscous carrier fluid, the long-term settling characteristics of these particles will lead to performance loss. Hence, MR dampers are an effective case study for the consequences of idle time.

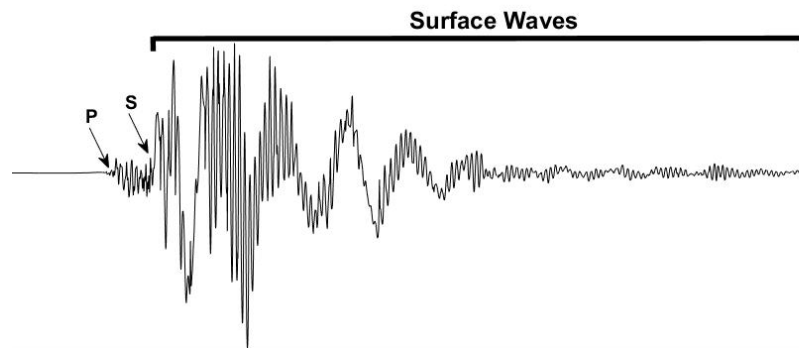


Fig. 1.1: General Earthquake Ground Motion Record

Earthquakes typically have extremely sudden and large peak ground accelerations due to the arrival of the Rayleigh (surface) waves as can be seen in the above figure. These first few seconds of the earthquake are critical for the structural control systems to resist to best protect the building. If the MR fluid particles within the damper have settled after being left idle for a very long time, the ability for the damper to exert the appropriate force or shear strength during this initial ground motion is greatly hampered. This may lead to uncontrollable deformation and damage to the structure.

Although the effects of idle time on structural control systems are a severe issue, there has not been much research done from the view of civil engineering structures. However, through research in other fields, MR damper technology has moved to provide solutions for settling behavior through innovative carrier fluids which prevent settling, even over very long idle-time periods. As such, this MR damper technology still has the potential be used as effective seismic protective systems. These innovative carrier fluids require more research for civil engineering applications and are outside of the scope of this thesis. This thesis will focus on unmitigated idle time using a model MR fluid with a relatively short settling time (on the order of one year for complete settling). The result of this model MR fluid can also be considered as accelerated testing for MR fluids with longer settling times.

Chapter 2 provides a literature review to discuss the background theory behind structural control systems, MR dampers, and other related topics. In Chapter 3, further detail is provided regarding the experimental set-up and the specifics of the large scale 200kN MR damper with a model MR fluid vulnerable to idle-time effects. Chapter 4 includes the implementation and calibration of the Bingham Plastic Model for the numerical simulation. Chapter 5 then addresses the creation of a numerical model to predict idle time behavior of the damper as well as sine wave characterization tests. RTHS testing and structural analysis under seismic ground motion will be presented in Chapter 6. Finally, the results and the implications of the research will be discussed in Chapter 7.

Chapter 2: Literature Review

2.1 Structural Control Systems

Structures are built to resist dynamic loads due to natural disasters through the building's strength, the ability of the structure to deform, and any other energy absorption mechanisms installed. In extreme cases, the resultant displacement will cause the structure to undergo permanent deformation and potentially fail. This is an important factor to control to prevent the collapse of the building or extensive localized damage which may inhibit evacuation procedures and damage people or goods within the building. By adding supplemental structural control systems, the ability to resist natural disasters and the resilience of the buildings can be improved. One such control strategy to reduce the impact of dynamic loading is to increase the damping to the structure by adding supplemental damping systems. Damper control systems use a variety of energy absorbing methods to remove energy from any external excitation. Common ways the input energy can be dissipated is through the use of friction, viscous fluids, and deformable devices (Yang, 2001).

Structural control systems can be broadly categorized into three separate categories: passive control systems, active control systems, and semi-active control systems. From the definitions in the 1997 work by Housner et. al., passive control systems dissipate energy away from the structure in response to a dynamic load without needing any power source (Housner et. al., 1997) while active control systems require an external power source. In active systems, the external power is applied using actuators, which respond to the structural motion through the application of a complimentary force, thereby dissipating or adding energy to the

system as necessary. This force is dependent on the dynamic response of the system which is measured and sent to the control system (Housner et. al., 1997). Lastly, semi-active control systems are ones that attempt to take the positives of active and passive control systems and apply them together. A semi-active control system is often realized as a controllable passive damper. This is because although there is some input of external power to modify the damping capabilities of the control system in response to the structural vibration, the control system is not directly able to inject energy in to the system (Housner et. al., 1997). This ability eliminates stability concerns and if the input control signal is disrupted, it is still possible for the device to act as a passive system (Phillips & Spencer, 2012).

Additionally, semi-active and active systems work well to mitigate multiple hazard types. That is, semi-active and active control systems have the potential to respond well to both earthquakes and strong wind events, while passive systems may not be able to do the same for multiple hazards. Unlike passive systems which may be tuned to a single frequency or to respond to a certain hazard loading type, semi-active and active systems can effectively respond to a range of frequency content even for a single hazard. An example of this, is the effectiveness of passive base isolation in mitigating seismic loading by shifting the natural frequency of the structure away from the high frequency content of earthquakes (Heydari, 2014). Due to the increased lateral deformation and reduced stiffness in the base, wind loading can lead to large displacements and accelerations, and depending on the system may result in resonance with wind loading (Soong & Spencer, 2000; Heydari, 2014). Similarly, another passive system, tuned mass dampers, work well for wind loading, but not for

seismic ground motion (Housner, 1997; Rai, 2009; Heydari, 2014). For this reason, the implementation of hybrid control systems in structures is a beneficial structural protective system. By combining different passive, active, and semi-active control systems, it becomes possible to greatly mitigate the risk from multiple hazards. A thorough literature review is provided in the paper by Housner (1997) and Rai et al. (2009) and multiple case studies are presented in the paper by Spencer (2008).

2.2 Passive Control Systems

Passive control systems work to dissipate the energy due to the structural response, thereby reducing it, by converting kinetic energy into other forms such as heat. Examples of passive control systems include viscoelastic dampers, metallic yield dampers, and friction dampers. These devices convert energy from the dynamic motion by doing work and dissipating energy as heat through frictional sliding, metallic yielding, or the deformation of viscoelastic fluids (Housner et. al., 1997; Yang, 2001). The following figure shows how inter-story viscoelastic fluid dampers, metallic yield dampers, and friction dampers can be implemented into a structure to reduce the dynamic response of the structure.

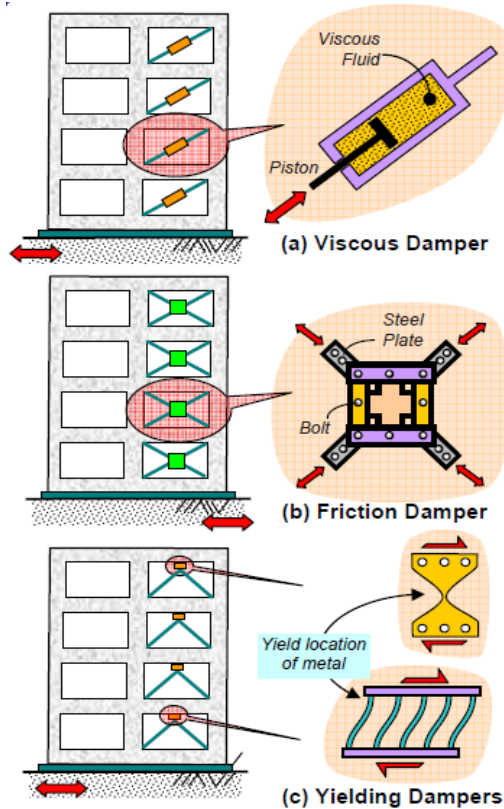


Fig. 2.1: Types of Passive Structural Control Systems (Murty, 2005)

Another type of passive device is seismic isolation systems or base isolators. These replace the conventional fixed base of a structure with deformable bearings. This allows the building to translate in the direction of the excitation, thereby dissipating energy in the deformable layer. It also allows the superstructure to nominally behave as a rigid body instead of oscillating about the base of the structure. Base isolation prevents the generation of high response accelerations in the superstructure and reduces the stiffness of the base which shifts the natural frequency of the structure away from high frequency earthquake ground motion content. Base isolation reduces the risk of structural damage by decreasing the response and preventing the possibility of resonance occurring (Housner, 1997; Rai, 2009; Heydari, 2014; Taywade & Savale, 2015). Isolators can be coupled with other passive, active,

or semi-active control systems to further enhance the structure's resilience. The figure below shows the effectiveness of such seismic isolators.

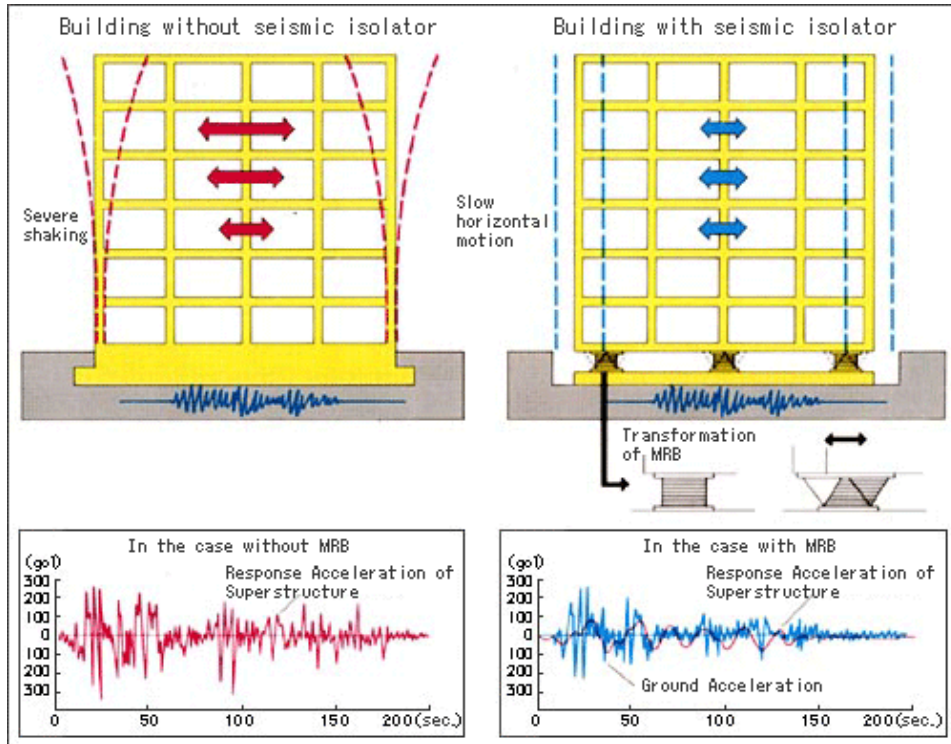


Fig. 2.2: Effects of Seismic Base Isolation (Bridgestone, 2017)

The last type of passive device considered herein directly enhances the damping capabilities of the building by using the inertia of large tuned mass dampers (TMDs) (Housner et. al., 1997; Yang, 2001). TMDs are seen in the literature to effectively reduce wind loading but not work as effectively for seismic excitation. This is due to the TMD being tuned to the natural frequency of the structure which restricts the protective capabilities to a narrow frequency range. Seismic excitation has a wider variety of frequency content within the same excitation and produces forced vibration response, which can lead to a reduction in the protective capability of purely passive TMDs. One example of a TMD is the one suspended between the 92nd

and 87th floors of Taipei 101 (Taipei-101, 2014), which uses its extremely large mass and inertia to reduce the vibration motion of the structure due to the persistent wind loading the building experiences. However, this structure also combines the TMD with other passive control systems, such as viscous dampers, to create a hybrid control system to better protect the structure (Taipei-101, 2014).

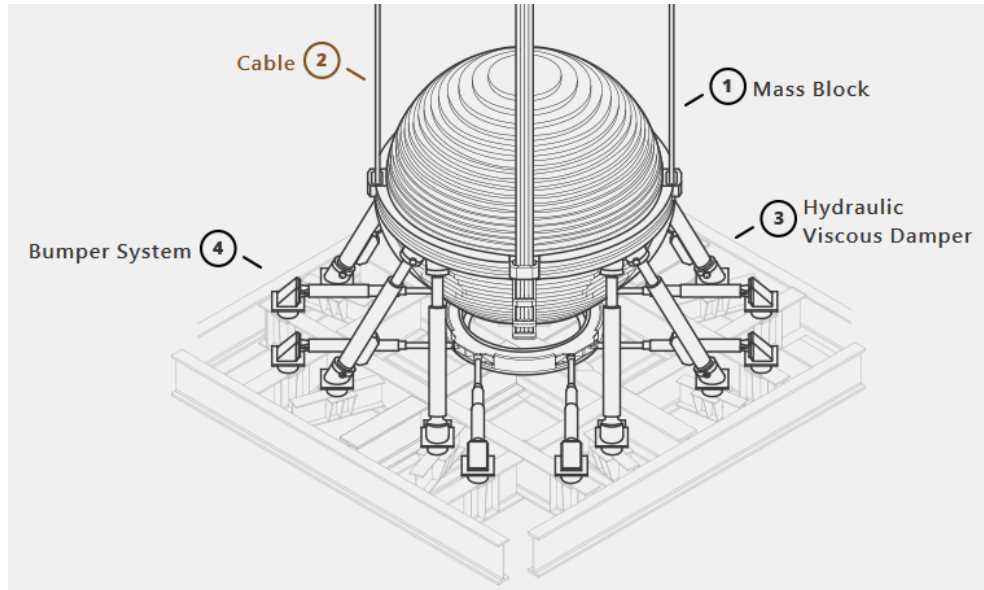


Fig. 2.3: Tuned Mass Damper on Taipei-101 (Taipei-101, 2014)

2.3 Active Control Systems

Active control systems are created through the combination of actuators, sensors, and a controller which can modify the damping force or other dynamic properties to reduce the structural response (Housner et. al. 1997). The key shortcoming of this method lies in the potential for the actuator to add energy to the system and amplify the response. This may occur due to poor control strategies or measurements (Housner et. al. 1997; Yang 2001). Additionally, if there is a loss of power to the control system all protection from the active protection is lost and the

actuator can become locked. However, when implemented well, especially when paired with other protective systems, active control systems can provide effective protection from seismic and wind loading (Yang, 2001; Spencer 2008; Rai et al. 2009). The schematic below shows the active control system and how the different components relate to one another.

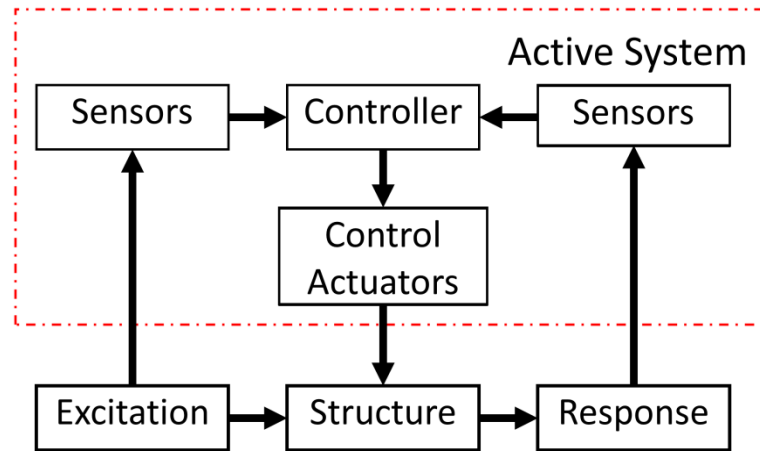


Fig. 2.4: Active Control System Component Block Diagram

Active control systems are most efficient when combined with passive systems to make hybrid control systems. Hybrid mass dampers (HMD) use a tuned mass damper and an active control actuator together to increase the stability of the system and reduce the energy requirements of the active control system (Housner, 1997; Spencer 2008). Similarly, hybrid seismic isolation systems combine base isolators with active control actuators in order to minimize displacement and energy requirements for the actuator. One major issue is that these actuators do not have the capacity nor have been developed enough to mitigate strong earthquakes. Generally, the initial capital and high energy requirements for active control systems are also very high (Yang, 2001; Spencer 2008; Rai et al. 2009). This combined with the

potential for destabilizing the system inhibit the system from being widely accepted and integrated in to more buildings.

2.4 Semi-Active Control Systems

Semi-active control systems are devices which also interface with sensors and the controller to reduce the structural vibration, but do not have an actuator. As such, the semi-active control system works to combine the favorable characteristics of both passive and active control systems. By having a variable response depending on the control algorithms, these devices can perform better than passive systems in reducing motion or damage due to any excitation while also taking up a smaller space (Housner; 1997; Rai et. al; 2009). Additionally, as semi-active systems do not use an actuator, they cannot introduce energy to the system which can destabilize the structure. They also require less energy than active systems, and if power sources are lost during an event, the semi-active systems can act as passive systems to provide some level of protection to the system (Spencer, 2008). Some examples of these include variable orifice dampers, controllable fluid dampers, and variable friction dampers (Housner et. al., 1997; Dyke et. al., 1998; Yang, 2001).

One semi-active control system that is very effective at reducing the structural response, is a type of controllable smart fluid damper known as magnetorheological (MR) dampers. These dampers contain a fluid whose strength can be varied using a magnetic field (Carlson 1996; Jolly, 1996; Jolly, 1998; Goncalves, 2005; Peng et. al., 2013; Spaggiari, 2013; Yang, 2001). These MR fluids will be discussed in the following section. MR dampers have potential as an effective device to control the structural response under multiple natural hazard loading types (Spencer, 2008; Rai et

al., 2009). Due to the relatively low energy requirements and inability to add energy to the structural system, semi-active control systems have the highest potential to be developed for common integration into future buildings (Housner, 1997; Spencer, 2008; Rai et. al. 2009). Furthermore, when used with the appropriate control methods, these systems can protect infrastructure over a variety of external excitations and perform significantly better than passive systems and are comparable to active systems (Housner, 1997; Spencer, 2008; Rai et al., 2009). Due to the low energy needs, these control systems could run on battery power which is an extremely beneficial feature due to the possibility of natural hazards affecting the main power supply (Dyke et. al., 1998; Jansen & Dyke, Housner et. al., 1997; Yang, 2001).

2.5 Hybrid Control Systems

Hybrid control systems may use a combination of passive, active, and semi-active control systems in order to protect the structure more effectively and to provide multi-hazard protection. Some systems which have been researched well and show effective reduction in the structural response under multi-hazard excitations are hybrid mass dampers (HMD) and the hybrid isolation systems. HMDs are a combination of a TMD and an active control system while hybrid isolation systems are a combination of semi-active or active control systems with base isolators. In both cases however, other protective systems may also be implemented in the building for further protection. Housner (1997), and Spencer (2008) provide a good overview and literature review on hybrid control systems. An example HMD implementation can be seen in the Sendagaya INTES building in Tokyo (Spencer 2008). This includes tuned mass dampers and hydraulic actuators, thereby reducing the structural response

passively while also providing active control capability. This building can be seen in Fig. 2.5 below.

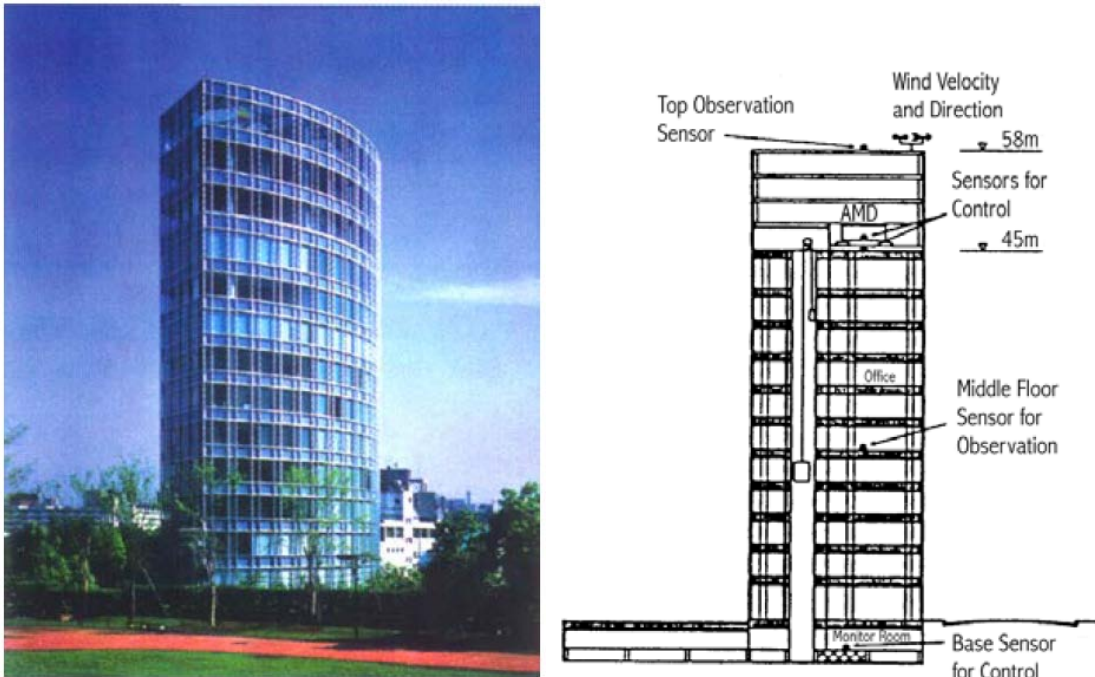


Fig. 2.5: Sendagaya INTES Building with HMDs (Spencer, 2008)

Similar approaches have been taken in other buildings such as the Kyobashi Seiwa Building in 1989 (Spencer, 2008) and the Ando Nighikicho Building (Rai et al. 2009) and studies have shown the effectiveness of the technology to reduce the structural response.

Due to the effectiveness and relative simplicity of purely passive base isolation systems (Housner, 1997), hybrid isolation systems have also been researched in several articles to reduce the negative effects of base isolation layers. As base isolation can reduce displacements and acceleration in the structure by making the base more flexible, there can be large base displacements. By combining the base isolation with active or semi-active control systems such as hydraulic

actuators or MR dampers, this displacement can then be reduced and controlled. This provides a substantial advantage over the purely passive base isolation systems.

2.6 Time-varying performance of structural control systems

Passive systems such as tuned mass dampers, friction dampers, viscoelastic dampers or viscous dampers may not require much maintenance or control but can still experience performance degradation over time (Housner 1997). This could occur due to corrosion in the friction damper, wear and temperature effects on the viscoelastic dampers, wear on the mechanical components of a viscous damper, loss of friction in sliding bearings, or de-tuning of a tuned mass damper due to structural damage or material degradation (Housner 1997; Riley & Reinhorn, 1997; Demetriou et al. 2014). Similarly, semi-active and active control systems could also undergo long-term performance degradation in the mechanical or material components or even the failure of the electronics which control the devices. This thesis discusses the behavior of semi-active MR dampers over time and the performance degradation of a model MR fluid which exhibits accelerated performance degradation due to idle time settling. As the particles settle out of the suspension they are no longer as responsive to the applied magnetic field and hence can lose a significant amount of their controllable force. Although this performance degradation is expected if the MR particles settle, there are not many studies which focus on the long-term performance degradation of seismic protective systems and use experimental testing on civil structures. One study by Khansefid and Ahmadizadeh (2016) discusses the effects of long-term structural degradation on active and passive structural control systems. It also provides the brief history of work done which takes the nonlinearity of structural

performance over time into account. Due to the uncertainty present in these structural control systems, engineers may be being unwilling to design with and implement these devices to protect their structures and the people using them. This is especially true for more regular or commonly built structures due to the increased construction and labor costs. At the same time however, these control systems are important in providing protection to the masses and by doing further research and testing and designing better devices and strategies to maintain their performance over time, these structural control systems may be implemented more in areas prone to natural hazards.

Civil infrastructure may last for decades before being exposed to any dynamic loading. Unlike mechanical systems, such as automotive suspension systems, which undergo repeated and frequent excitation, civil protective systems are prone to remain at rest for extended periods of time. Additionally, the life cycle of civil structures is generally on the order of decades while for mechanical systems, the same is not true. Maintenance for mechanical systems may be less time consuming and more cost effective than civil systems, especially when comparing to civil protection systems like base isolation, or dampers that are within the main structure. To fix, replace, retrofit, or maintain civil protection systems may require the building to be shut down for months or even years depending on the extent of the work needed, due to the inaccessibility of these systems. For example, base isolation is most commonly found in the base or foundation of the structure, while friction dampers, viscous dampers, or metallic yield dampers are often implemented within the walls of the structure on the frame of the structure (Housner, 1997; Murty, 2005; Rai et al. 2009). Both of these

location types are difficult to access quickly and easily and require extended periods of renovation. As such, by performing further research into the effects of time on the performance degradation of these systems, it will be possible to design appropriate counter measures and maintenance strategies. By mitigating the loss in performance and maintaining the integrity of the structural protective systems, the burden on the owners will also be reduced and make these technologies more cost-effective and worthwhile to implement in their structures.

2.7 Magnetorheological (MR) Fluids

Magnetorheological (MR) Fluids, are a type of smart material, along with piezoelectric materials, electrorheological fluids, and shape memory alloys (Kciuk & Turczyn, 2006), which have the ability to temporarily modify their rheology due to an applied magnetic field. The first known record of MR fluid properties come through the research done by Jacob Rainbow at the US National Bureau of Standards (Goncalves, 2005). MR fluid is a homogeneous non-colloidal suspension of magnetizable particles in a viscous carrier fluid, e.g. carbonyl iron particles in a mineral oil. The particles are typically around 2-10 microns in diameter and make up around 20-40% of the volume of the MR fluids. The viscosity of the fluid is important to allow the particles to remain suspended within the fluid. This is additionally supported using additives to prevent gravitational settling. However, if the fluid is too viscous or the volume fraction of particles too low then the dynamic range may be reduced. Dynamic range is the range of forces that can be developed between the low off-state and high on-state forces.

When a magnetic field is applied, these fluids can convert from free-flowing liquids to semi-solids in the matter of milliseconds and develop significant and controllable shear strength (RSC 2014). This is similar to electrorheological fluids which exhibit increased shear strength under an applied electric current. According to Jolly et. al. (1996), MR fluids develop a monotonically increasing yield stress with an increase in the applied field. This occurs due to formation of induced dipoles which allow for the construction of linear particle chains along the magnetic field. These structures form perpendicular to the direction of fluid flow within milliseconds, which allow them to almost instantaneously resist fluid motion and hence increase the yield shear strength and viscosity of the fluid (Spencer et. al. 1997; Spaggiari, 2013; Kciuk & Turczyn, 2006; Jolly et. al., 1996; Jolly et. al., 1998; Goncalves, 2005; Premalatha et. al., 2012; RSC 2014).

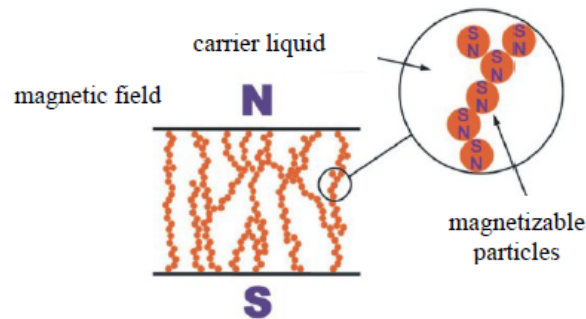


Fig. 2.6: MR Fluids Under Magnetic Field (Kciuk & Turczyn, 2006)

This increase in strength combined with the short rise time allow for much more efficient tracking of the dynamic loading and hence more effective vibrational damping. This almost instantaneous variable shear strength is ideal to counteract external dynamic loading through energy dissipation. Additionally, as the force is not exerted by a mechanical device like an actuator, even with these large damping

forces, energy will not be added to the structure and destabilize it. Instead, it will dissipate the energy through the conversion of kinetic energy into work and heat when the MR fluid shears (Carlson et. al., 1996; Jolly et. al., 1996; Spencer et. al. 1997; Dyke et. al., 1998; Jolly et. al., 1998; Jolly et. al., 1999; Li et. al., 1999; Goncalves, 2005). As such, MR fluids possess a number of beneficial traits which can be utilized to best counteract dynamic loading on structures. Additionally, compared to electrorheological fluids, MR fluids are not as sensitive to temperature fluctuations or the presence of contaminants, making it easier to maintain, build, and use in a variety of locations around the world (Kciuk & Turczyn, 2006; Maleki-Jirsaraei et. al., 2010; Premalatha et. al., 2012). These reasons push it far beyond electrorheological fluids in terms of viability for commercial applications, including semi-active control systems for civil engineering applications (Carlson et. al., 1996; Jolly et. al., 1996; Spencer et. al. 1997; Dyke et. al., 1998; Jolly et. al., 1998; Yang, 2001; Spaggiari, 2013; Peng et. al., 2013).

2.8 Magnetorheological (MR) Dampers

The use of MR fluids in semi-active control systems is through controllable fluid devices known as magnetorheological (MR) dampers. These dampers can operate over large temperature ranges, produce significant forces even at low velocities, and possess a high dynamic range. Furthermore, MR dampers can provide these features in a relatively small device while also have no moving parts, thereby reducing maintenance and increasing the rise time due to the applied magnetic field (Yang, 2001; Goncalves, 2005; Jiang et. al., 2010). This is an additional bonus as compared to active systems or some passive systems which may take significantly

more area within the structure, more materials to construct, and more input energy requirements.

The three basic operational modes for MR fluid devices include the valve (or pressure driven flow) mode, the direct shear mode, and the squeeze mode as shown in the figure adapted from Jolly et. al., 1998:

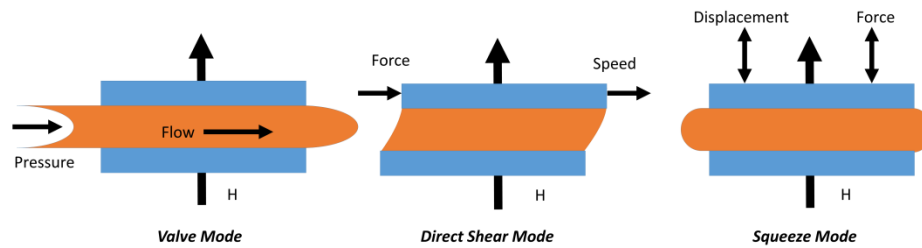


Fig. 2.7: Basic Operational Modes of MR Fluid Devices

In each of these modes, the magnetic field is applied over the entire volume in order to solidify the MR fluid. This allows for the availability of high reversible shear strengths in the fluid. In the valve mode, the MR fluid flows between fixed parallel plates under an applied magnetic field. This develops a pressure driven flow also known as Poiseuille flow. In the shear mode, the fluid flows between sliding parallel plates which slide with a relative velocity to one another. Both valve and shear modes are typically used in MR dampers, with the shear mode also being used in MR brakes and clutches. Lastly, in the relatively uncommon squeeze mode, the applied field can cause the linear particle chain to act somewhat like a column, resisting lateral displacement. For this mode, it is assumed that the lateral flow of the fluid has Poiseuille-like behavior (Carlson et. al., 1996; Jolly et. al., 1998; Goncalves, 2005; Spaggiari, 2013).

Lord Corporation have developed MR fluid devices for commercial purposes and some large-scale dampers for research purposes (Carlson et. al., 1996; Jolley et. al., 1998). One such research prototype is located at the University of Maryland, College Park. This is a second-generation Lord Corporation 200 kN (45 kips) damper, with an available stroke of ± 292.1 mm (± 11.5 in.) and a total length of 1.47 m (Christenson et. al., 2008; Jiang et. al. 2010; Phillips et. al., 2010).

Unlike the three basic operating modes mentioned above, this MR damper uses something more akin to a pinch mode. In pinch mode, the poles are arranged axially along the flow path and hence generate a non-uniform magnetic field which targets the fluid in the narrowest part of the orifice. This can be seen in the following figure from (Goncalves & Carlson, 2009):

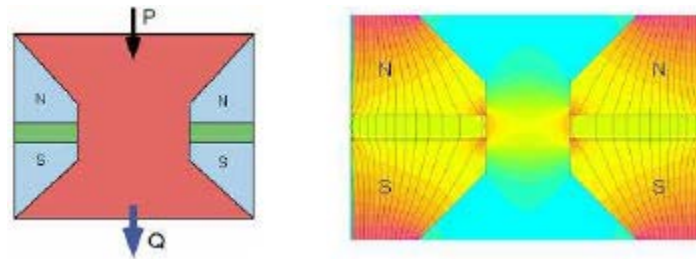


Fig. 2.8: Illustrations of Pinch Mode Action (Goncalves & Carlson, 2009)

For the Lord Corporation damper, a single set of coils were wrapped around the piston to create a choke point which inhibits fluid flow from one side of the piston to the other when a magnetic field is applied. This consists of the use of a magnetic gradient pinch to solidify MR fluid only near the axially distributed poles versus the entire fluid. This not only allows for improvements in energy efficiency, but also could allow for the use of cheaper, less refined materials which would also drive capital costs low. Although the damper itself may contain a large volume of MR

fluid, for this mode of use for the MR fluids, small active volumes are required. In the case of the Lord damper, the pinch mode is being used to prevent flow through the annular duct around the piston, thereby increasing the shear strength. This can also be approximated as a valve mode due to the small annular gap size.

2.9 Bingham Plastic Model

The simplest model for describing the behavior of the MR fluid is the Bingham plastic model as per the model by Stanway et al. (1985) and the equation from Phillips (1969), referenced in Spencer et al, (1997) Yang et al., (2002) and Goncalves (2005) among others:

$$\tau = \tau_0(H) * sgn(\dot{\gamma}) + \eta\dot{\gamma} \quad |\tau| > |\tau_0| \quad (Eq. 2.1. a)$$

$$\dot{\gamma} = 0 \quad |\tau| < |\tau_0| \quad (Eq. 2.1. b)$$

Where τ = yield stress caused by the applied field; $\dot{\gamma}$ = shear strain rate; H = amplitude of the applied magnetic field; and η = field-independent post-yield plastic viscosity, which is defined as the slope of the measured shear stress versus the shear strain rate (Stanway, et al. 1985; Spencer et al, 1997; Jolly, 1998; Yang et. al., 2002; Goncalves, 2005; Kciuk & Turczyn, 2006).

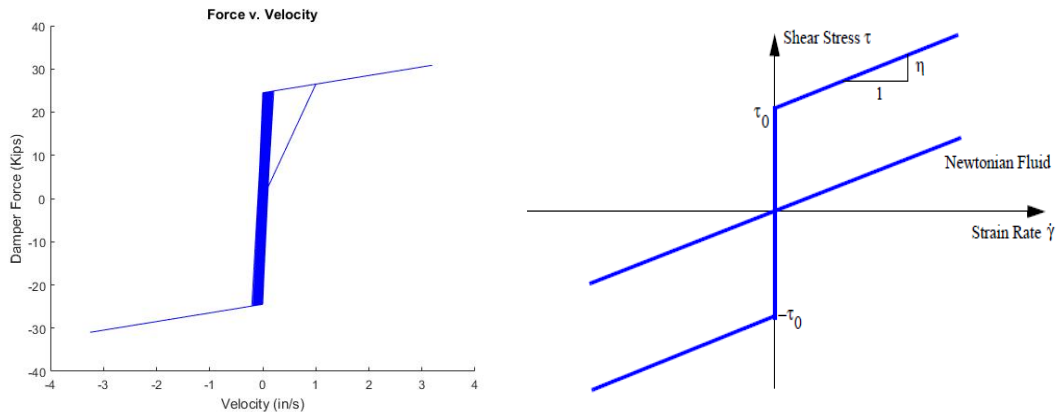


Fig. 2.9: Generic Bingham Plastic Model

The MR fluid acts as a Newtonian fluid without an applied field and produces an increasing shear stress with increasing strain solely due to the viscosity. However, when there is an applied magnetic field we see a much larger stress develop, and hence observe the potential for the fluid's controllability and ability to respond to large forces. (Spencer et al, 1997; Jolly, 1998; Yang et al., 2002; Goncalves, 2005; Kciuk & Turczyn, 2006). According to Premalatha et al., MR fluids may be able to exhibit apparent viscosities 10^5 times larger under the applied magnetic field (Premalatha et al., 2012).

Chapter 3: Experimental Setup

For this thesis, the use of sine wave testing and real-time hybrid simulation (RTHS) testing was crucial to verify and identify the effects of idle time. To perform these experiments, a second generation large-scale MR damper manufactured by the Lord Corporation was used. Semi-active devices such as the MR dampers serve as an effective case study for idle time effects due to the potential of the MR particles to settle over time. Prolonged idle time may cause the degradation of many structural control systems. Through the use of idle time settling of MR particles, we can gain an appreciation for the importance of the long-term performance of these devices in civil engineering applications.

For this thesis, six sine wave characterization tests were used to calibrate the Bingham Plastic Model discussed in Chapter 4. Additionally, three idle time sine wave characterization tests were performed in order to generate an idle time model presented in Chapter 5. Furthermore, one idle time RTHS test was performed to validate the idle time model and to measure the performance degradation of the physical damper. Additional RTHS tests were performed to accurately compare the idle time performance to the fully-mixed case. Further information on the structural model and the RTHS testing will be provided in the Chapter 6.

3.1 Physical Substructure

The second-generation MR damper produced by the Lord Corporation is a large scale 200 kN (~45 kip) damper with a total length of 1.47 m and a total available stroke of ± 0.2921 m (± 11.5 in.) (Christenson, 2008). To compensate for the temperature-

controlled expansion of the MR fluid during operation, an accumulator charged to 5.17 MPa (750 psi) with N₂ gas is used (Christenson et al., 2008). This allows the damper to maintain nominal performance up to 27^o C. The damper includes a single internal piston with an electromagnet which can be controlled via the input current. This provides the pinch-mode operational mode for the MR damper. The MR damper properties are shown in Table 3.1 and the MR damper is shown in Fig. 3.1.

Table 3.1: MR Damper Properties

MR Damper Properties	
Total Available Stroke (m)	0.5842
Max Velocity (m/s)	0.2491
Inner Diameter, ID (m)	0.2032
Inner Radius (m)	0.1016
Annular Gap Thickness (m)	0.002
Radius of Piston (m)	0.0996
Radius of Shaft (m)	0.04
Total Volume (m ³)	0.01660
Active Volume (m ³)	0.00009
Coil Resistance (Ω)	4.8
Inductance (H) at 1 A/ 2 A	5.0 / 3.0
Length (m)	3.47
Weight (kN)	2.734

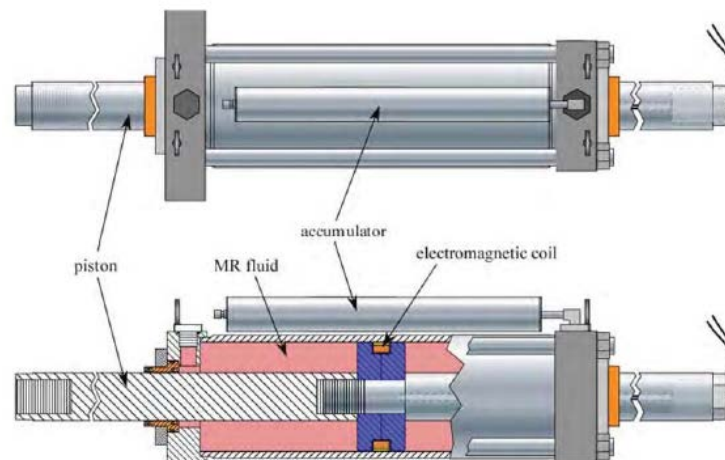


Fig. 3.1: Lord Corporation MR Damper (Jiang et. al., 2010; Phillips et. al., 2010)

The damper is connected to a MTS 245 kN (55 kips) actuator which has a stroke of ± 0.2540 m (± 10 in.) and is double ended (MTS). This is capped using the control software for protection purposes to a maximum of ± 0.1524 m (± 6 in.). Both devices are bolted to an I-beam which is connected to a 0.6096 m (24 in.) thick strong floor at the University of Maryland, College Park's Structural Lab area. This can be seen from the Fig. 3.2 and 3.3 below. As can be seen, the damper is mounted to the I-beam using a 0.0508 m (2 inch) thick reaction angle plate, while the left end of the actuator is connected to a reaction angle plate. Both angle plates are bolted to the I-beam to resist the large forces and deformation that could be generated by the actuator and damper during testing. The main body of the actuator is also tied down to resist any vertical displacement or bending the actuator may undergo. This setup has been used successfully with some variations in other large-scale damper testing (Yang et al., 2002; Phillips et al., 2010; Phillips & Spencer, 2012).

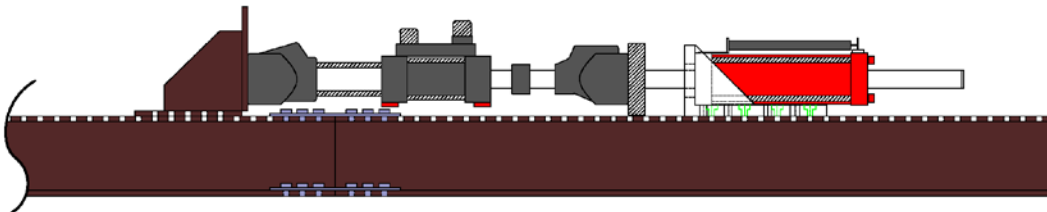


Fig. 3.2: Schematic of Actuator and MR Damper Setup on Top of I-beam



Fig. 3.3: Actuator and MR Damper Setup

The actuator is driven by the UMD high-bay main hydraulic power unit which supplies hydraulic oil at 20.7 MPa (3000 psi) and 227 lpm (60 gpm). The hydraulic oil is sent to the MTS SilentFlo hydraulic system manifold which then regulates the pressure and flow of the hydraulic oil and is rated at 189 lpm (50 gpm). The actuator uses two MTS servo valves rated at 57 lpm (15 gpm) each, which are controlled through a MTS FlexTest 60 controller and the MTS 793 control software.

3.2 Numerical User Interface and Control Equipment

The setup also includes the use of a dSPACE I/O control board model 1103 which interfaces with MATLAB and Simulink and can be used to give external commands to the MTS controller. The MR damper's electromagnetic coils are controlled using a pulse-width modulator (PWM) which controls the current supplied to the device. The PWM is made up of an Advanced Motion Controls PS2x300W unregulated power supply which supplies a 72V DC output to the 30A8 analog servo-drive, which has a maximum continuous current of 15 A and a maximum peak output of 30 A. The ability of the PWM to provide quick response times with minimal power losses allow for accurate control of the damper. A command signal of ± 10 V via dSPACE is used to control the current with a ratio of 1 V / 1 A. To protect the equipment and AC supply from the high amperage current and high frequency noise, a Schaffner FN2080-12-06 line filter is used on the AC input to the power supply, and a ferrite core is used at the DC output to the damper. The current produced by the PWM is used along with the electromagnet within the MR damper piston head to generate a variable strength magnetic field as per the structural control requirements. The PWM equipment configuration can be seen in Fig. 3.4 and 3.5 below.

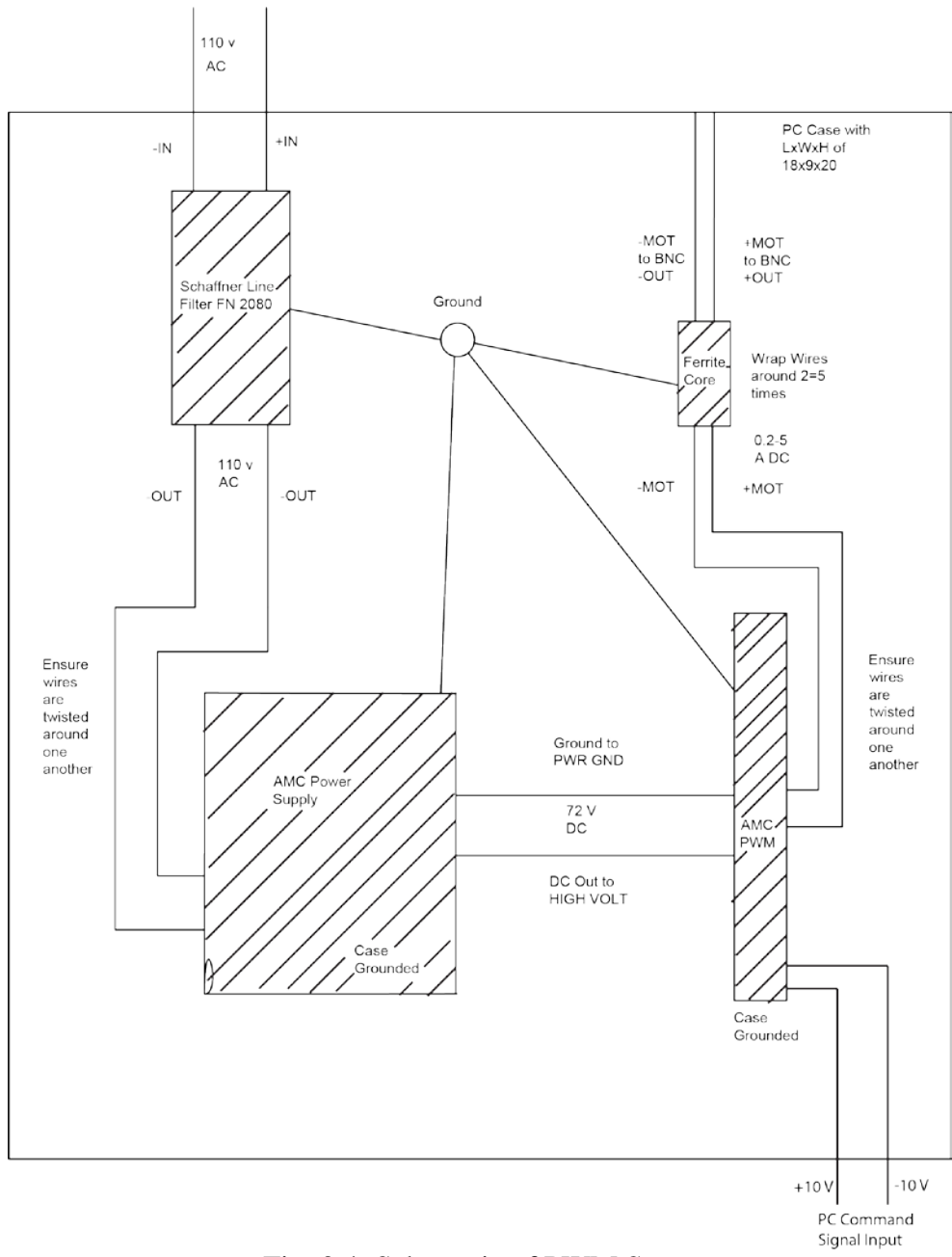


Fig. 3.4: Schematic of PWM Setup

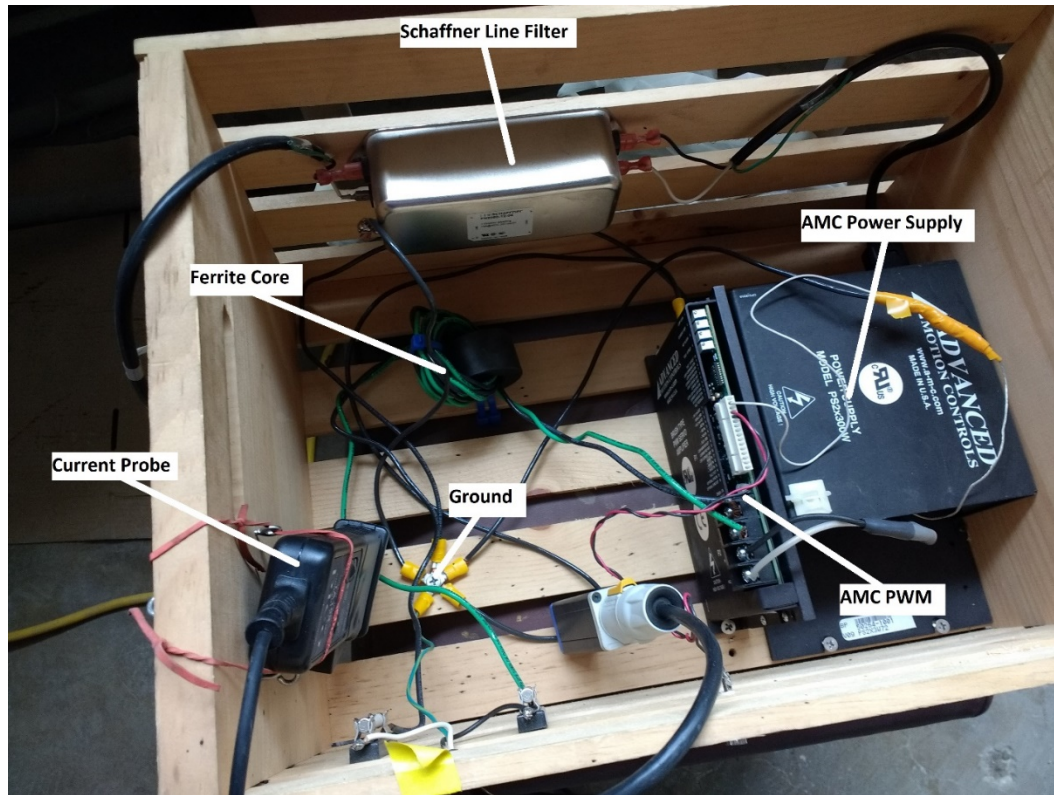


Fig. 3.5: Picture of PWM Setup

An MTS load cell were used to record the damping force and an internal LVDT was used to collect displacement data of the actuator. The MTS load cell can measure up to 250 kN (55 kip) forces. To measure temperature, three temperature gauges were used on the sides and top of the MR damper. These Omega temperature gauges are connected to Omega analog-to-digital converters with a sensitivity of 1 mV/°F (Omega). For sinusoidal testing, the MTS controller was adequate in order to run tests and collect the data for both idle time testing and for model calibration and verification. However, to perform RTHS testing using earthquake ground motion records on a numerical structure, a simulation was created using MATLAB and Simulink and that model interfaced with the dSPACE I/O control board. It does this by converting the Simulink model and all numerical components into C code and

sending it to the dSPACE board through MATLAB's Real-Time Interface. The testing parameters can then be controlled using the dSPACE Control Desk software.

The Simulink model performs calculations for the state-space matrices and equations of motion, outputs current to the damper depending on the structural control type (passive-off, passive-on, or semi-active), and provides the displacement commands to the actuator. Additionally, dSPACE and the computer model collect data from the various sensors through the dSPACE I/O board. This allows for an effective way to run experimental testing and collect data from test excitations beyond that of simple sine waves, i.e. earthquake ground motions for RTHS testing.

3.3 Real-Time Hybrid Simulation Setup

A 5 story base isolated structure with an MR damper in the base isolation layer is used for structural analysis and real-time hybrid simulation (RTHS) testing in this thesis and is presented in Chapter 6. RTHS was used to test the numerical model while interfacing the physical substructure, i.e. the MR damper. In RTHS, there is the possibility for time delays and time lags to be introduced due to the response time of the physical testing equipment which may lead to inaccuracy and instability in the numerical model. A model-based actuator controller was used to compensate for the time delays and time lags. The NSEL report by Phillips and Spencer (2012) provides a thorough background on the different types of RTHS testing frameworks and control algorithms. The RTHS Testing Block Diagram is shown in Fig. 3.6.

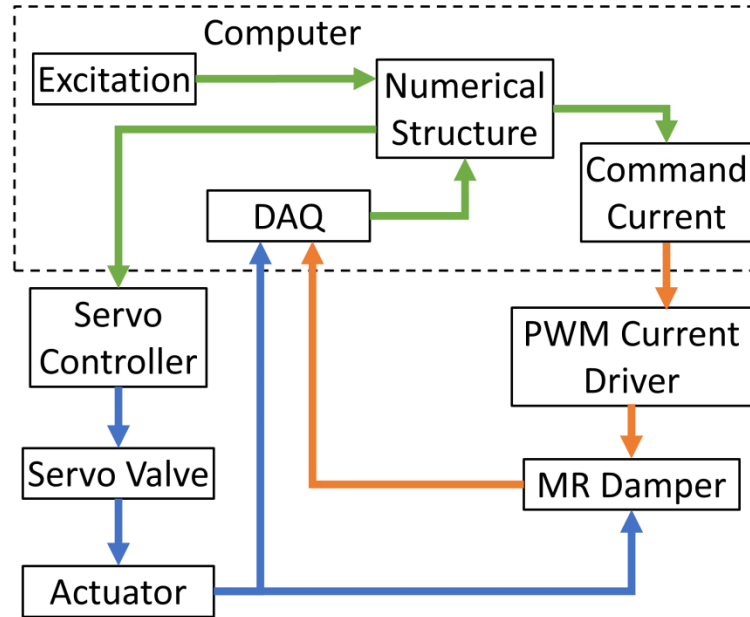


Fig. 3.6: RTHS Block Diagram

Chapter 4: Bingham Plastic Damper Model Creation

For the purposes of this thesis, a Bingham plastic model was developed to represent the MR damper in the numerical simulation. Due to the simplicity of the Bingham model, which only has two variable parameters, it allowed for an easier integration with the idle time numerical model discussed in Chapter 5. To create the numerical model for the 200 kN Lord Corporation MR damper, first the response of the MR damper was determined through a set of characterization tests. The model was then verified through the use of additional sine wave tests and RTHS tests under earthquake ground motion. The Bingham plastic model can be considered equivalent to a Coulomb friction element and a viscous dashpot connected in parallel.

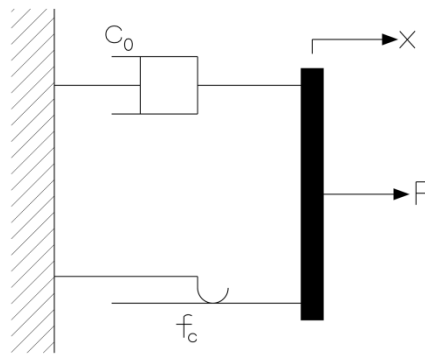


Fig. 4.1: Bingham Plastic Model

$$F = f_c(I) * \text{sgn}(\dot{x}) + c_0(I)\dot{x} \quad (\text{Eq. 4.1})$$

where F = Damper Force; f_c = Coulomb friction force; \dot{x} = velocity; I = applied current; and c_0 = viscous damping coefficient.

The parameters from the equation above were determined by fitting the model to six sets of sine wave data tests run using the physical components of the experimental set up. The sine wave testing varied over three currents (0 A, 1 A, and

2.5 A) and two frequencies (0.5 Hz and 1 Hz) with a fixed displacement of ± 25.4 mm (± 1 in). These six sets of sine wave data can be seen in Fig. 4.2 to 4.4 below.

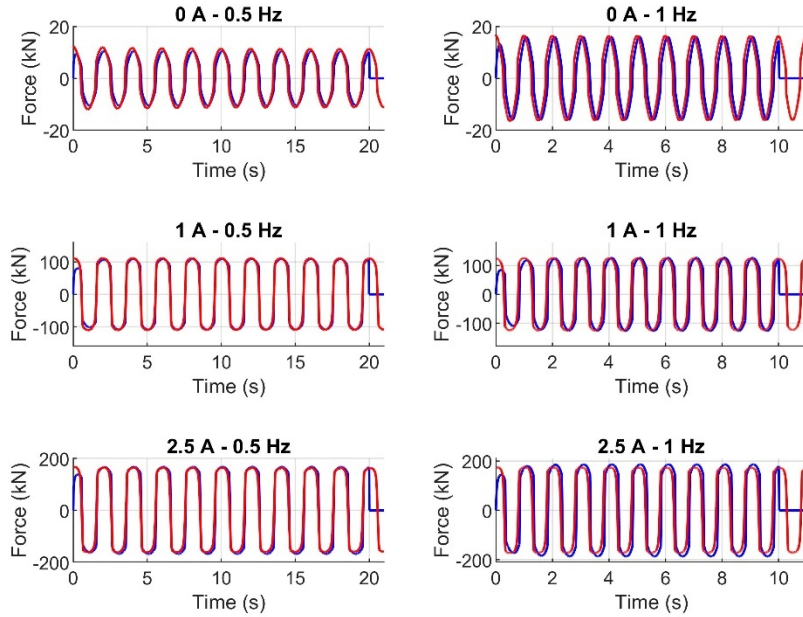


Fig. 4.2: Force-Time Plots for Calibrated Model (Blue) and Sine Wave Test Data (Red)

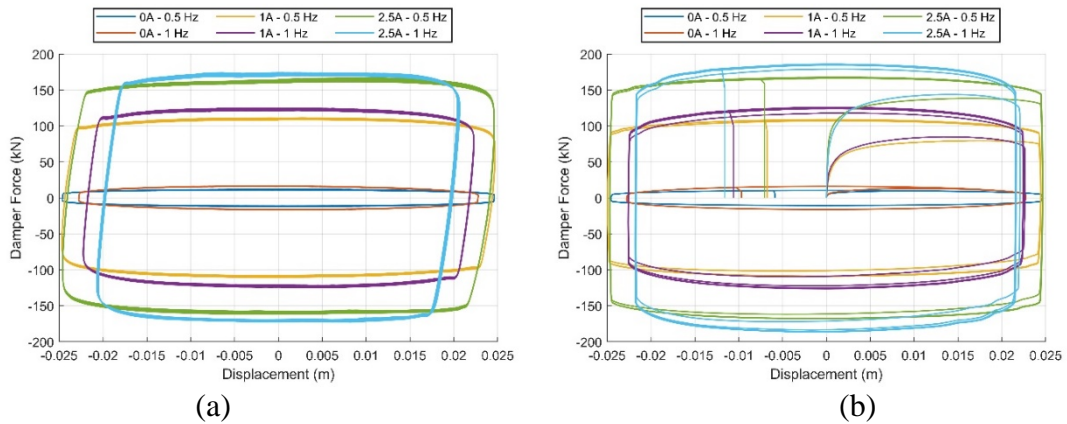


Fig. 4.3: Force-Displacement Plot from Experimental Data (a) and Numerical Model (b)

(b)

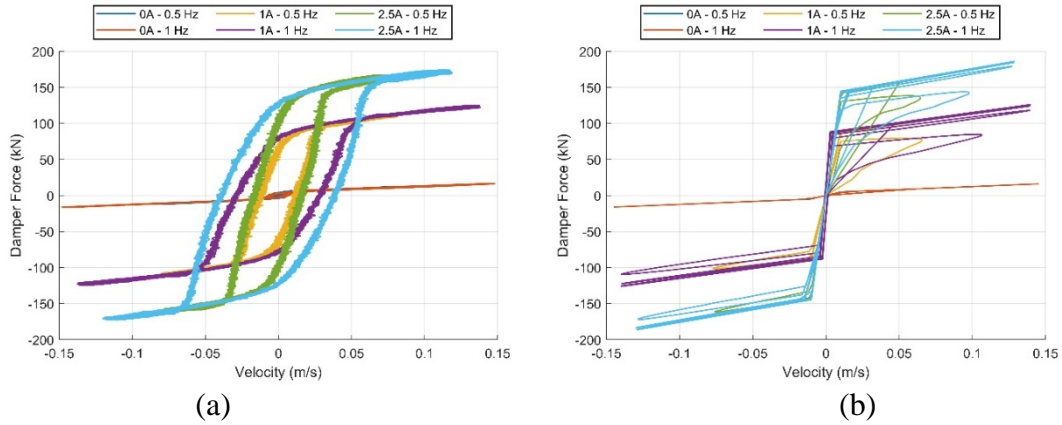


Fig. 4.4: Force-Velocity Plot from Experimental Data (a) and Numerical Model (b)

The parameters vary with the applied current using an exponential function to model the appropriate force behaviors depending on the current. The parameters are displayed in Table 4.1 below.

$$f_c(I) = f_{c,b} + (f_{c,a} - f_{c,b}) * \exp(-f_{c,c} * I) \quad (Eq. 4.2)$$

$$c_0(I) = c_{0,b} + (c_{0,a} - c_{0,b}) * \exp(-c_{0,c} * I) \quad (Eq. 4.3)$$

The parameters with the subscript ‘a’ referred to the parameter’s value at a current of 0 A and those with the subscript ‘b’ referred to the parameter’s value at a current of 2.5 A. Parameters with the subscript ‘c’ were used to vary the rate that the exponential function rose to pass through the three points for 0 A, 1 A, and 2.5 A sine wave data.

Table 4.1: Bingham Plastic Fitted Parameters

$f_{c,a}$ (kN)	$f_{c,b}$ (kN)	$f_{c,c}$ (A ⁻¹)	$c_{0,a}$ (kN*s/mm)	$c_{0,b}$ (kN*s/mm)	$c_{0,c}$ (A ⁻¹)
4.1	170	0.7	0.0825	0.365	1.15

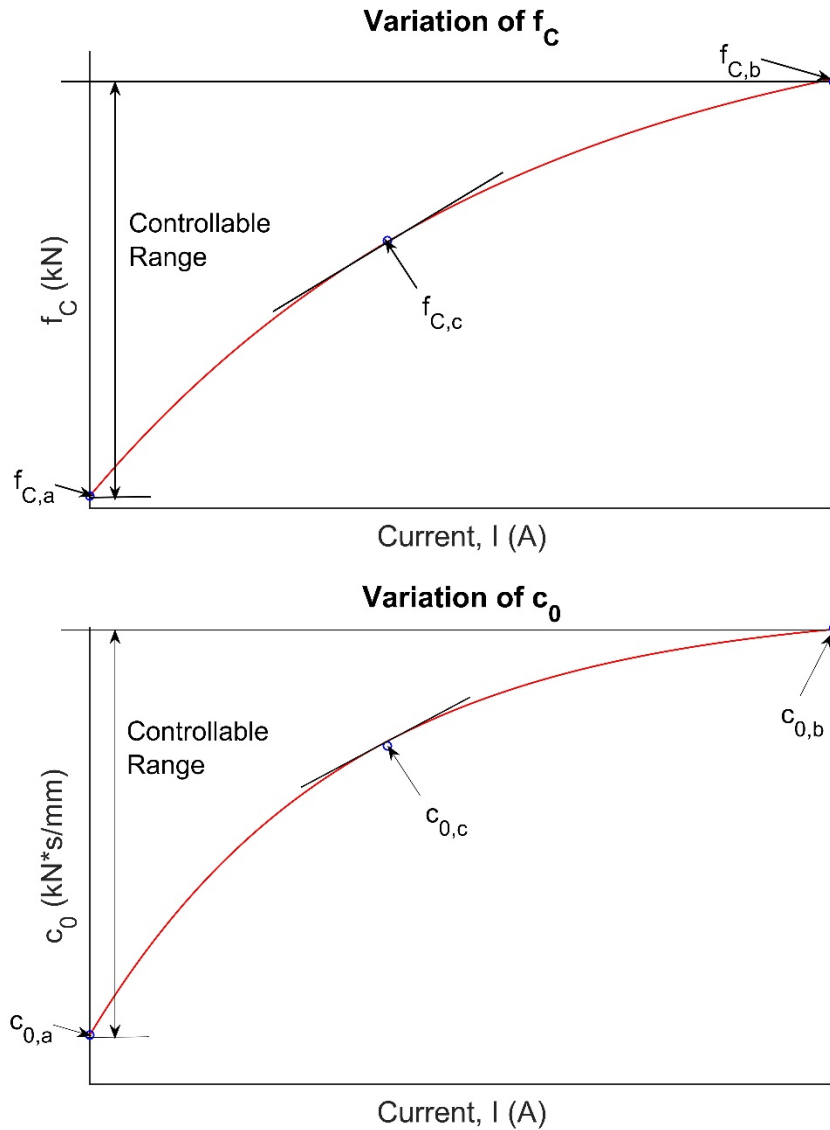


Fig. 4.5: Variation of Bingham Plastic Parameters

Due to the simplicity of the model, we see that there is poor tracking of the force-velocity behavior and it is displayed as an instantaneous shift after crossing zero velocity. However, we see in the experimental data that this is not true due to the effects of nonlinearity in the force-velocity response and the region near zero velocity where the acceleration and the velocity have opposite signs (Spencer et al., 1997). As such, the model is modified using a transition function to introduce some of that behavior within the Bingham Plastic model. This can be seen in Fig. 4.6 below.

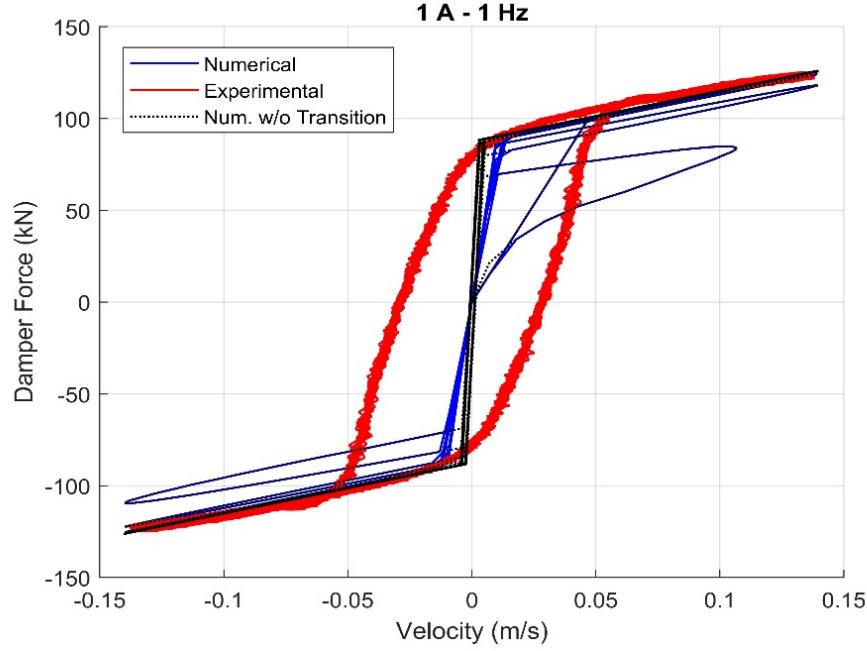


Fig. 4.6: Effect of Transition Function on Bingham Plastic Model

The transition function (TF) is dependent on the velocity. The Bingham plastic model output force is multiplied by TF to get the final output force.. The equation is as follows with $\dot{x}_{TF} = 10$ mm/s:

$$TF = \begin{cases} \frac{|\dot{x}|}{\dot{x}_{TF}} & \text{if } |\dot{x}| \leq \dot{x}_{TF} \\ 1 & \text{if } |\dot{x}| > \dot{x}_{TF} \end{cases} \quad (Eq. 4.4)$$

This damper model will be used for all numerical simulations throughout the paper. In the next chapter, the numerical model will be combined with a generalized idle time model to include the idle time settling effects on long-term performance of the MR damper. This will allow for the study of the consequences and risk of long-term performance degradation in structural control systems. The next section discusses the creation of a generalized idle time model.

Additionally, to properly model the physical substructure within the numerical simulation, a time delay in the current must be modeled. This is due to the time delay

created when sending the command signal to the damper, and the dampers rise time to respond to the command, both of which are almost simultaneous in the numerical simulation (Jiang et al., 2010; Jiang & Christenson, 2012; Phillips & Spencer, 2012). This delay which replicates the current dynamics, is modeled through the use of transfer functions and is shown in Eq. 4.5.

$$H(s) = \frac{y(s)}{u(s)} = \frac{1}{0.7s + 1} + \frac{1}{0.03s + 1} \quad (\text{Eq. 4.5})$$

where u = system input, y = system output, and s is the Laplace-domain.

Chapter 5: Idle-Time Behavior of MR Fluids

One major concern with MR fluids, is the potential for the particles to settle out of the fluid. For the Lord Corporation second-generation damper, the carbonyl iron particles have a diameter between 3 and 5 microns and make up between 40% and 45% of the volume of the MR fluid (Jolly, 1998). A higher percentage of iron particles in the fluid can result in a higher on-state force but can also mean a lower off-state force. This is because the number of particles that are homogeneously suspended in the fluid determine the number of particle chains which can form and resist fluid flow. As such, maximum damping strength will be reduced which may lead to severe consequences especially if the structural design does not have other redundancies built in to it. To counteract this, the MR fluids can be stabilized using additives which prevent settlement or by using different carrier fluids (Jolly, 1998; Carlson et. al. 1996; Goncalves, 2005; Premalatha et. al., 2012).

The ability for MR dampers to mitigate earthquake damage may potentially decrease over long periods of time in which the dampers remain idle (Phillips et. al., 2011). Phillips provides an example of this behavior in the same NSEL report using sine wave tests performed after a 6-month idle time settling period. The force in the initial run for these repeated sinusoidal tests at 7.62 mm (0.3 in.) amplitude, 1 Hz frequency, and a constant current of 2.5 A, was around 9.26% of the expected force given those parameters. For the fully mixed case, we see this expected absolute maximum force to be around 139 kN (31.30 kips). This data was analyzed for use in this thesis and can be seen in Fig. 5.5.

In the development of control systems for civil engineering applications, idle time effects are important due to the long design lives of structures and the long return periods of severe earthquakes over that lifetime. Between earthquake events, there is the potential for a significant reduction in performance due to idle time effects. As such, it is critical to research and understand this behavior to appropriately design strategies to mitigate this idle time effect on the force response of MR dampers. This topic has not been fully researched from a civil engineering perspective or with large-scale structural laboratory tests. This thesis hopes to explore idle time effects and their consequences in better detail. Additionally, by gaining further insight into how idle time affects MR damper performance, we can also get a better understanding of the risk involved with long-term degradation of other structural control systems. To best research this in a reasonable time frame, a model MR fluid was used which exhibited accelerated performance degradation. This behavior is reflective of the experimental setup used for this research not the true potential of MR damper technology. I.e., there are methods to extend the settling time of MR fluids, which, properly adapted to civil engineering applications, could mitigate some of the performance loss discussed herein.

5.1 Idle Time Factors Affecting Performance

Three main phenomenon have been identified which can be used to better explore, understand, and model the idle time settling effects. These include the settling of the particles during the idle time, the mixing of the particles when subjected to a dynamic loading, and the resultant participation of the particles in

modifying the controllable shear strength of the MR fluid. The interaction of these three factors can be seen in the below figure:

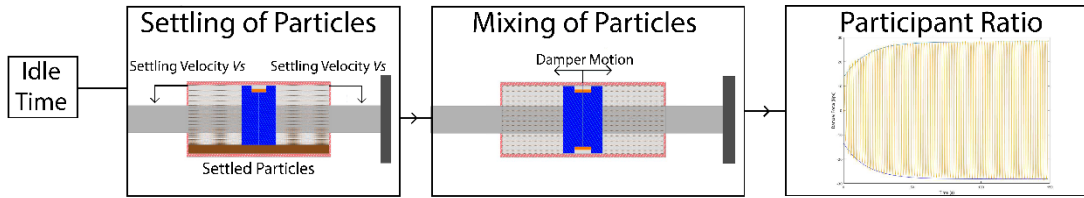


Fig. 5.1: Relationship of the Three Factors Which Create the Participant Ratio

5.1.1 Particle Settlement

The first of these parameters is the settlement of the particles while the damper is inactive due to the difference in particle and carrier fluid densities. The settling and caking of MR particles at the bottom of the damper plays a major role on the rate of force recovery and the maximum force recovered. This effect has been discussed in papers by Ngatu & Wereley (2007), Sugiyama et al. (2013), and Wahid et al. (2016) among others. Ngatu and Wereley (2007) discuss the sedimentation characteristics of MR Fluids and the balance between suspension stability and maximum yield stress through the analysis of multiple MR fluids. The paper by Sugiyama et al. (2013) presents a new design for an MR grease damper which was created to directly counter sedimentation characteristics of the MR fluids. Although it provides an effective alternative to MR fluids available with reduced settling characteristics, an increased viscosity in the operating range of the damper is not desirable. The paper by Wahid et al., goes through an extensive review of the limitations within MR fluids and the improvements that have been made to improve the long-term performance (2016). Regarding settlement, the paper describes studies related to the use of additives to improve the stability of the MR Fluids. Most studies

use idle times of at most a few months to a year, though more often shorter, as it is not often feasible to go beyond that. Instead, the initial settling rate is measured and used as a measure of stability. Additionally, the effects of that settlement on structural control performance for civil applications has not been studied using laboratory or RTHS testing.

When the damper is neither in motion nor subject to an active current, the particles are unable to be mixed by the piston or held in situ by the magnetic field. Hence, the problem is simplified to the settling of solid particles in a viscous fluid media. The carbonyl iron MR particles have a higher density than the carrier fluid they are surrounded in and, even with additives to prevent settling, can eventually aggregate at the bottom and be difficult to disperse back into the fluid (Premalatha et. al., 2012). Due to this settling, the particles can no longer be magnetized. This settling behavior can be described through the use of Stokes' Law with the fluid in the laminar regime $Re_p < 0.3$ (Atiemo-Obeng, 2004):

$$V_t = \frac{g_c d_p^2 (\rho_s - \rho_l)}{18\eta} \quad (Eq. 5.1)$$

where V_t is the settling velocity, g_c is acceleration due to gravity, d_p is the diameter of the particle, ρ_s is the density of the solid particles, ρ_l is the density of the carrier fluid, and η is the viscosity. Additionally, to account for the presence of other particles, the hindered settling velocity applies (Atiemo-Obeng, 2004):

$$V_{ts} = V_t (1 - \chi)^n \quad (Eq. 5.2)$$

where V_{ts} is the hindered settling velocity, V_t is the settling velocity, χ is the volume fraction of the solid particles, and n is a function based on the Reynolds number, 4.65 for $Re_p < 0.3$ (Atiemo-Obeng, 2004). This can be used to approximate the degree of

settling of the particles over the time in which the MR fluid devices remain idle. Depending on the degree of settling, the particles may or may not be able to fully return to a completely homogeneous suspension in the event of a sudden natural disaster. Due to this, the actual damper force may not properly track the desired damping force, hence not achieving the design dynamic range of the control system.

5.1.2 Mixing Behavior & Participant Ratio

Once the MR damper begins moving, we see that over time the particles are mixed back into a uniform suspension. This phenomenon occurs in varying time periods depending on the severity of the initial settlement. Solid-liquid phase interactions are explored in a number of papers but tend to be related to industrial mixing applications. For the MR damper, the mixing occurs through the motion of the piston shaft in an axial direction unlike most industrial processes which use radial or axial impellers (Nienow 1985; McKee et al. 1995; Atiemo-Obeng, 2004; Guazzelli, É. 2006; Ein-Mozaffari, F. & Upreti, S. R. 2010;).

One way to determine the effects that settlement will have on the damping force is to look at the participant ratio of the magnetizable particles. As per the paper by Peng et al. (2013), depending on the degree of settlement, the maximum participant ratio will vary, and hence, so will the maximum shear strength. This simulation was done using a large-scale atomic/molecular massive parallel simulator to best simulate the particle motions and interactions. Four cases were analyzed where Case 1 refers to a completely suspended fluid, Case 2 refers to 30% settlement, Case 3 refers to 70% settlement, and Case 4 refers to a completely settled fluid. The dynamic yield strength of the fluid is calculated at a shear rate of 1000 sec^{-1} .

According to Peng et al. (2013), for fluids with a larger portion of settled particles, the participation ratio is lower which leads to a reduction in the maximum shear stress exhibited. The resultant forces were 100%, 85%, 65%, and 35% of the expected for each of the four cases respectively (Peng et al. 2013). Although, the concept of participation ratio was used when envisioning the idle time model for this thesis, the resultant effects of the percent of settled particles on the force response of the damper and the numerical model did not follow the paper's estimates.

In the case of dynamic loading, this weakened strength can lead to severe consequences. Fig. 5.2 shows the expected damping force under a 25.4 mm (1 in.) amplitude and 0.5 Hz frequency sinusoidal wave displacement with a constant current of 2.5 A. The expected damping force for an applied sinusoidal displacement with a constant current (and hence magnetic field) should provide a constant force amplitude, which for this case was observed to be around 178 kN (40 kips).

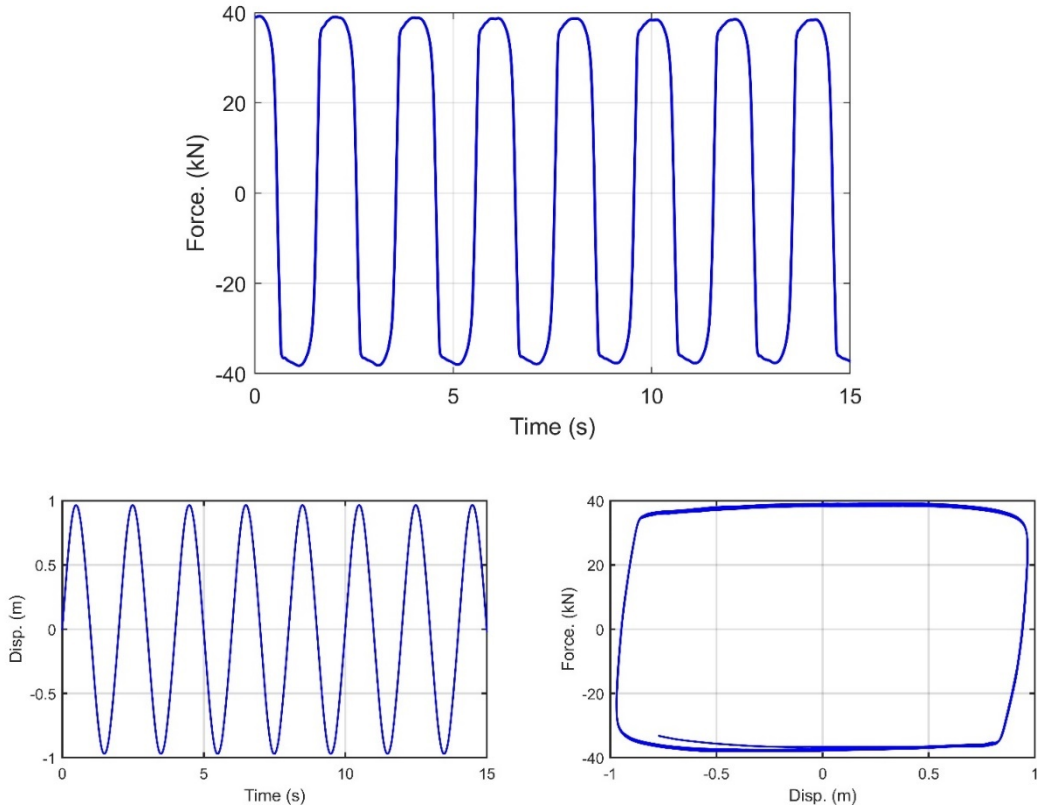


Fig. 5.2: Sine Wave (1 inch, 0.5 Hz, & 2.5 A) Test Data – Fully Mixed

5.2 Idle-Time Sine Wave Testing Results

To better understand the idle time behavior for the MR damper of interest, a series of characterization tests were completed over different periods of idle time.

These tests had the following parameters with a constant supplied current of 2.5 A.

Table 5.1: Idle Time Sine Wave Test Parameters

	Case 1	Case 2	Case 3
Idle Time Duration	0.25 years	0.5 years	2.5 years
Amplitude	25.4 mm (1 inch)	7.62 mm (0.3 inch)	25.4 mm (1 inch)
Frequency	0.5 Hz	1 Hz	0.5 Hz

Case 1 is the idle time data collected after 3 months of inactivity. The rise time for such a short idle time is extremely quick, only on the order of ~2 seconds and can be seen in Fig. 5.3 (a).

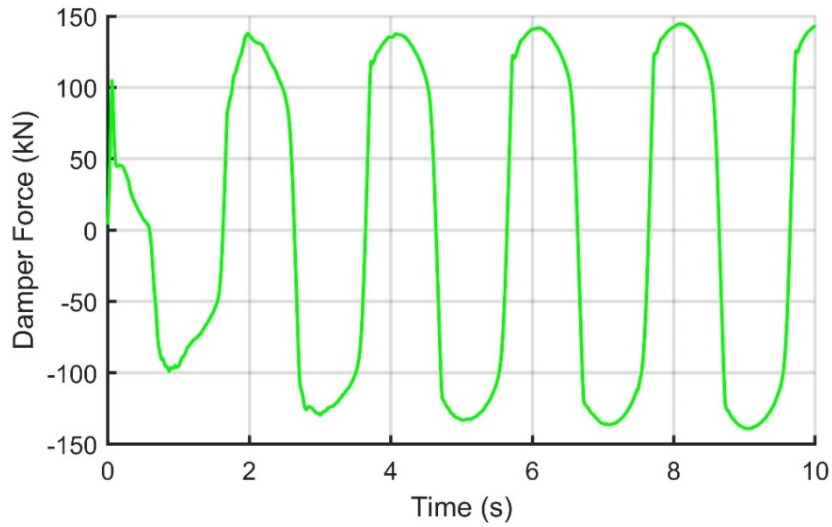


Fig. 5.3 (a): Force-Time Plot for 0 – 10 Seconds of 3 Month Idle Time Data

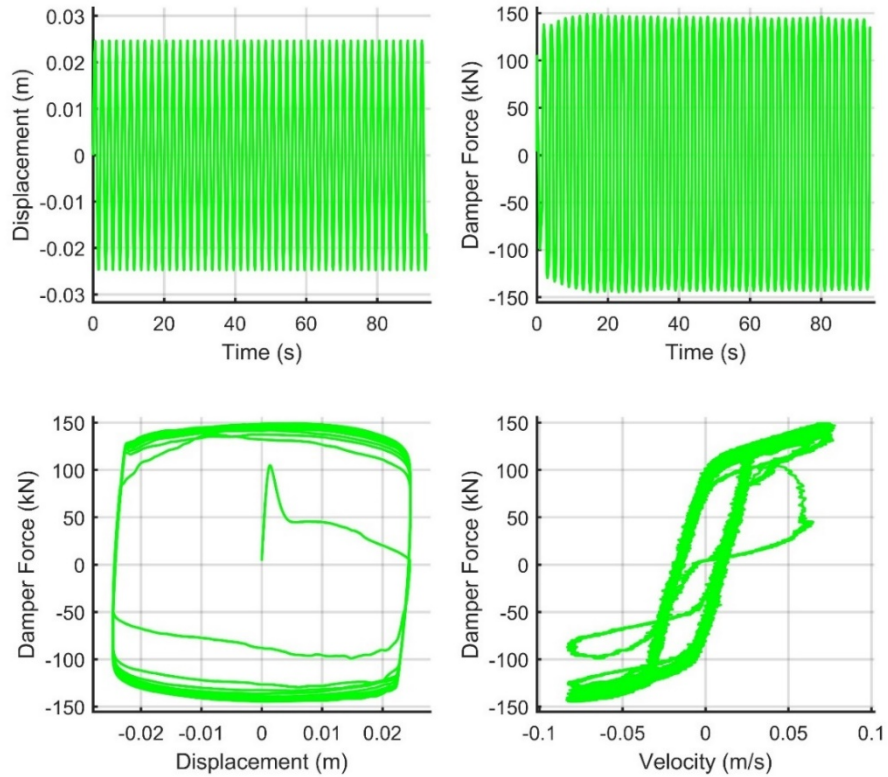


Fig. 5.3 (b): 3 Month Idle Time Sinusoidal Test Data – UMD Structures Lab

Case 2 was the idle time data collected by Dr. Phillips and published in his NSEL report (Phillips et. al., 2011) as shown in Fig. 5.4 and 5.5. This test was performed after the damper had been idle for 6 months. Rather than collecting the

data until the maximum force response stabilized, this data was collected through 5 separate runs using the same 0.3 inch amplitude, 1 Hz frequency sine wave displacement input. As such, the 5 sets of data were stitched into a single set of data to better observe the behavior and use for analysis. These results can be seen in Fig. 5.4. Using this data, a combined plot was generated which showed the total recovery through mixing over the 5 runs. This can be seen in Fig. 5.4 and Fig. 5.5.

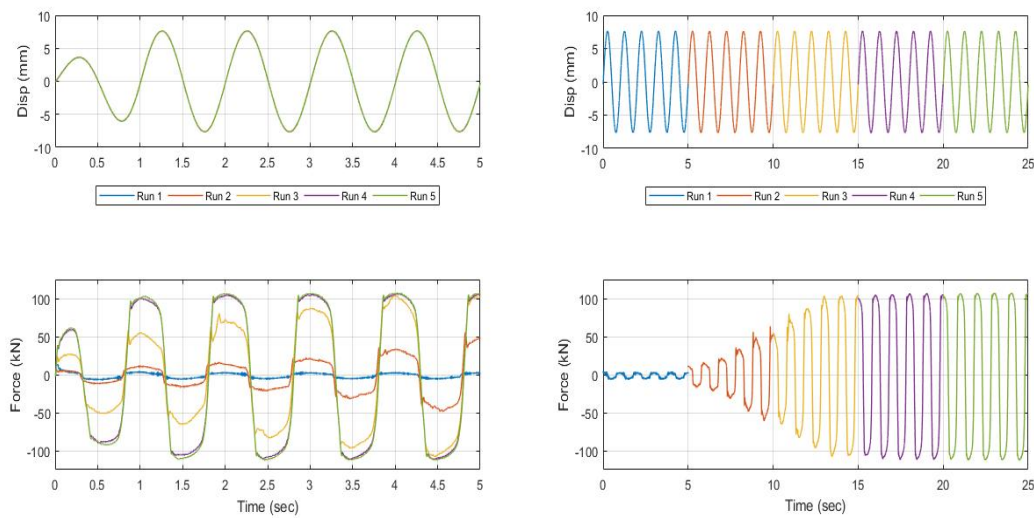


Fig. 5.4: 6 Month Idle Time Sinusoidal Test Data (Left) Stitched (Right)

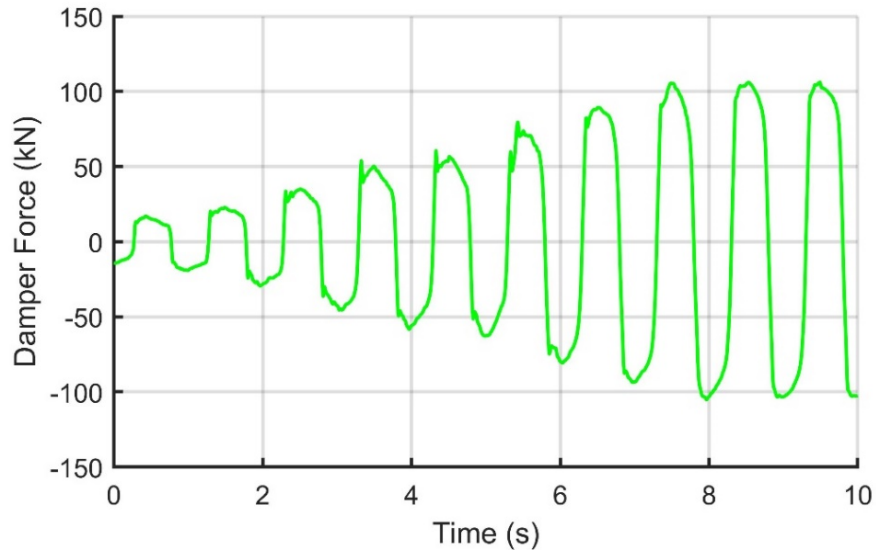


Fig. 5.5 (a): Force-Time Plot for 0 – 10 Seconds of 6 Month Idle Time Data

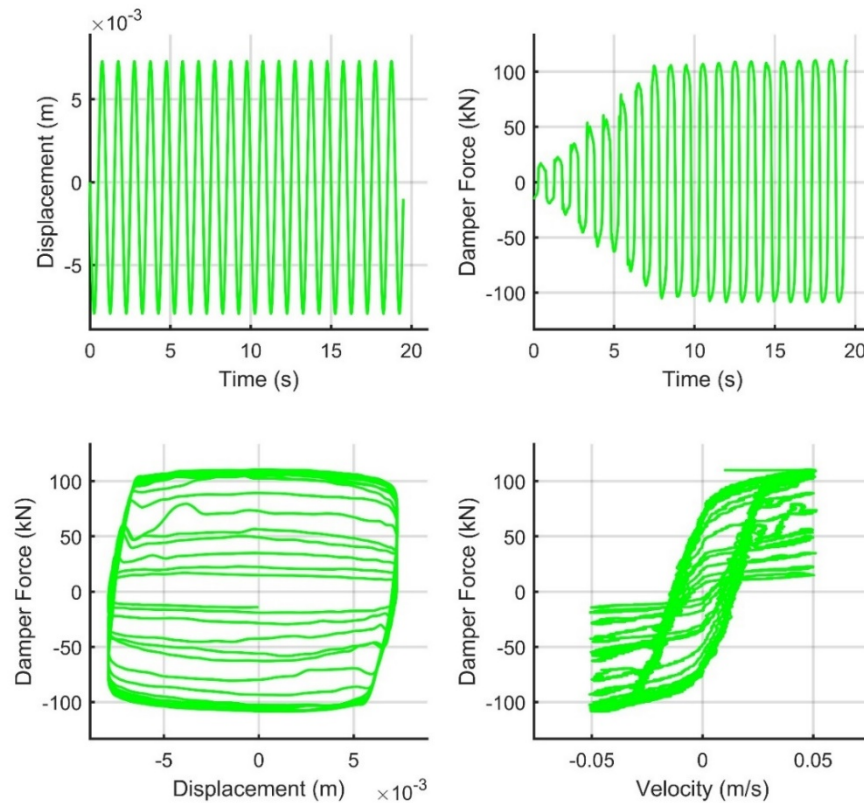


Fig. 5.5 (b): 6 Month Idle Time Sinusoidal Test Data

Case 3 was conducted after the damper had been sitting idle for approximately 2.5 years before being set up at UMD. This is a lower-bound estimate, given our records. The measured damper force begins at roughly 20 kN (4.51 kips) which is approximately 12.26% of the expected value of 163.61 kN (36.78 kips). This is a very severe decrease in the capacity of the MR damper and could lead to excessive deformation and failure of a structure.

This data was collected on August 26th, 2017 and September 6th, 2017 and then stitched together. This stitching was required due to some technical difficulties with the initial setup of the equipment. For the August 26th, 2017 test, the bolts on the angle plate supporting the MR Damper were not sufficiently tightened, leading to backlash as the direction of excitation changed. This can be clearly seen in the

corners of the hysteresis curve in the following figures. The backlash was remedied and the testing continued a few days later.

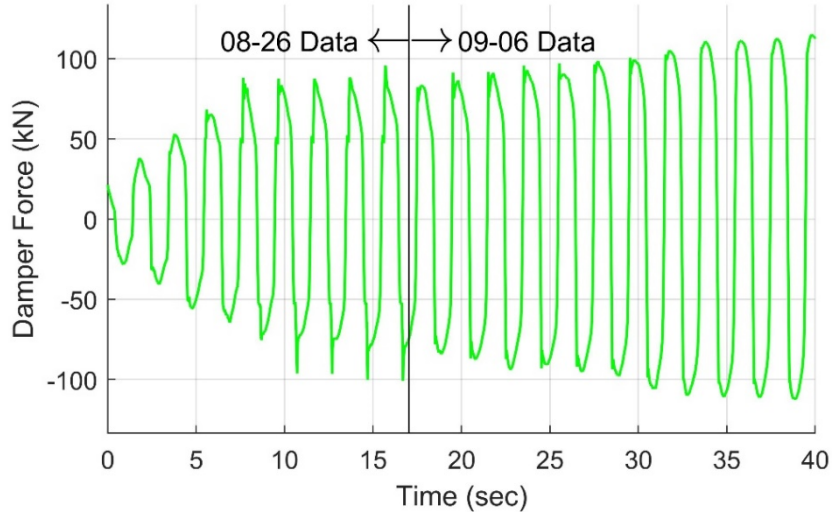


Fig. 5.6 (a): Force-Time Plot for 0 – 40 seconds of 2.5 Year Idle Time Data (Stitched)

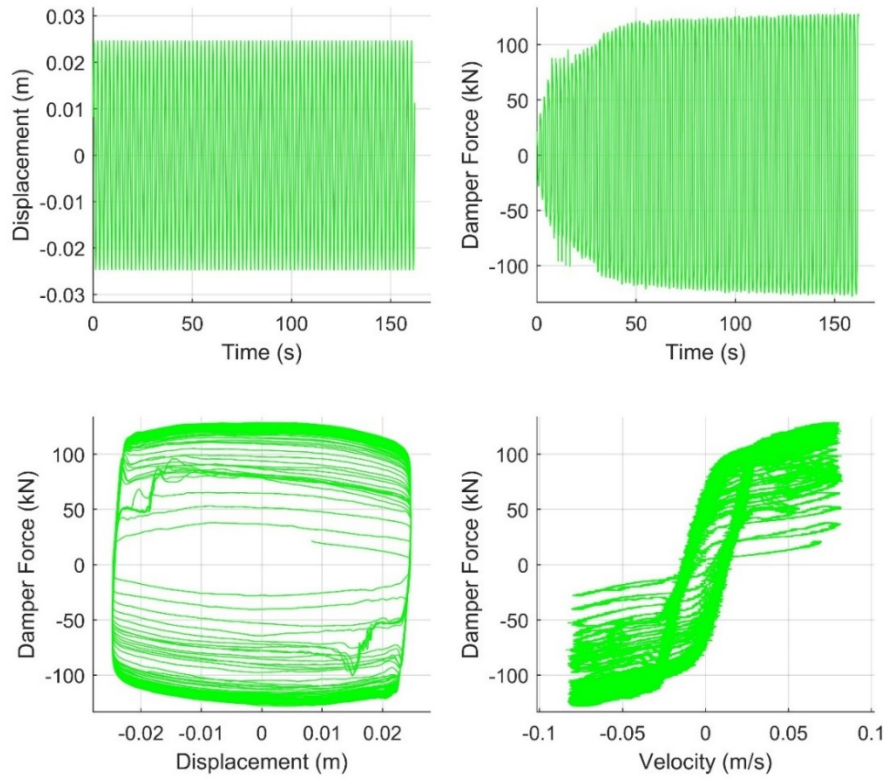


Fig. 5.6 (b): 2.5 Year Idle Time Sinusoidal Test Data – UMD Structures Lab

When compared to the 3 month idle time sine wave test data, we see a very slow rise time, a lower initial force, and a reduced capacity for the final maximum force. This will lead to a drastic reduction in ability for the damper to respond within the first few seconds, which is the same period over which most earthquakes exhibit the largest magnitude of excitation. Furthermore, if the mixing due to ground motion excitation is not sufficient, it is not possible to fully recover the force. I.e., it is hypothesized that mixing over a short displacement range does not fully mix the entire damper. The recovery of the absolute maximum achievable force is only realized after cycling the damper at much higher displacement amplitudes. The summary table below shows the key values for each of the different data sets.

Table 5.2 (a): Idle Time Sine Wave Test Data Summary Table (S.I. Units)

Results	Case 1			Case 2			Case 3		
	0.25 year	25.4 mm	0.5 Hz	0.5 year	7.62 mm	1.0 Hz	2.5 year	25.4 mm	0.5 Hz
Fully Mixed Force (kN)	163.61			139.23			163.61		
Max Experimental Force (kN)	143.46			106.98			127.84		
% of Fully Mixed Force	87.68			76.84			78.14		
Initial Experimental Force (kN)	45.28			12.89			20.06		
% of Fully Mixed Force	27.68			9.256			12.26		
Calc. 90% of Experimental Force (kN)	129.11			96.28			115.06		
90% of Experimental Force (kN)	129.31			96.30			115.08		
Rise time to 90% of Exp. Force (secs)	1.918			12.46			25.97		
Calc. 95% of Experimental Force (kN)	136.28			101.63			121.45		
95% of Experimental Force (kN)	136.34			101.60			121.30		
Rise time to 95% of Exp. Force (secs)	1.956			12.97			36.02		

Table 5.2 (b): Idle Time Sine Wave Test Data Summary Table (U.S. Units)

Results	Case 1			Case 2			Case 3		
	0.25 year	1 in.	0.5 Hz	0.5 year	0.3 in.	1 Hz	2.5 year	1 in.	0.5 Hz
Fully Mixed Force (kip)	36.78			31.30			36.78		
Max Experimental Force (kip)	32.25			24.05			28.74		
% of Fully Mixed Force	87.68			76.84			78.14		
Initial Experimental Force (kip)	10.18			2.897			4.509		
% of Fully Mixed Force	27.68			9.256			12.26		
Calc. 90% of Experimental Force (kips)	29.03			21.65			25.87		
90% of Experimental Force (kips)	29.07			21.65			25.87		
Rise time to 90% of Exp. Force (secs)	1.918			12.46			25.97		
Calc. 95% of Experimental Force (kips)	30.64			22.85			27.30		
95% of Experimental Force (kips)	30.65			22.84			27.27		
Rise time to 95% of Exp. Force (secs)	1.956			12.97			36.02		

5.3 Generalized Idle Time Model

To better understand the consequence of idle time behavior, an empirical MR damper model was created that includes both current-dependent behavior and idle time effects. The model is based on the Bingham plastic model that was introduced in Chapter 4. The model is dependent on the initial idle time settling effects and the mixing effects due to the velocity of the damper. Through the mixing of the MR fluid, more particles will be suspended throughout (and beyond) the region that the damper moves through. Once the fluid is fully mixed and all particles are fully suspended, we will see the intended behavior of the device.

The displacement range that the damper moves through also affects the mixing and including this would improve the accuracy in the model. However, for the purposes of this study, the generalized idle time model does not explicitly consider

the effects of displacement. It was observed that a majority of the force recovery can be empirically attributed to the velocity over the short testing duration (for both sine wave and RTHS testing). The velocity is related to the flow rate of MR fluid from one chamber to the other. A block diagram of the model can be seen in Fig. 5.7 below. Variables that will be elaborated on herein include the idle time IT , settling quotient SQ , participant ratio PR , flow rate Q . In short, the idle time is used to estimate the amount of settled particles, which is converted into a participant ratio. As the MR damper is cycled, this participant ratio increases until the damper is fully mixed.

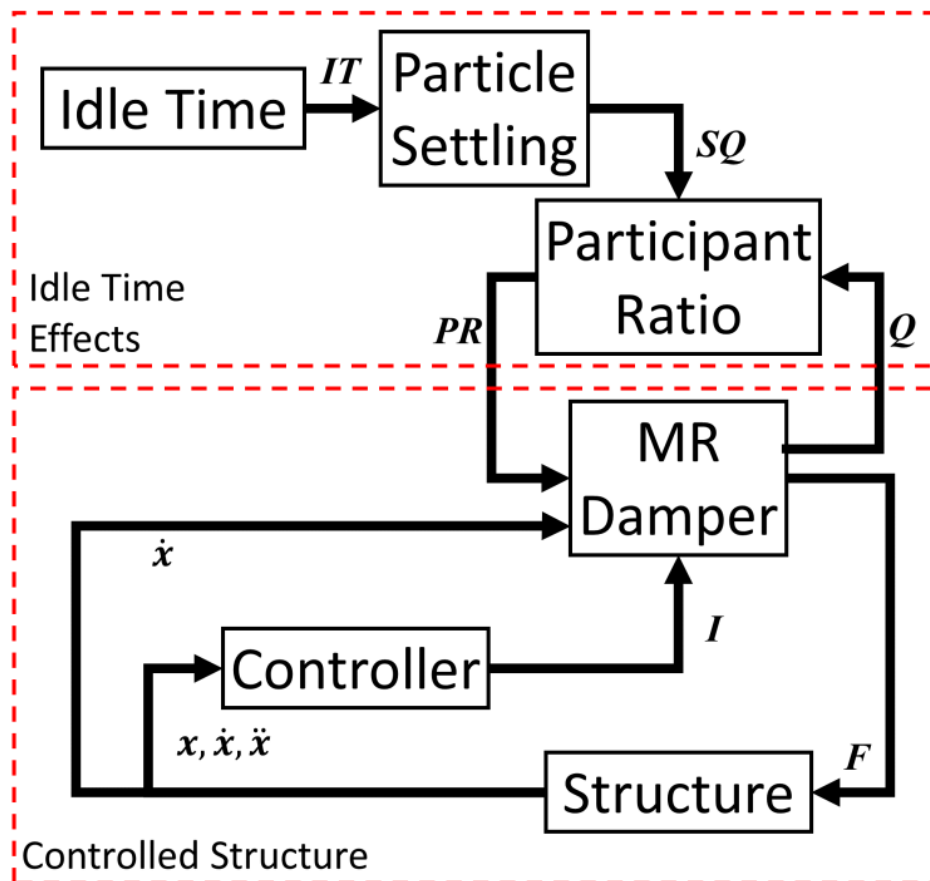


Fig. 5.7: Block Diagram of Generalized Idle Time Model

This model directly affected the Bingham Plastic model's parameters. Models for the particle settling, participant ratio, and the mixing effects were calibrated against the three sets of idle time sinusoidal tests shown in Chapter 4. Additionally, this numerical model was verified using a 3 month idle time RTHS test which will be further discussed in Chapter 6.

As mentioned above, the model is created of three parts. The first is dependent on the idle time of the MR fluid before excitation. This was accomplished through the use of the hindered settling velocity and the idle time *IT* to find the thickness of the settled layer at the bottom of the damper. To determine this, the damper fluid properties are needed. As this information was not readily available for the second-generation Lord Corporation MR damper, an assumption was made regarding the fluid properties using the first-generation Lord Corporation MR damper (Jolly, 1998; Yang, 2001). These MR fluid parameters are based on a Lord Corporation MR Fluid MRX-140ND and shown below.

Table 5.3: Assumed MR Fluid Parameters

MR Fluid Properties	
Density of Fluid (kg/m ³)	3640
Density of Solid (kg/m ³)	7870
Density of Liquid (kg/m ³)	820
Apparent Plastic Viscosity (Pa*s)	2.0
Diameter of Particles (μm)	5
Volume Proportion of Solids	40%

The density of MR fluids are typically between 3 – 4 g/cm³ (Yang, 2001). This model fluid is based on the assumption of a 40% volume fraction of 5-micron carbonyl iron particles suspended within a hydrocarbon oil carrier fluid. This carrier fluid is assumed to have a density between mineral oil CAS 8042-47-5 (Sigma-

Aldrich, 2018) and Polyalphaolefin Oil Molykote ® L – 1268 Synthetic Compressor Oil (RSC, 2014; Engineering360, 2018). Additionally, the apparent plastic viscosity is chosen to be 2.0 based on papers by Jolly (1998), Yang (2001), Seval Genç (2002), and Goncalves (2005).

To determine the idle time settling effects, first the maximum height of the settled solids needed to be determined. This was done by using the equation for the volume of a partially filled cylinder with the assumed 40% volume proportion of solid particles already in a settled state. This equation from Weisstein (2018) is given below:

$$V(L, R, h) = L \left[R^2 \cos^{-1} \left(\frac{R-h}{R} \right) - (R-h)\sqrt{2Rh - h^2} \right] \quad (Eq. 5.3)$$

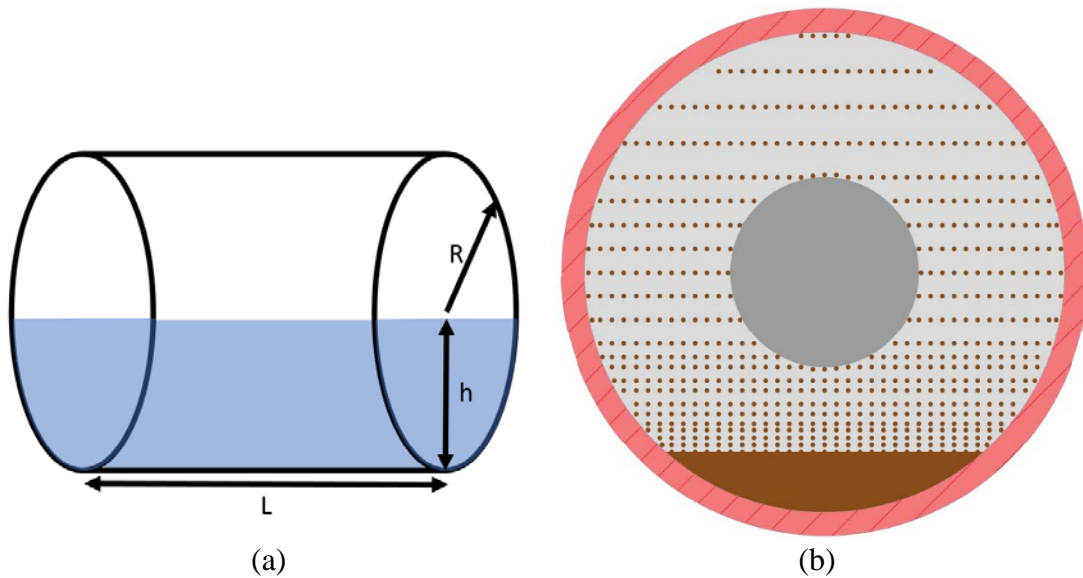


Fig. 5.8: (a) Horizontal Cylindrical Segment Volume Calculation, (b) Example of Settling Particles Visualized as Layers Sinking

To determine the volume of the MR fluid particles, the total volume of MR fluid within the second-generation Lord Corporation damper was first calculated. Two methods were used to determine the total volume of the MR fluid in the damper. The first used the excess stroke length and the knowledge that the inner diameter was the same, to determine the extra volume within the damper. This was then added to the 5 L volume within the first-generation MR damper (Jolly 1998) to approximate the total volume of MR fluid within the second-generation damper. The second method was to use the damper measurements and assumptions based on the first-generation damper to calculate the total volume. These can be seen in the tables below.

Table 5.4 (a): Calculation of Total MR Fluid Volume in Large-Scale 200 kN Damper

Method 1: Adding Extra Volume Due to Longer Stroke		
Extra length	0.4242	Difference between 1st & 2nd Gen
Extra Volume	0.01162	Using Extra Stroke Length
Total Volume (m ³)	0.01662	Extra Volume + 1st Gen Volume
Approximate total volume (m ³)	0.01660	Rounded to 3 significant figures
Vol of Particles in MR Fluid (m ³)	0.00665	Using 40% Volume Proportion

Table 5.4 (b): Calculation of Total MR Fluid Volume in Large-Scale 200 kN Damper

Method 2: Calculation Using Assumed Dimensions		
Inner Area (m ²)	0.0324	Based on Inner Diameter
Piston Area (m ²)	0.0312	Based on ID - Gap Thickness
Shaft Area (m ²)	0.00503	Based on Shaft Radius
Stroke (m)	0.584	
t (m)	0.0127	Assumed Piston Thickness
P _t (m)	0.191	Piston Width
inside L (m)	0.775	Stroke - P _t
V _{ID}	0.0189	Excluding piston width
V _{shaft}	0.00293	Excluding piston width
V _{gap}	0.000241	Over piston width
Total V	0.0163	= V _{ID} - V _{shaft} + V _{gap}

From these two methods, the first method had less uncertainty due to the lack of the need for internal dimensions of the damper, and as such was used when determining the maximum height of the settled particle layer as per Table 5.5. The maximum height was then used along with the hindered settling velocity to determine the time taken for the particles to fully settle out of the suspension. Finally, this was used along with the idle time to determine the percentage of particles settled henceforth termed settling quotient SQ . This was done as per the following formulas:

$$Settling\ Time_{Max} = \frac{Inner\ Diameter - Max\ Height\ of\ Settled\ Particle\ Layer}{Hindered\ Settling\ Velocity} \quad (Eq. 5.4)$$

$$Initial\ \% Settled\ Particles = SQ = \left(\frac{Idle\ Time}{Settling\ Time_{Max}} \right) * 100 \quad (Eq. 5.5)$$

Table 5.5: Calculation of Maximum Height of Settled Particle Layer

Maximum Height of Settled Particle Layer	
Approx. total solid height (m)	0.0858
Max Height of settled solids (m)	0.0831
Height to bottom of shaft (m)	0.0616
Height of solid around shaft (m)	0.0215
Calculated Volume (m ³)	0.00665
Optimization (V - V _{calc} = 0)	-3.82E-10

These equations provide the initial SQ before mixing begins. The initial condition, as described by SQ directly affects the initial participant ratio prior to mixing, final participant ratio after mixing, and rate at which mixing affects participant ratio. These parameters are described by the empirical relationship with SQ given below.

$$a_{PR} = PR_{initial}(SQ) = b_{initial} + (a_{initial} - b_{initial}) * \exp(-c_{initial} * SQ) \quad (Eq. 5.6)$$

$$b_{PR} = PR_{final}(SQ) = b_{final} + (a_{final} - b_{final}) * \exp(-c_{final} * SQ) \quad (Eq. 5.7)$$

$$c_{PR} = PR_{rise}(SQ) = b_{rise} + (a_{rise} - b_{rise}) * \exp(-c_{rise} * SQ) \quad (Eq. 5.8)$$

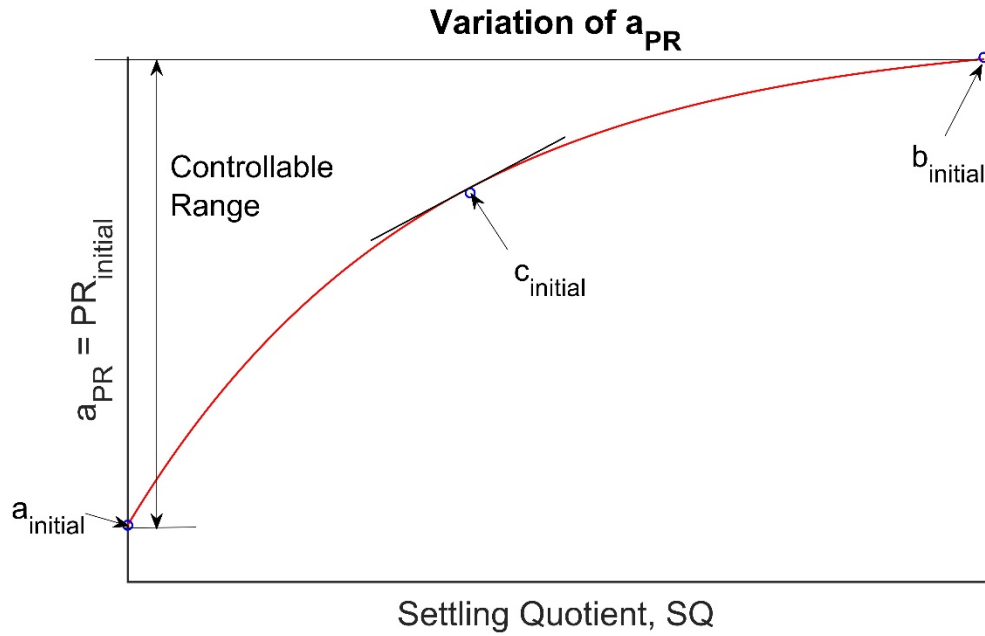


Fig. 5.9 (a): Variation of Participant Ratio Model Parameter, a_{PR}

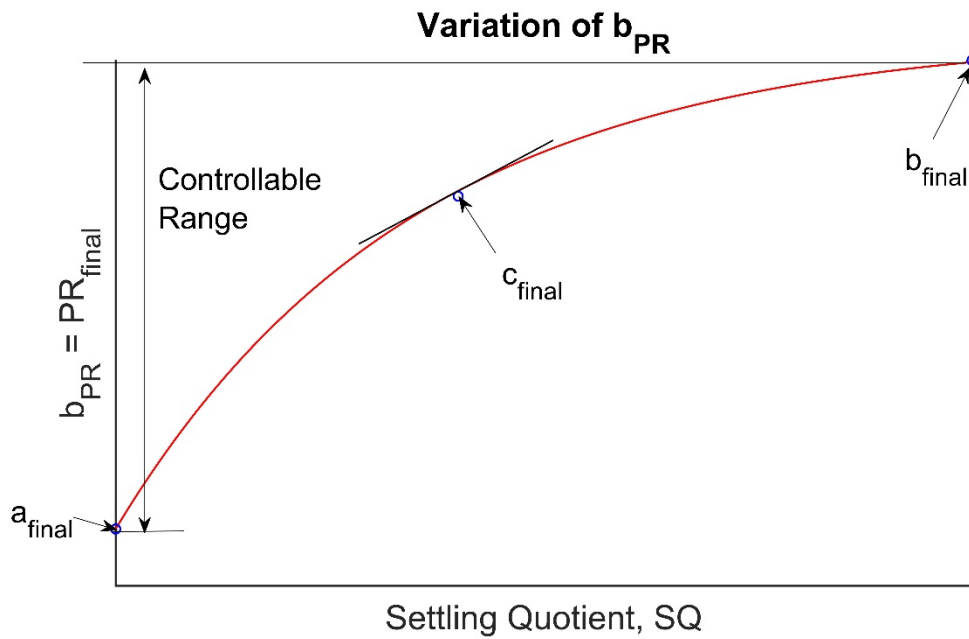


Fig. 5.9 (b): Variation of Participant Ratio Model Parameter, b_{PR}

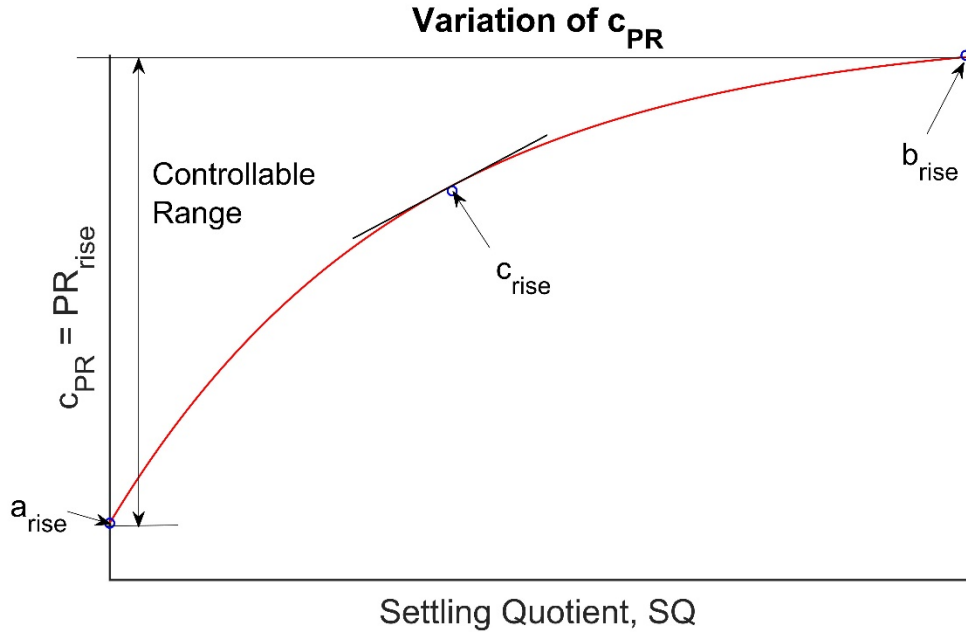


Fig. 5.9 (c): Variation of Participant Ratio Model Parameter, c_{PR}

Table 5.6: Parameters for Participant Ratio Formula

Parameter	Value	Parameter	Value	Parameter	Value
$a_{initial}$	1.0	a_{final}	1.0	a_{rise}	5.474
$b_{initial}$	0.10	b_{final}	0.605	b_{rise}	0.0
$c_{initial}$	7.0	c_{final}	4.5	c_{rise}	3.650

The participant ratio PR is defined as 1 minus the fraction of particles that have settled, similar to the Peng et al. (2013) paper. The variable a_{PR} (Eq. 5.6) provides the lower limit of the PR and is a function of the settling quotient, SQ . a_{PR} is based on the initial percent settled for each of the cases: fully mixed, 3 month idle time, 6 month idle time, and 2.5 year idle time. Similarly, b_{PR} (Eq. 5.7) provides the upper limit of PR . Although this creates a false ceiling based on SQ , as per the observed behavior in the idle time sine wave test data, the force response is not able to reach the fully-mixed state even after long periods of mixing. This is most likely due to the magnitude of the excitation not causing the damper to cycle throughout its stroke length. Considering this behavior, coupled with the relatively short durations

of earthquake excitation, it is predicted that the behavior response will not be able to reach 100% force capabilities and hence the false ceiling does not introduce significant errors in the approximate performance of the damper. Lastly, c_{PR} (Eq. 5.8) provides the rate at which the PR upper limit is achieved under mixing.

The next component is to model the effects of damper motion in mixing the particles back into suspension. This empirical model is based on the volumetric flow rate Q (where $Q = |\text{velocity}| * \text{cross-sectional area}$) and an exponential function which outputs PR .

$$\text{Participant Ratio} = PR(Q) = b_{PR} + (a_{PR} - b_{PR}) * \exp(-c_{PR} * \int Q dt) \quad (\text{Eq. 5.9})$$

This function (Eq. 5.9) uses the parameters determined from equations 5.6-5.8 to create a new exponential function which is dependent on the displaced volume as measured by the integral of the flow rate. This is given the notation $\int Q dt$ and is the integral of the absolute value of the velocity of the damper multiplied by the cross-section of the MR damper. The model for PR includes the diminishing returns of mixing already-mixed fluid through the exponential function.

As can be seen, the parameters for the participant ratio are all functions of the settling quotient SQ (in decimals). This allows the force recovery to be determined according to the time that the device has been idle. The functions for $PR_{initial}$ and PR_{final} are based on and fit to the initial and final participant ratios for the three cases as per Table 5.2.

Through the use of the settling SQ and mixing components Q , the participant ratio PR is determined at each time step in the simulation. PR is then used to modify the damper parameters. PR directly multiplies each of the Bingham damper

parameters with the subscript ‘b’, i.e. $f_{c,b}$ and $c_{0,b}$. This allows PR to directly modify the controllable force in the Bingham Plastic model. The model for $PR(Q)$ was combined with the Bingham Plastic Model as per the Simulink/MATLAB model shown in Fig. 5.11-5.12. The updated equations are also provided below.

$$f_c(I, PR) = PR * f_{c,b} + (f_{c,a} - PR * f_{c,b}) * \exp(-f_{c,c} * I) \quad (Eq. 5.10)$$

$$c_0(I, PR) = PR * c_{0,b} + (c_{0,a} - PR * c_{0,b}) * \exp(-c_{0,c} * I) \quad (Eq. 5.11)$$

$$F = f_c(I, PR) * \text{sgn}(\dot{x}) + c_0(I, PR)\dot{x} \quad (Eq. 5.12)$$

where F = damper force; f_c = Coulomb friction force; \dot{x} = velocity; I = applied current; c_0 = viscous damping coefficient; PR = Participant Ratio determined from Eq. 5.9; and the parameters with subscripts ‘a’, ‘b’, and ‘c’ are the same as presented in Chapter 4.

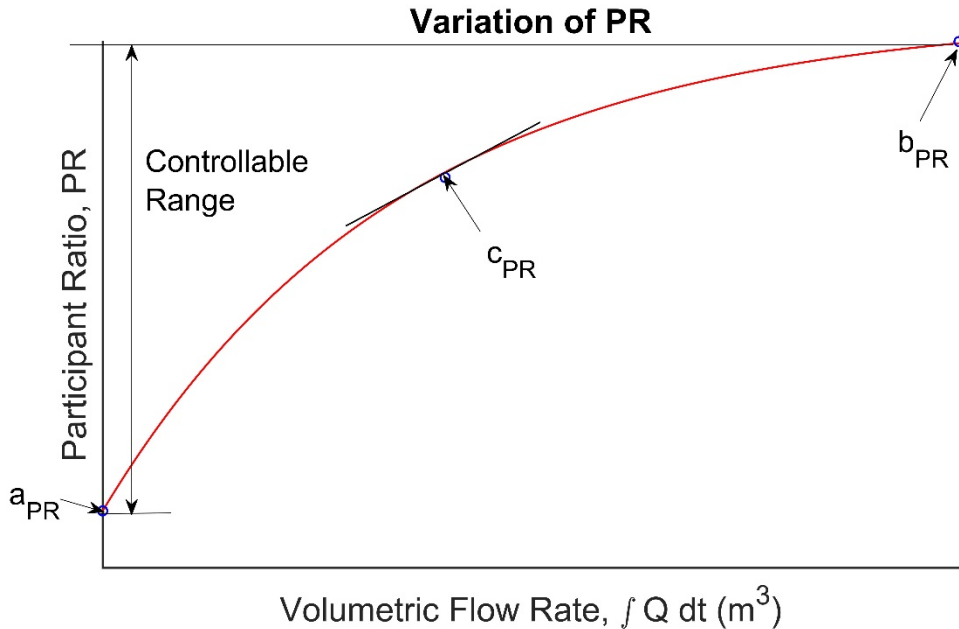


Fig. 5.10: Variation of Participant Ratio Model

Numerical simulations were performed and the results comparing the numerical model against the experimental idle time sine wave tests described above are shown in Fig. 5.13 – 5.15. As can be seen in these figures, the model tracks the performance of the dampers under different idle times well. Model verification through real time hybrid simulation (RTHS) testing is discussed in the next section. Additionally, Chapter 6 will also include the use of this model to run numerical simulations under different idle time durations.

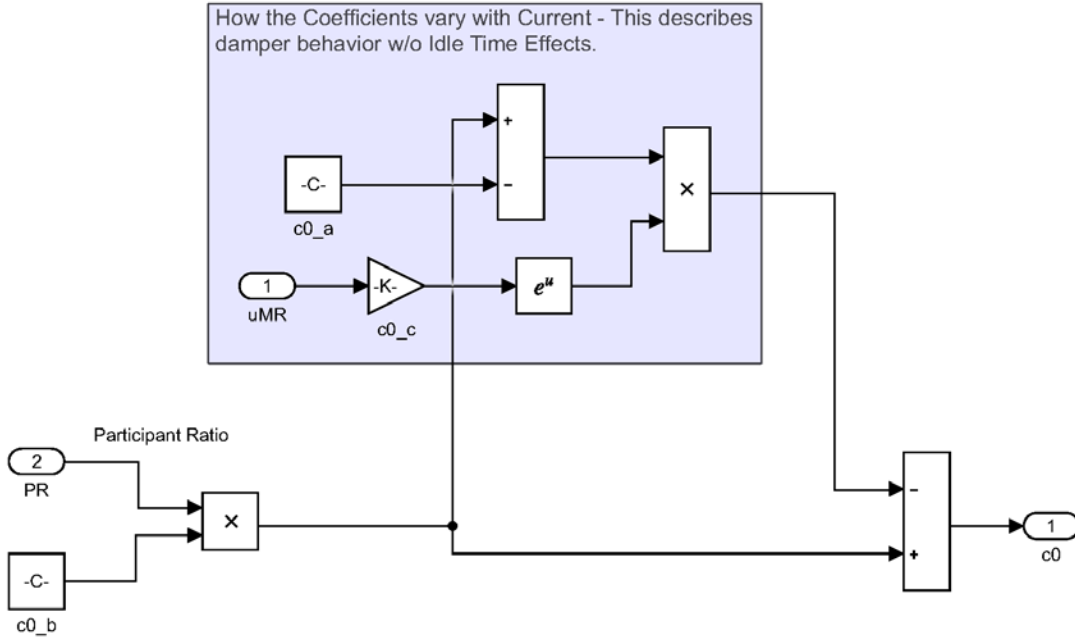


Fig. 5.11: Example of Bingham Plastic Coulomb Friction Component Calculation Including Idle Time Effects

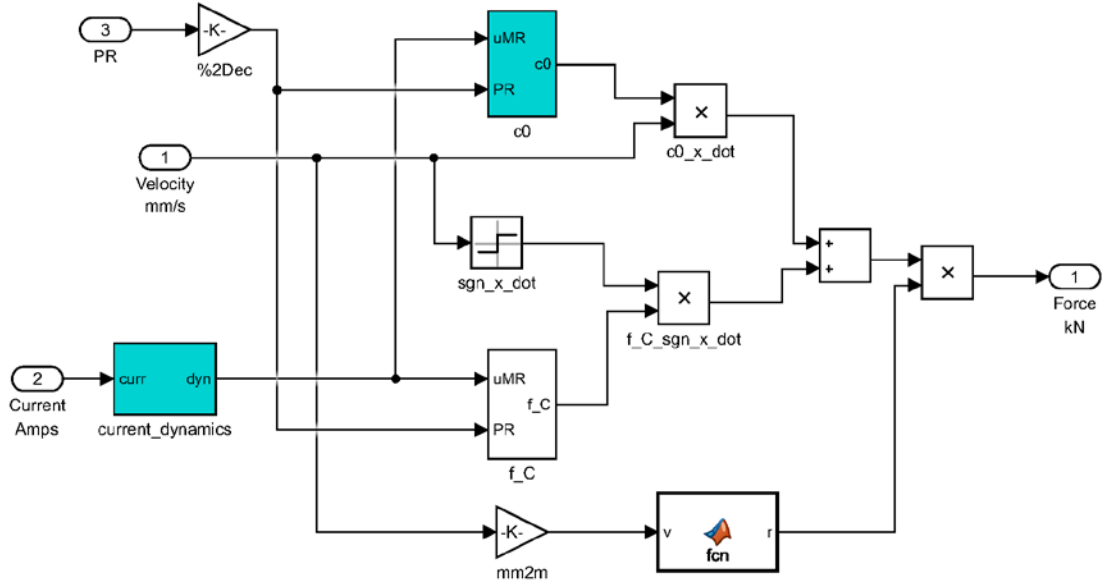


Fig. 5.12: Simulink Model of Bingham Plastic with Idle Time Effects Affecting the Parameters

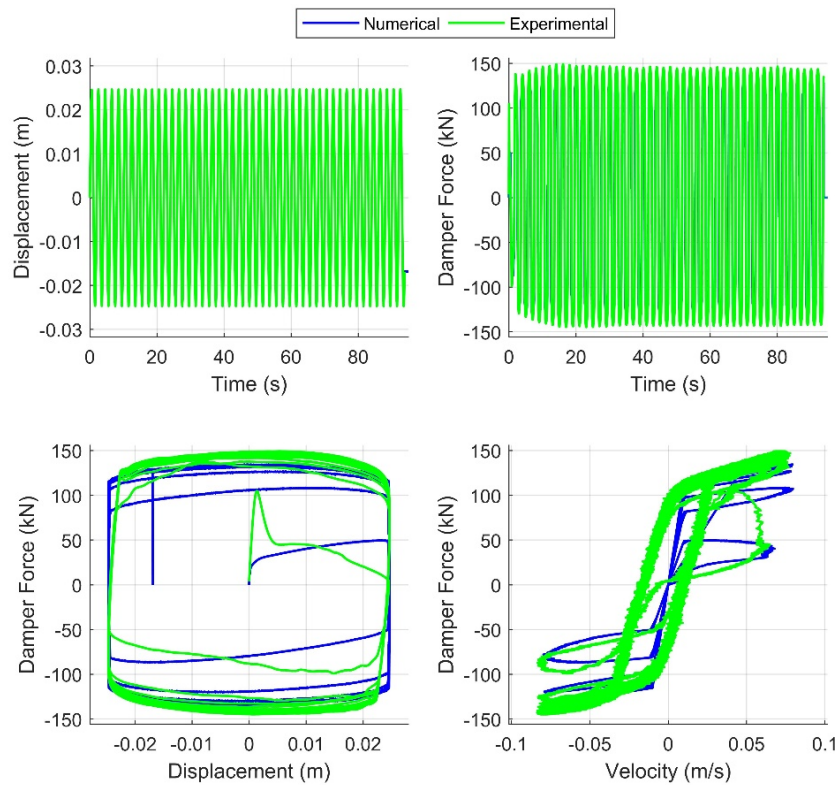


Fig. 5.13: Case 1 – 0.25 Year Idle Time Sine Wave (1 inch, 0.5 Hz, 2.5 A) Displacement

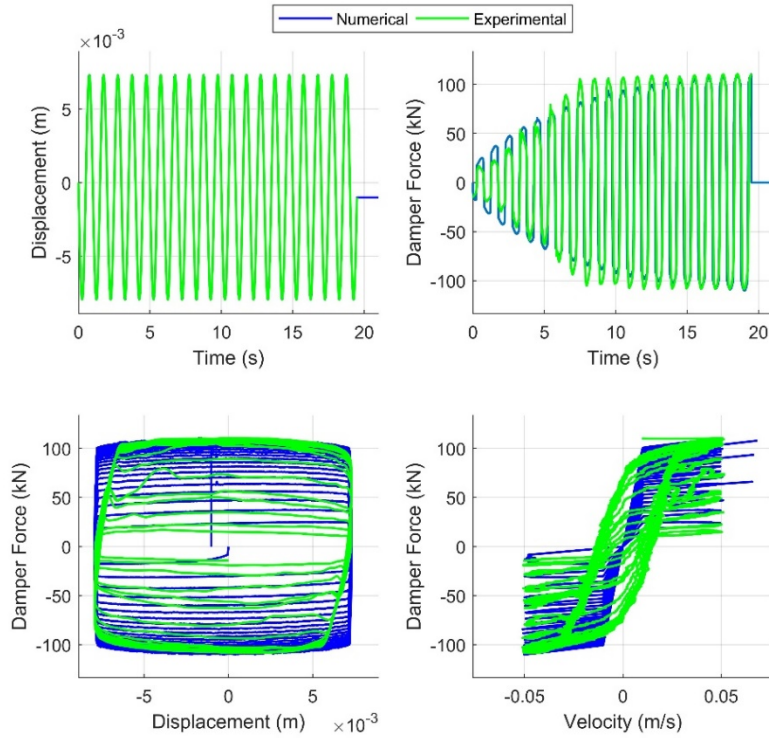


Fig. 5.14: Case 2 – 0.5 Year Idle Time Sine Wave (0.3 inch, 1 Hz, 2.5 A)
Displacement

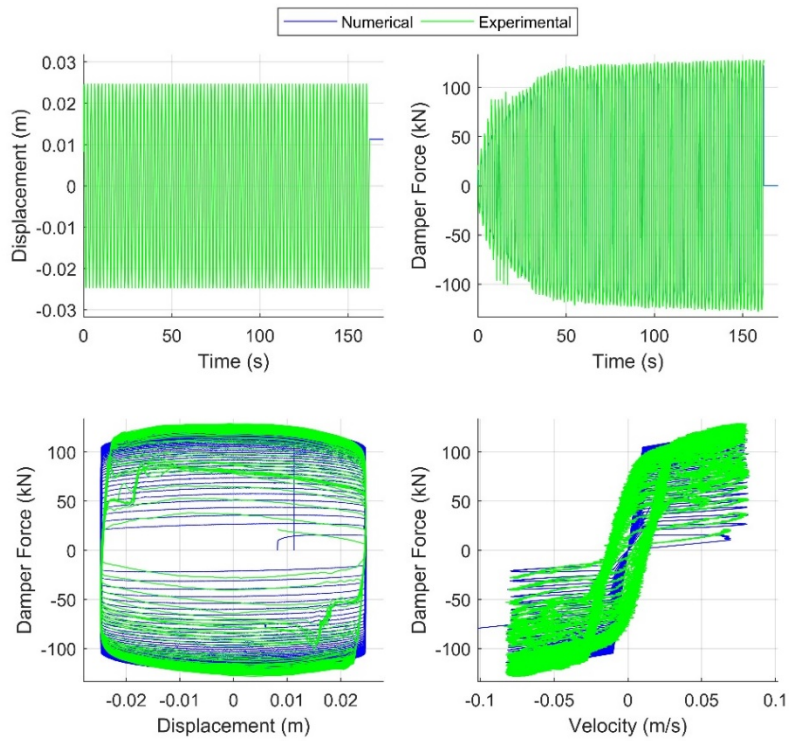


Fig. 5.15: Case 3 – 2.5 Year Idle Time Sine Wave (1 inch, 0.5 Hz, 2.5 A)
Displacement

Chapter 6: Impact of Idle Time on Seismic Performance of Structures

6.1 Structural Model

Once the numerical model was created and calibrated against different sine wave characterization tests, it needed to be validated under realistic operating conditions. The model is verified through the use of a real time hybrid simulation (RTHS). After validation, the model is then used to run additional numerical simulations on the structural response under different idle time settling durations and earthquake ground motions to gain a better understanding of the decrease in performance over variable idle time. Both RTHS and numerical simulations use a 5 story, 6 degree-of-freedom (DOF) base isolated building subject to an earthquake ground motion. An MR damper is installed in the isolation layer, which is either modeled physically for RHTS or numerically for simulations. The structural parameters are shown below in Table 6.1 and were used in the equation of motion $\mathbf{M}\{\ddot{x}\} + \mathbf{C}\{\dot{x}\} + \mathbf{K}\{x\} = -\mathbf{M}\{\ddot{x}_g\}$ to generate the state space matrices used to analyze the structural response shown in Fig 6.2.

Table 6.1: 5-story Base Isolation Structural Parameters

Floor	Floor Mass M (metric ton)	Damping Coefficient C (kN*s/m)	Story Stiffness K (kN/m)
Base	244.8	209.8	3,287
1	212.3	1,044	404,784
2	212.3	904.1	349,116
3	212.3	888.5	343,452
4	212.3	779.4	299,448
5	212.3	592.4	228,708

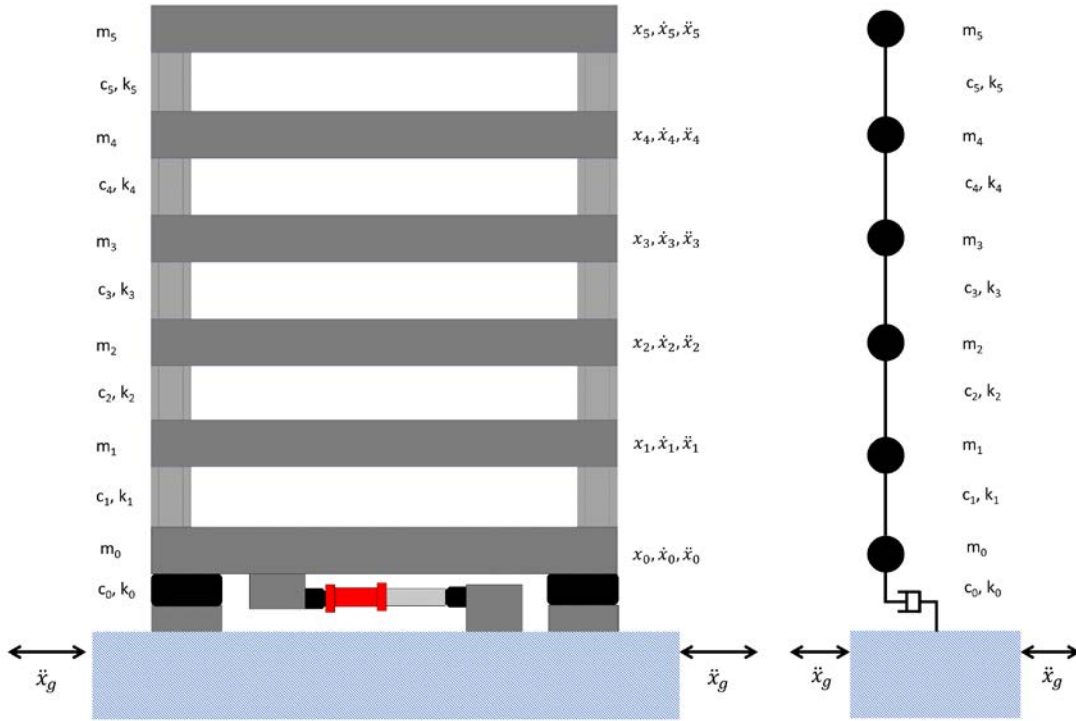


Fig. 6.1: 5-story Base Isolated Building with MR Damper

$$\mathbf{M}(\text{kg}) = \begin{bmatrix} 244800 & 0 & 0 & 0 & 0 & 0 \\ 0 & 212292 & 0 & 0 & 0 & 0 \\ 0 & 0 & 212292 & 0 & 0 & 0 \\ 0 & 0 & 0 & 212292 & 0 & 0 \\ 0 & 0 & 0 & 0 & 212292 & 0 \\ 0 & 0 & 0 & 0 & 0 & 212292 \end{bmatrix}$$

$$\mathbf{K}(\text{kN/m}) = \begin{bmatrix} 408071.3 & -404784 & 0 & 0 & 0 & 0 \\ -404784 & 753900 & -349116 & 0 & 0 & 0 \\ 0 & -349116 & 692568 & -343452 & 0 & 0 \\ 0 & 0 & -343452 & 642900 & -299448 & 0 \\ 0 & 0 & 0 & -299448 & 528156 & -228708 \\ 0 & 0 & 0 & 0 & -228708 & 228708 \end{bmatrix}$$

$$\mathbf{C}(\text{kg/s}) = 1.0\text{e}+06 \times \begin{bmatrix} 1.2542 & -1.0444 & 0 & 0 & 0 & 0 \\ -1.0444 & 1.9486 & -0.9041 & 0 & 0 & 0 \\ 0 & -0.9041 & 1.7927 & -0.8885 & 0 & 0 \\ 0 & 0 & -0.8885 & 1.668 & -0.7794 & 0 \\ 0 & 0 & 0 & -0.7794 & 1.3718 & -0.5924 \\ 0 & 0 & 0 & 0 & -0.5924 & 0.5924 \end{bmatrix}$$

Fig. 6.2: Matrices Used to Represent 6DOF Structure (without MR damper)

The structure has a fundamental natural frequency of 0.25 Hz and without the effects of the MR damper, has a damping ratio of 4.97%, 3.17%, and 5.07% at the first, second, and third modes of vibration which is typical of a steel frame building with a low-damping isolation system. The first 6 mode shapes for the structure along with their natural frequencies are shown in Fig. 6.3 below.

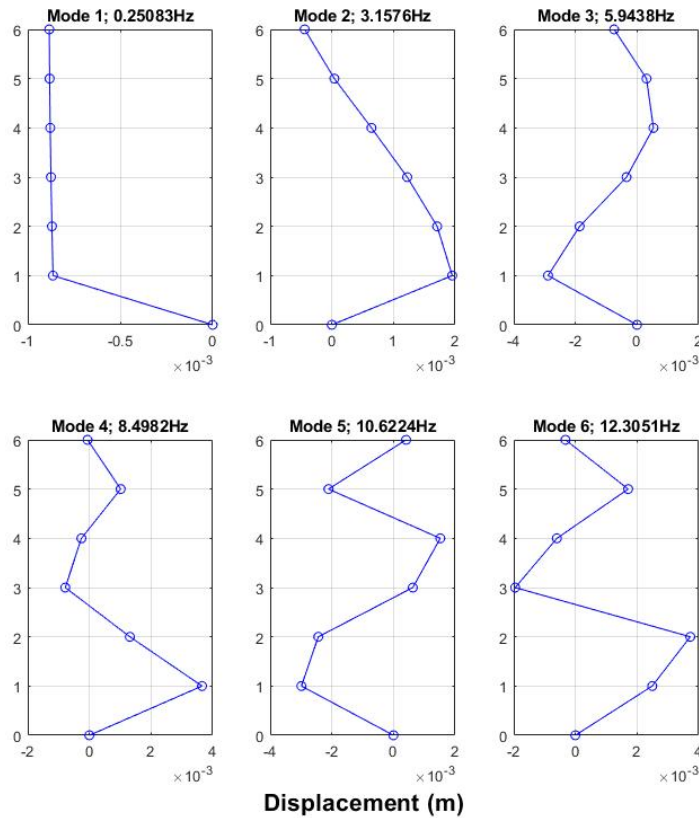


Fig. 6.3: Mode Shapes and Natural Frequencies for 6DOF Lumped Mass Structure

The MR damper (for both simulation and RTHS) is connected to the 6DOF structural model using a loop of action and reaction. All mass is assumed to be in the 6DOF model, so the earthquake ground motion is only applied to the 6DOF model. For numerical simulations, the Bingham plastic MR damper model is given an input of the relative velocity taken from the 6DOF model's isolation layer. The calculated

restoring force is applied to the 6DOF model. For RTHS, the physical MR damper is excited using an actuator to track the displacement of the 6DOF model's isolation layer. The measured restoring force is applied to the 6DOF model. In both cases, the loop of action and reaction continues until the entire ground motion response is evaluated.

6.2 Earthquake Ground Motion Records

For this thesis, the RTHS test was performed using the NS component of the Hachinohe ground motion record during the Tokachi-oki earthquake of May 16, 1968 (Ohtori et. al. 2004). Only one earthquake excitation was considered for RTHS due to the time required for the MR fluid particles to settle before testing. The ground motion records used were the El Centro record of the Imperial Valley earthquake of 1979, the Sylmar County Hospital parking lot record of the Northridge earthquake of 1994, and the Kobe Japanese Meteorological Agency (JMA) record of the Hyogo-ken Nanbu earthquake of 1995 (Ohtori et. al. 2004). The details of the earthquakes are provided in Table 6.2-6.3.

Table 6.2: Earthquake Ground Motion Records Details

Designation	Earthquake	Station	Direction	PGA (m/s ²)
Case a: Hachinohe	Tokachi-oki, 1968	Hachinohe	N-S	2.250
Case b: Northridge	Northridge, 1994	Sylmar	N-S	8.268
Case c: Kobe	Kobe, 1995	JMA, Kobe	N-S	8.178
Case d: El Centro	Imperial Valley, 1940	El Centro	N-S	3.417

6.3 Semi-Active Controller

For the RTHS test and numerical simulations, the causal approximation of rate-independent linear damping created by Keivan (2017) was used as the semi-active controller. This controller works to approximate the ideal rate-independent linear damping force (RILD) by passing the response displacement through an all pass filter transfer function and multiplying by $k*\eta$, where k is the stiffness of the isolation layer and η is a loss factor (Eq. 6.1). This paper (Keivan, 2017) provides the resultant equation as described below in Eq. 6.1.

$$H_{RILD}(\omega) = k\eta \frac{i\omega - \omega_f}{i\omega + \omega_f} \quad (Eq. 6.1)$$

where ω = frequency, ω_f = frequency with exact $\pi/2$ phase advance, i = imaginary number, m = mass, k = stiffness, and η is the loss factor. The η value used within the semi-active controller for this simulation was 0.8, which provided effective reduction of displacement in the isolation layer. This also produced a desired damper force between the passive off and passive on limits such that semi-active control (i.e., variable current) can be used. Ideal RILD should give a $\pi/2$ phase advance over all frequencies. In the casual approximation of Eq. 6.1, the ω_f parameter is selected as the fundamental natural frequency of the structure, as this is the anticipated dominant frequency of vibration.

This desired force was then used as an input to an over-driven, back-driven clipped optimal (ODBDCO) control algorithm. As presented in the NSEL report by Phillips & Spencer (2012), this controller works by supplying a positive or negative current to the MR damper to track the desired force output. First a positive current is applied to generate a force in the damper. Depending on the error between the desired

and measured force, this current can exceed the maximum current (2.5 A) to achieve a quicker rise in the force. If the force produced exceeds the desired force, then a negative current is applied instead to drop the force back down (Phillips & Spencer, 2012). Through this method, the over-driven and back-driven behavior is repeated to track the desired RILD force from the causal approximation equations above (Eq. 6.1 & 6.2).

6.4 Experimental Testing

For RTHS, only the Hachinohe ground motion was studied due long wait time required to develop idle time conditions. The magnitude was scaled to 50% of the original record to accommodate the physical limitations of the testing equipment. This reduced the risk of damage to the testing equipment by keeping the excitation within the allowable velocity limitations of the actuator. For accurate comparison with numerical models, the same earthquake magnitude scaling was applied to numerical simulation comparisons. The structural response data that was collected was not scaled back in any way to represent the 100% earthquake ground motion record, i.e. RTHS and numerical simulation used the reduced earthquake to analyze the numerical structure's response.

For this thesis, one 3 month idle time RTHS test was performed, followed by four subsequent RTHS tests to collect data for partially mixed to fully mixed cases. The repeated tests were run until the results stabilized, i.e., when consecutive tests had the same force and displacement behavior, which occurred at the third test. Additionally, the fourth and fifth tests were performed after the damper underwent a ± 76.2 mm (± 3 in.) 0.2 Hz sine wave displacement to try to fully mix the damper fluid.

As verification that the RTHS proceeded well, the displacement tracking performance of the actuator is observed. This is seen in Fig. 6.4 and shows that the experiment proceeded well. Additionally, the MR damper controller (ODBDCO controller) can also be seen to track the desired force and current well.

In the data collected, it was observed that although the damper was able to match the desired force required by the controller, it was unable to produce that force easily. Unlike in the fully mixed cases, the current required within the first 10 seconds was much higher which can be seen in Fig. 6.6 below. Additionally, the large required current to overcome the diminished performance leads to overshooting of the force. Once the measured force exceeds the desired force, the over-driven back-driven clipped optimal controller (ODBDCOC) turns off the current which causes the force to drop and vice-versa. Although in general, this is how the ODBDCOC controller works, within the first few seconds of the idle time test data, this behavior is slightly exacerbated due to the reduction in the physical ability of the damper to respond to the command current, i.e. the force response has some difficulty tracking the desired force. Even with this difficulty however, the controller is still able to track the force quite well by modifying the current to larger magnitudes. This can be seen in the first ten seconds as per Fig. 6.6. below.

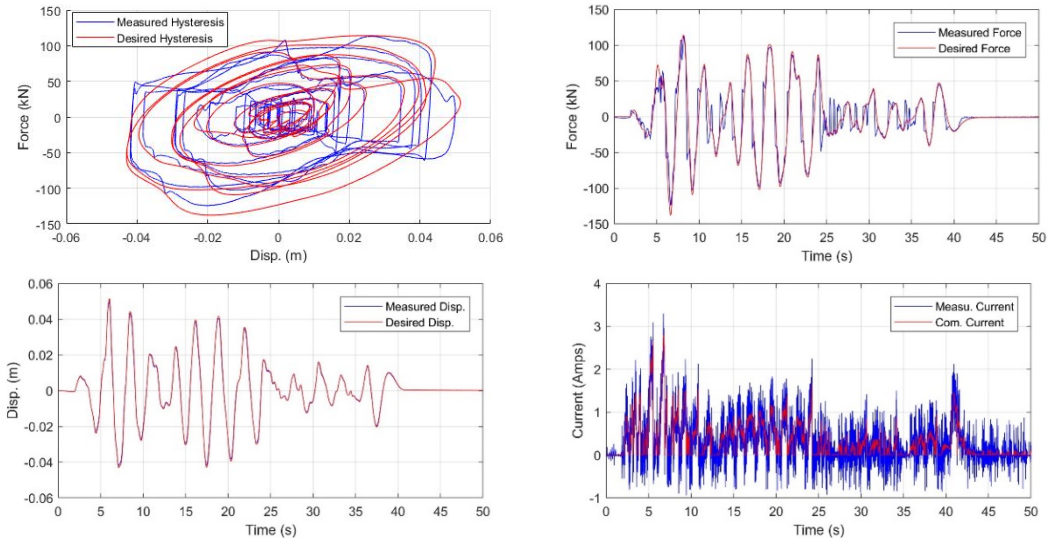


Fig. 6.4: Idle Time RTHS Test 1 Data and Tracking Performance

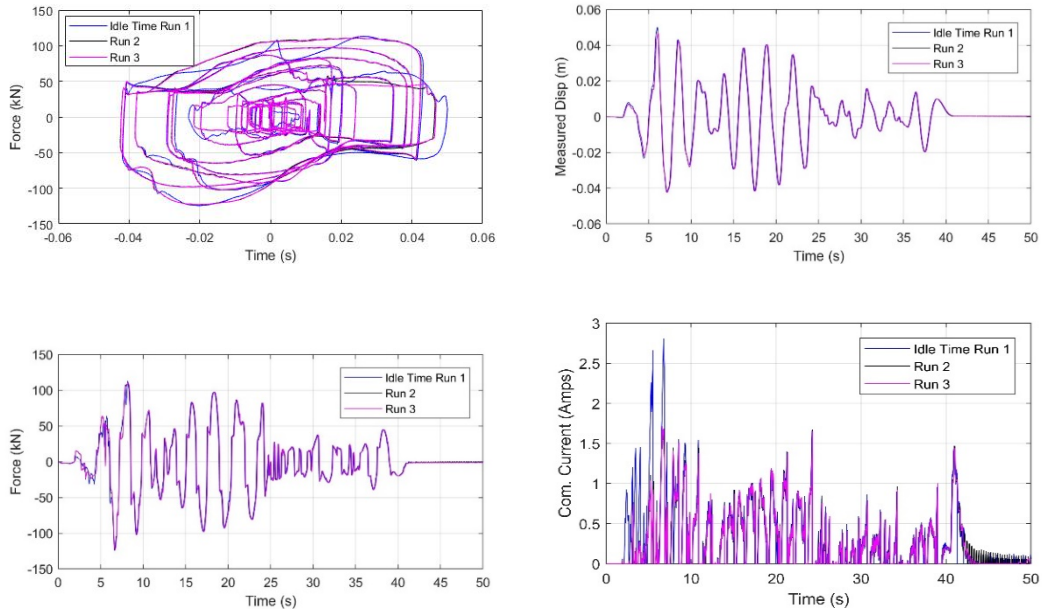


Fig. 6.5: Idle Time RTHS Comparison with “Fully-Mixed” Case

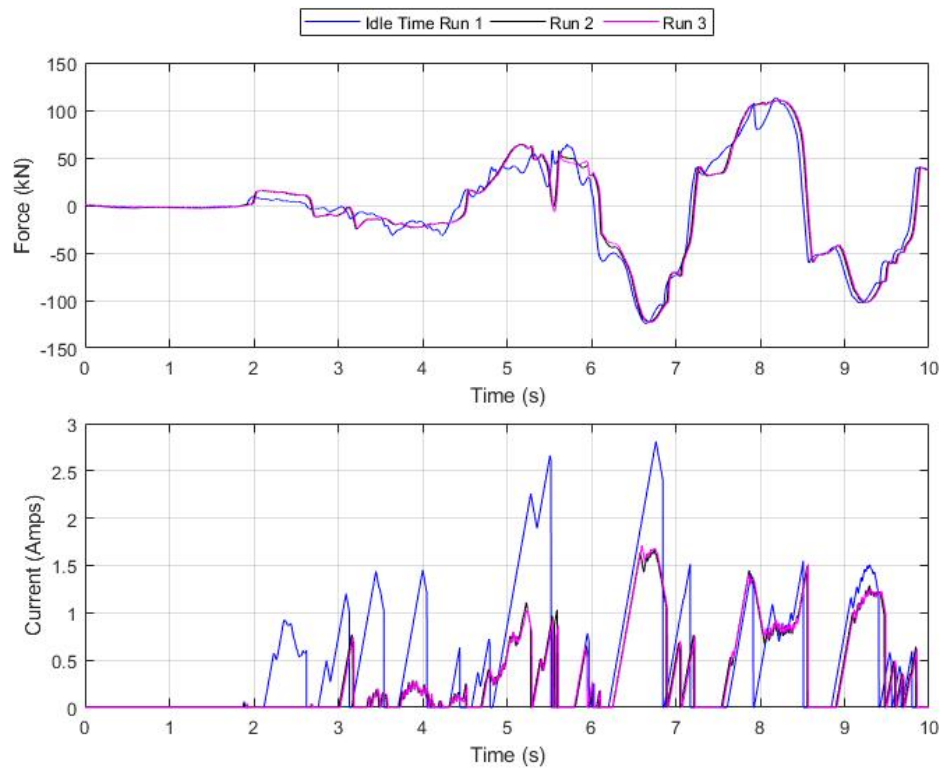


Fig. 6.6: Idle Time RTHS Comparison Plots from 0 – 10 Seconds

To verify the numerical model, the results from the 3 month idle time RTHS test are plotted against the numerical simulation and the fully mixed cases. These results are presented in Fig. 6.7. As can be seen from this figure, there is also good force and displacement tracking between the numerical and experimental results. However, the current response is not accurately captured in the numerical model. Although there is clear evidence in Fig. 6.8 that the current from the numerical simulation was predicted to be larger than the “fully-mixed” case, it did not achieve the levels that the idle time RTHS test data shows. This may be due to a number of reasons, such as errors in the idle time model due the assumptions made, uncertainty in the exact period that the damper was idle, or errors introduced by the limitations of the Bingham Plastic model, among others.

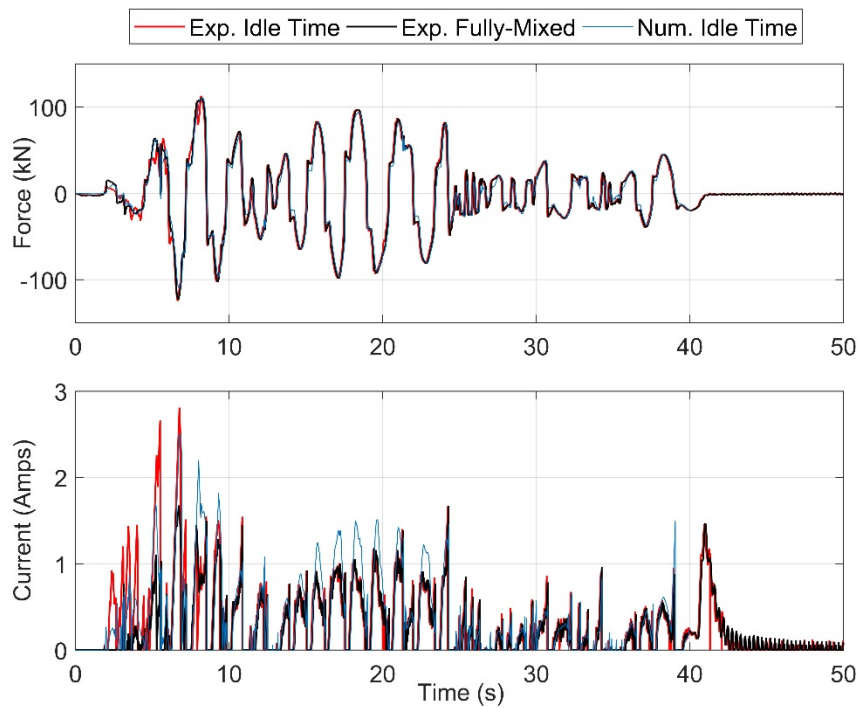


Fig. 6.7: Comparison of Numerical Simulation and RTHS Testing

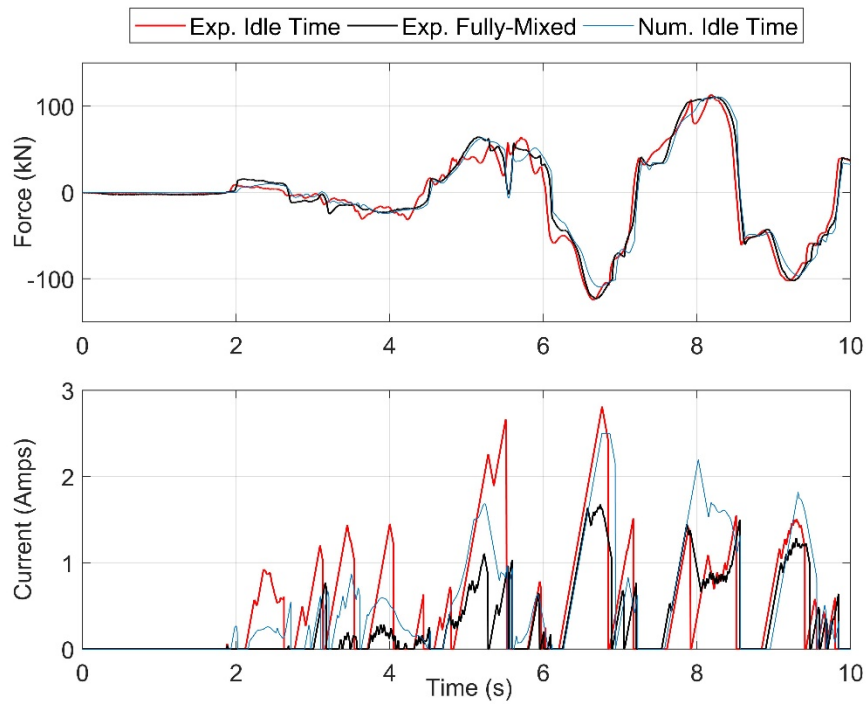


Fig. 6.8: Comparison of 0 – 10 sec Numerical Simulation and RTHS Testing

This idle time RTHS test supports the claim that over time, the performance of the damper degrades. However, for the conditions evaluated, the damper was still able to handle the required force from the semi-active control algorithm. This is because the desired force was still achievable by the MR damper by using a larger current that would have been needed under fully mixed conditions. If the desired force were higher or the idle time were longer, there may not be enough “excess capacity” to reach the desired force under the idle time conditions. Under stronger earthquake ground motion excitation or longer idle times, it is predicted that this behavior may lead to large differences between the desired and measured (achievable) forces and hence larger drift in the structure. This performance degradation is something to be aware of to further improve upon the technology and develop maintenance strategies for MR dampers, as well as to apply similar study techniques to analyze and improve other structural control systems.

To better understand the effects of the idle time effects on the performance of MR dampers, numerical simulations to analyze the 6DOF under different earthquake ground motion records were performed. This set of tests analyzed the structure under the earthquake ground motion records listed in Table 6.3 so that each earthquake had roughly the same PGA value.

Table 6.3: Earthquake Ground Motion PGA Scaling

Earthquake Record	Original PGA (g)	RTHS Test Scaling	Num. Simulation Scaling	Scaled PGA (g)
Hachinohe	0.2254	50.00%	50.00%	0.1127
Northridge	0.8517	-	13.23%	0.1127
Kobe	0.8300	-	13.58%	0.1127
El Centro	0.3570	-	31.56%	0.1127

The cases used are: 50% Hachinohe (Case a), 13.23% Northridge (Case b), 13.58% Kobe (Case c), and 31.56% Elcentro (Case d) earthquake ground motion records. The numerical simulations were run using passive-off control, passive-on control with 2.5A constant current, and semi active control using the causal approximation of RILD and an ODBDCO controller to gain a better understanding of the behavior of the damper. The comparison between fully-mixed case and 2.5 year idle time has been presented. The results between different earthquakes and between different control modes (passive-off, passive-on, and semi-active) are shown in Fig. 6.9 – 6.11.

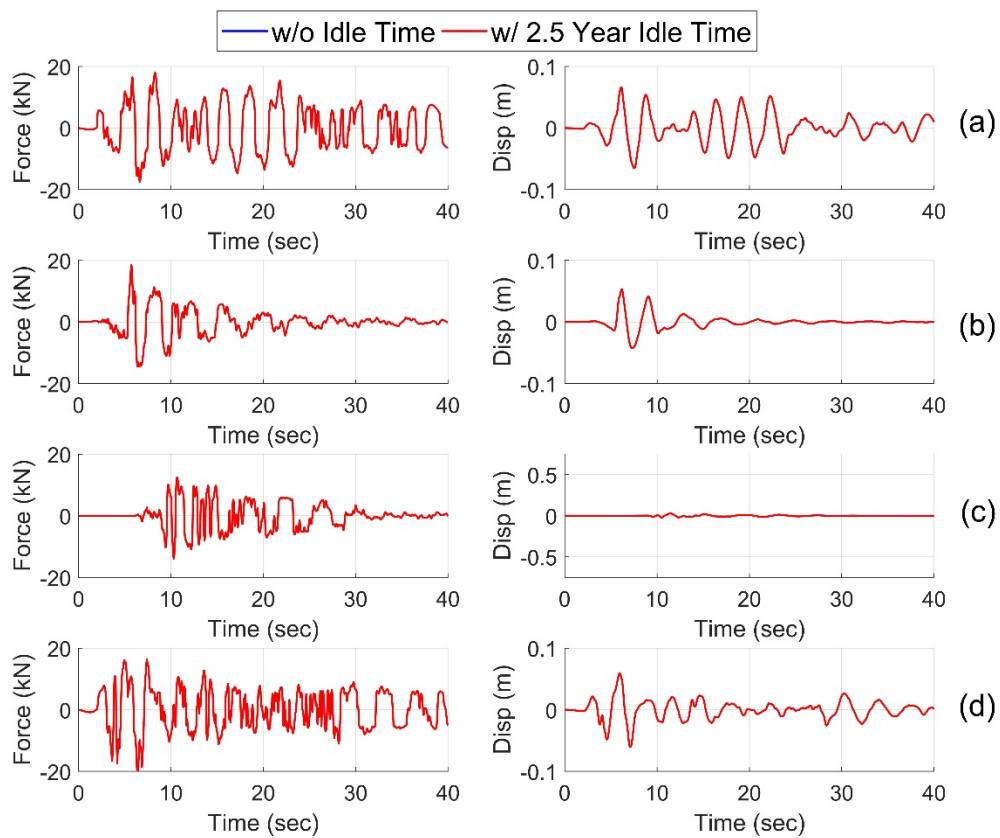


Fig. 6.9: 2.5 Year Idle Time with Passive-off Control Under Hachinohe (Case a), Northridge (Case b), Kobe (Case c), and Elcentro (Case d) Ground Motion

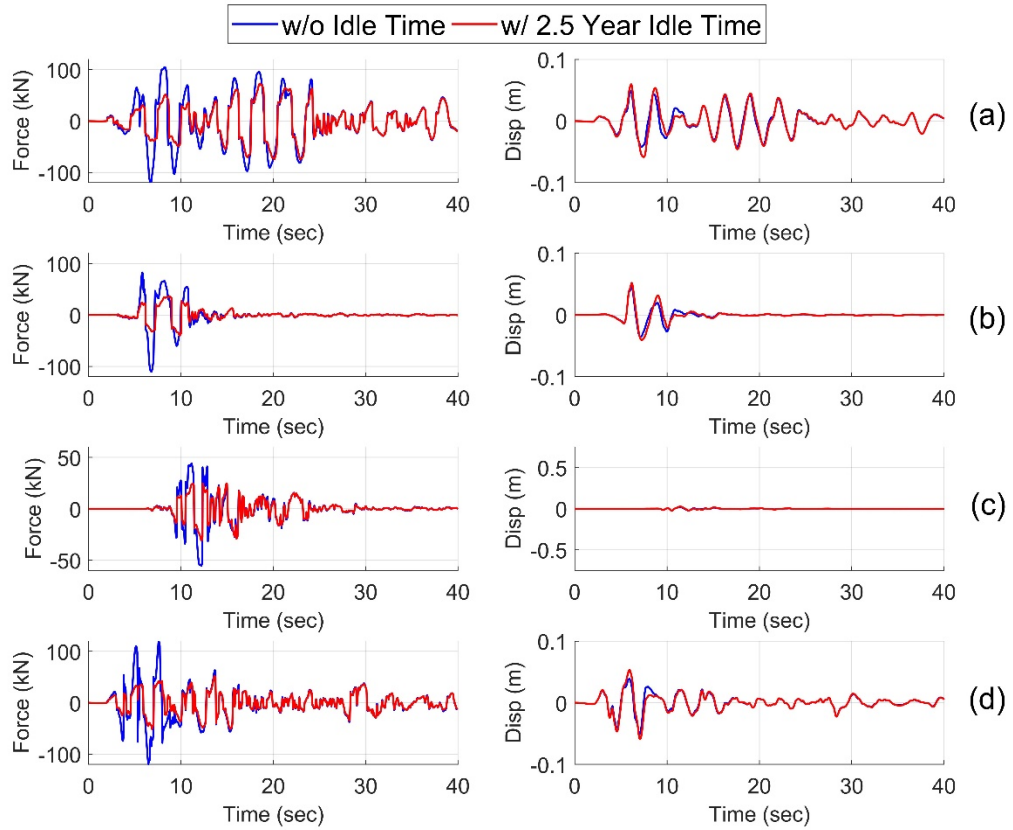


Fig. 6.10: 2.5 Year Idle Time with Causal Semi-Active Control Under Hachinohe (Case a), Northridge (Case b), Kobe (Case c), and Elcentro (Case d) Ground Motion

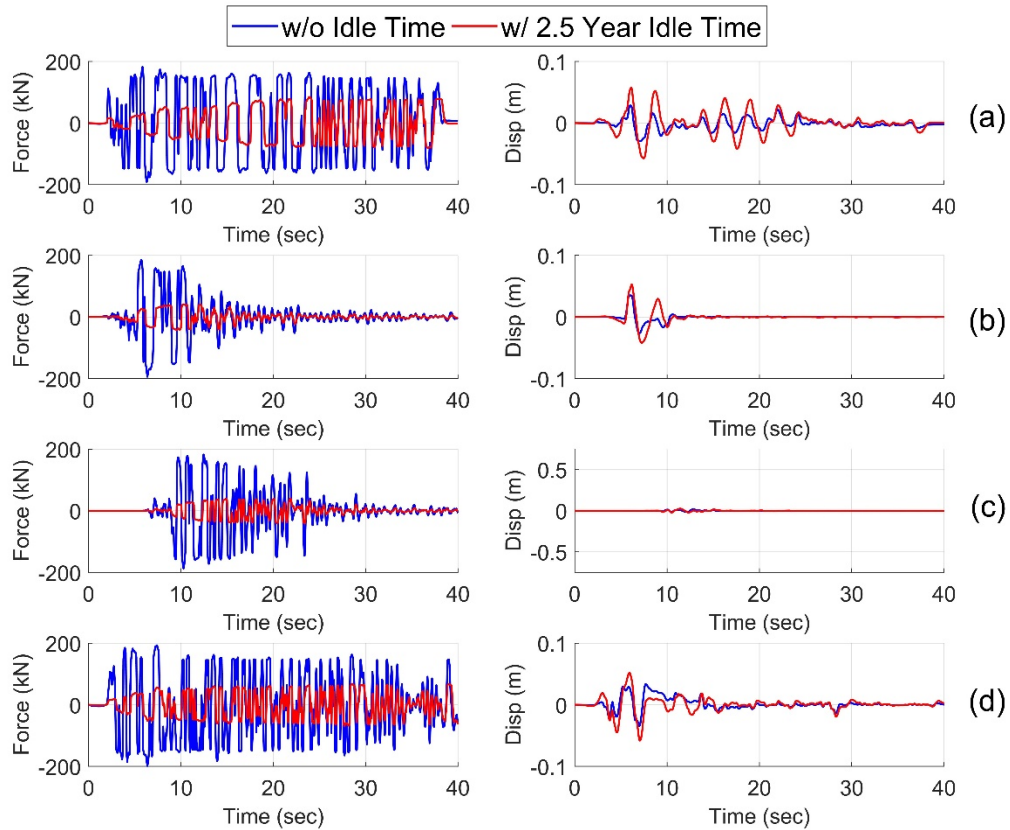


Fig. 6.11: 2.5 Year Idle Time with Passive-On Control Under Hachinohe (Case a), Northridge (Case b), Kobe (Case c), and Elcentro (Case d) Ground Motion

6.5 Numerical Simulations for Long-Term Performance

Additionally, an analysis was performed which tracked the maximum force response of the damper and displacement for the structure under over a range of idle times. The maximum absolute acceleration of the structure was also tracked to see what other effects the reduced capabilities of the damper would have on the structure. For this numerical analysis, the same magnitude scaling for all the earthquake ground motion records from Table 6.3 was used to have their peak ground acceleration (PGA) values be roughly the same at ~ 0.11 g. This would allow us to observe the effects of the idle time on the performance degradation of the structural response

under a range of frequency content. This idle time settling period spanned from 0 to 1.0 years at 0.05 year intervals. The numerical simulations were run using the same three control types, i.e., passive-off control, passive-on control with 2.5A constant current, and semi active control using the causal approximation of RILD and an ODBDCO controller. The results in Fig. 6.12 predict a decrease in maximum absolute damping force over the increasing idle time duration. It also predicts an increase in the maximum absolute displacement (Fig. 6.13) in the base isolation layer and in the acceleration of the superstructure (Fig. 6.14). This can be attributed to the decrease in performance due to the idle time settling of the particles which is also the reason for the saturation in the maximum absolute force and displacement at 0.8531 years. This specific idle time value is dependent on the minimum time required for the complete settling of the particles and as discussed in chapter 5, is dependent on the viscosity of the fluid. In this thesis, the viscosity was assumed to be 2 Pa*s which led to the time of 0.8531 years, however, if more accurate values of the viscosity of the fluid can be determined when the damper is idle, the predictions and effectiveness of the model will be improved. Furthermore, if different MR fluids were used this behavior can be delayed for decades. The results for passive-off (Fig. 6.15-6.17) and passive-on (Fig. 6.18-6.20) control are also displayed below.

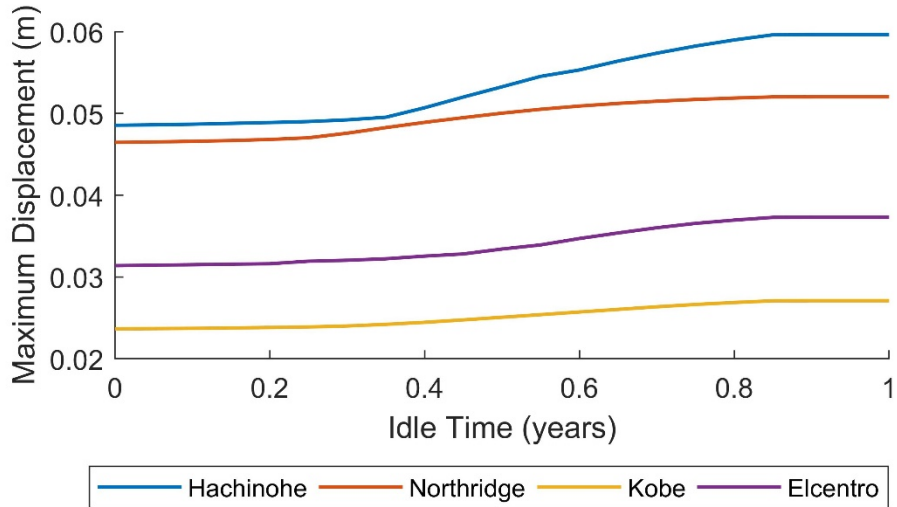


Fig. 6.12: Max. Displacement of Base Isolation Under EQ Ground Motion with Causal Semi-Active Controller

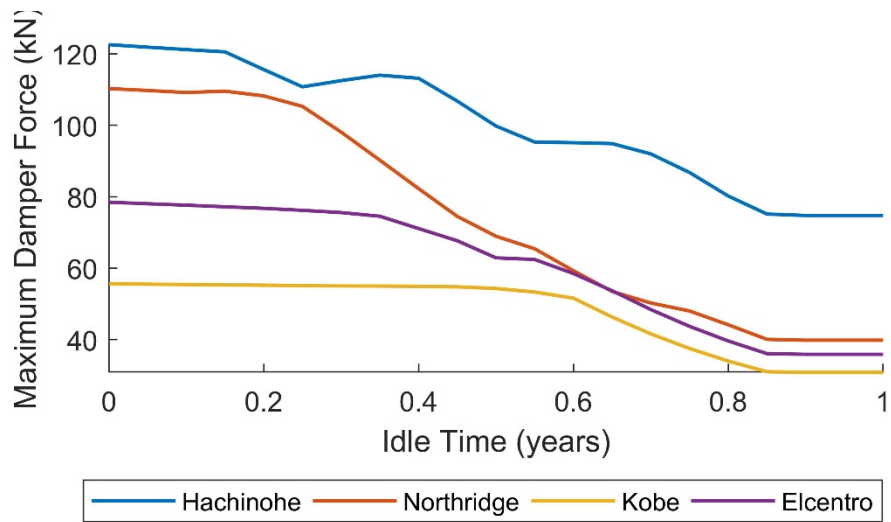


Fig. 6.13: Max. Damping Force Under EQ Ground Motion with Causal Semi-Active Controller

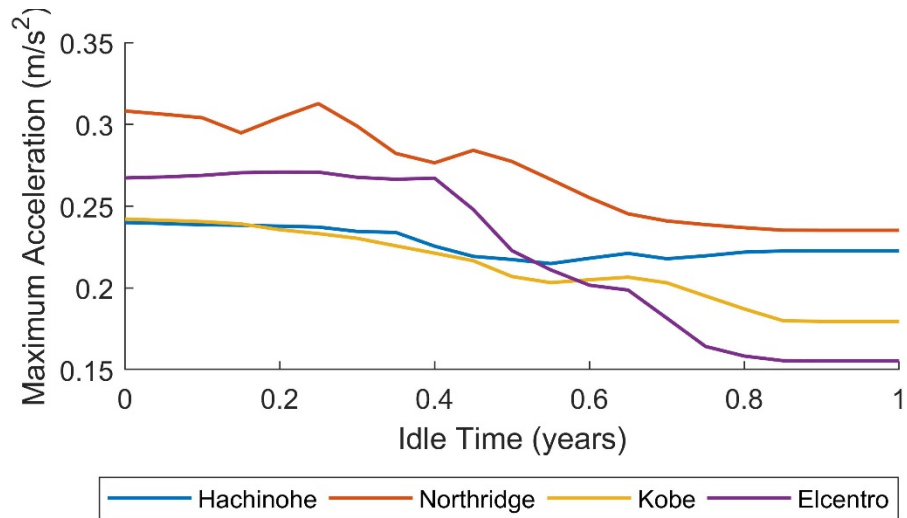


Fig. 6.14: Max. Acceleration of Superstructure Under EQ Ground Motion with Causal Semi-Active Controller

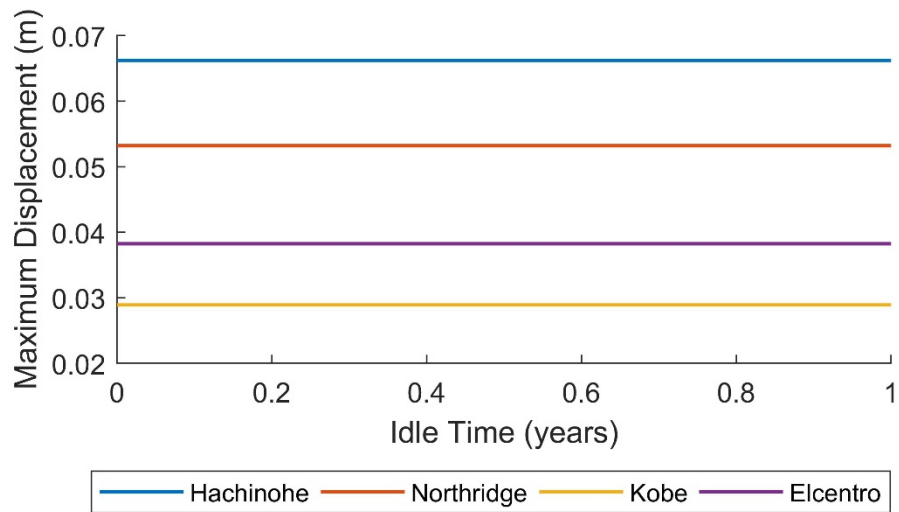


Fig. 6.15: Max. Displacement of Base Isolation Under EQ Ground Motion with Passive-Off Controller

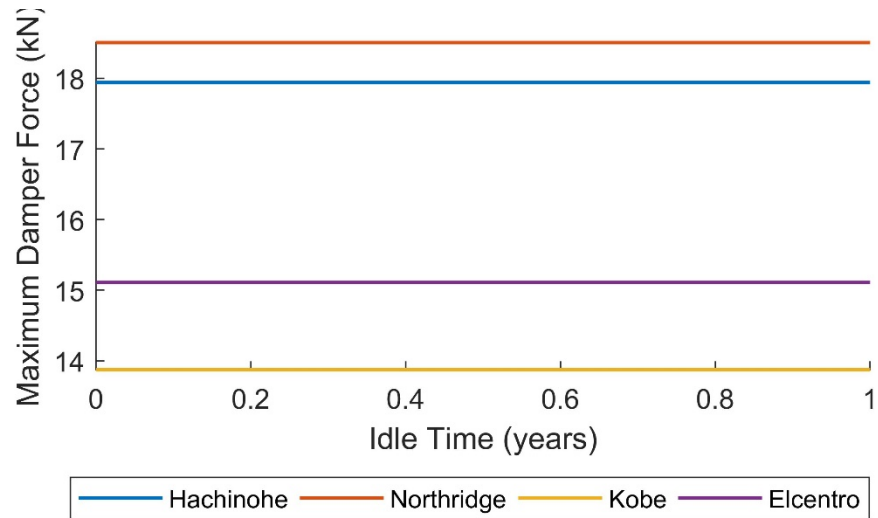


Fig. 6.16: Max. Damping Force Under EQ Ground Motion with Passive-Off Controller

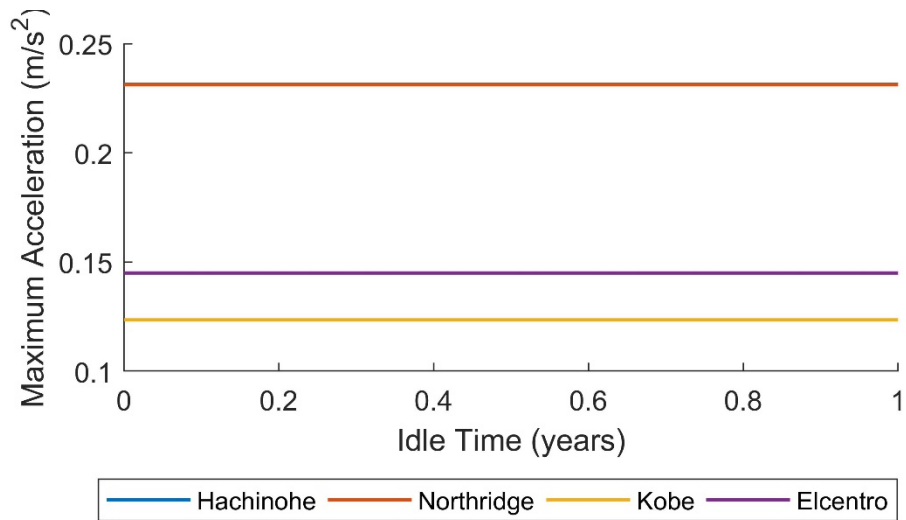


Fig. 6.17: Max. Acceleration of Superstructure Under EQ Ground Motion with Passive-Off Controller

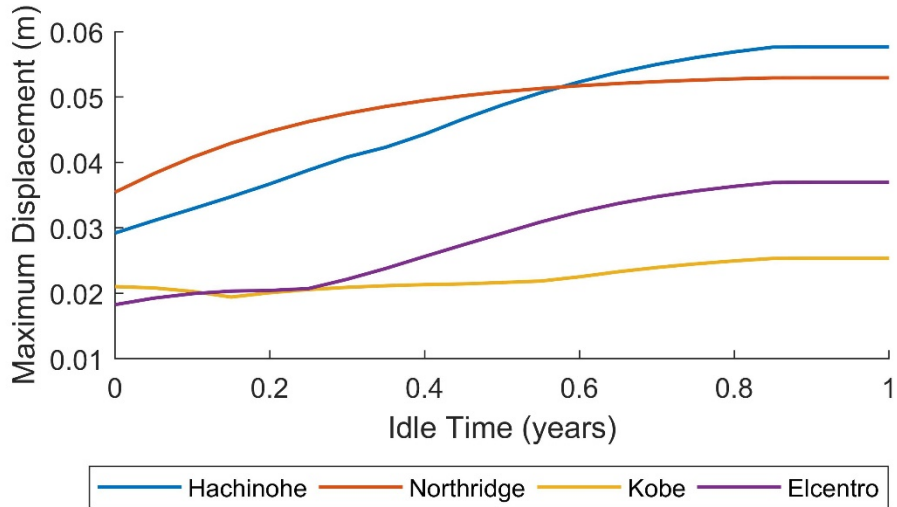


Fig. 6.18: Max. Displacement of Base Isolation Under EQ Ground Motion with Passive-On Controller

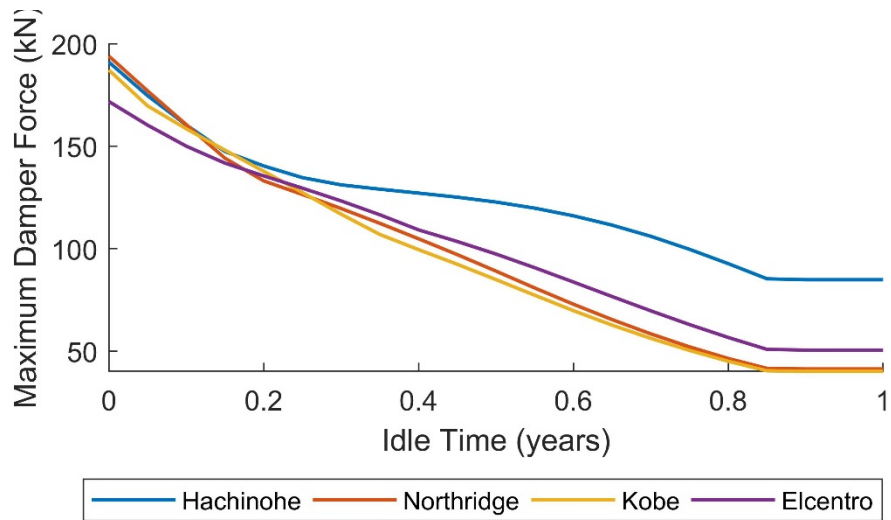


Fig. 6.19: Max. Damping Force Under EQ Ground Motion with Passive-On Controller

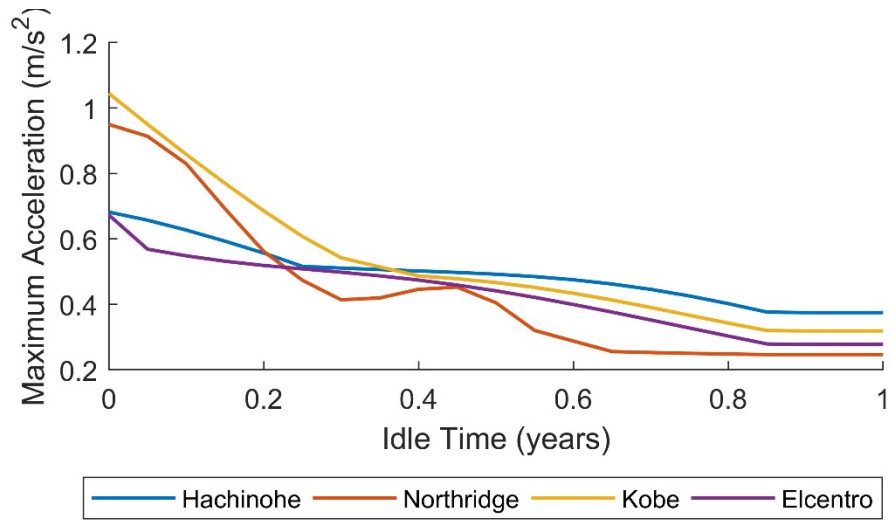


Fig. 6.20: Max. Acceleration of Superstructure Under EQ Ground Motion with Passive-On Controller

Chapter 7: Conclusion and Future Studies

Structural protective systems are key to improving the design of engineered structures under dynamic loads. By providing these systems with an adequate certainty in the long-term performance, it becomes a much more attractive and useful tool for engineers to implement in their structures. Through the analysis, design and study of different control strategies, structural protective systems, and maintenance strategies for those systems, the field of seismic protection engineering will continue to grow and protect people around the world. This thesis presented the study of long-term performance degradation of structural protective systems on the structural response. Through the use of MR dampers as an analog for structural protection systems, these ideas can be examined and tested with equipment available in a repeatable and controlled manner. By studying the long-term performance degradation of the MR damper through idle time and fully-mixed RTHS testing, it is possible to predict and verify the hypothesis regarding the extent and effects of performance degradation on the structural response under seismic ground motion excitation. As can be seen in Chapter 5 and 6, there is a clear decrease in the ability for the damper to achieve a force under a given current over time. This can be compensated for by driving the current higher than normally required in order to achieve the desired force response, as was seen in the experimental RTHS test under a 3 month idle time. In general, there may not be excessive capacity to overdrive the current to make up for the idle time performance loss. This is particularly true if the desired force is large or idle time is long. This loss in performance and the resultant change in the damper behavior may lead to severe effects.

From this thesis it is seen that under a certain level of excitation and within sufficiently maintained control systems, the MR damper behavior is within acceptable limits and allows for the protection of the building. However, once that limit is crossed, it is difficult for the structural protective systems to appropriately respond to the same extent that they are designed to do. This depends on the scale of the ground motion excitation, the structural components and protective systems and the number of devices implemented, among other factors. These negative effects are predicted to be worse for longer idle time settling periods which will occur due to the long lifetimes of civil structures and the significant periods of time between seismic events. This can also affect the resilience of the structure and the engineering design capacities of the structures and will need to be addressed appropriately. Even at a fully settled state, the MR damper still provides protection, damage mitigation, and control over the structural response through a passive off state in which the MR damper acts as a viscous damper (the observable lower bound with large idle times).

This thesis presented the results of idle time settling effects, however, it did so through the use of a model MR fluid that exhibited accelerated settling as compared to a fluid that may be used in practice. For this specific damper and fluid, it can be seen that even within a year there is severe performance degradation. This model MR fluid was used in order to determine the consequences of long-term performance degradation due to sedimentation. However, particle sedimentation can effectively be delayed by decades using newer MR fluids that have been researched. This can be achieved by using a type of carrier fluid known as thixotropic fluids (Xie et al, 2016). These fluids exhibit very high viscosities when the fluid is undisturbed but can

quickly convert to a lower viscosity even at relatively low shear rates. This property allows the particles to remain suspended due to the high viscosity while also providing fluidity when the damper needs to act (Zhang et al., 2010; Xie et al., 2016). Future studies would involve the development of these kinds of MR fluids for civil applications, which would provide effective seismic protective capabilities and prevent the settling of the MR fluid particles. By using different mixtures of magnetic particles and thixotropic carrier fluids, the damper's controllable range would also be affected and needed to be accounted for in the damper mechanical configuration and the MR fluid design. The damper design must ensure that peak performance of the damper would be maintained even after decades of idle time. Further testing needs to be done to determine the maximum viscosity the fluid can have when the damper undergoes motion. This is important because if the viscosity is too high, amplified accelerations may be generated in the structure. Through further RTHS testing, these limits can be determined.

Additionally, to better understand and model the settling behavior of the MR fluid particles, advective models proposed for the settling particle motion can be used rather than the simplified settling quotient from Chapter 5. These can be further refined through column tests to measure the stratification of the fluid as per the method described by Chambers & Wereley (2017). By using fluids with accelerated settling, experiments can be performed within shorter time frames and through physical processes such as the use of a centrifuge, specific settling and participant ratios can be created for experimentation.

Through this thesis and future research, MR damper technology will be able to have better long-term performance and make it more worthwhile to investors and owners to use such technologies to protect their structures and the public. This reduction in risk will not only lead to more widespread acceptance of the technology, but also increase public safety in the face of natural hazards. These same methods and concepts can be applied to study other structural control systems to determine targeted maintenance strategies or improvements in the design to prevent long-term performance degradation. By appropriately designing for these long-term performance degradation sources, it will be possible to ensure that the structural protective systems achieve their design response levels.

References

- Advanced Motion Controls (2018). Retrieved April 3rd, 2018 from <https://www.a-m-c.com/>
- Atiemo-Obeng, V. A., Pnney W.R., Armenante, P. (2004). Solid-Liquid Mixing. In Paul, E. L., Atiemo-Obeng, V. A., & Kresta, S. M. (Eds.). *Handbook of Industrial Mixing: Science and Practice* 543-584. John Wiley & Sons.
- Avraam, M. T. (2009). *MR-Fluid Brake Design and its Application to a Portable Muscular Rehabilitation Device*. (Doctoral dissertation) Facultedes Sciences Appliquees. Universite Libre de Bruxelles.
- BBC News (2017, September 20). Mexico: Huge earthquake topples buildings, killing more than 200. *BBC News*. Retrieved Feb 4th, 2018 from <http://www.bbc.com/news/world-latin-america-41327593>
- Bridgestone (2017). Seismic Isolators. *Bridgestone*. Retrieved Feb 4th, 2018 from http://www.bridgestone.com/products/diversified/antiseismic_rubber/images/img_antiseismic_rubber_10.gif
- Carlson, J. D., Catanzarite, D. M., & St. Clair, K. A. (1996). Commercial Magneto-Rheological Fluid Devices. *International Journal of Modern Physics B*, 10(23n24), 2857-2865.
- Chambers, J. M. & Wereley, N.M. (2017). Vertical Axis Inductance Monitoring System to Measure Stratification in a Column of Magnetorheological Fluid. *IEEE Transactions on Magnetics*, 53(1).

- Chavez, N., Almasy, S., Sanchez, R., & Simon, D. (2017, September 20). Central Mexico earthquake kills more than 200, topples buildings. *CNN*. Retrieved Feb 4th, 2018 from <http://www.cnn.com/2017/09/19/americas/mexico-earthquake/index.html>
- Christenson, R., Lin, Y., Emmons, A., & Bass, B. (2008). Large-Scale Experimental Verification of Semiactive Control through Real-Time Hybrid Simulation. *Journal of Structural Engineering*, 134(4), 522–534.
[https://doi.org/10.1061/\(ASCE\)0733-9445\(2008\)134:4\(522\)](https://doi.org/10.1061/(ASCE)0733-9445(2008)134:4(522))
- CNN Library (2017, October 30). 2017 Atlantic Hurricane Season Fast Facts. *CNN*. Retrieved Feb 4th, 2018 from <http://www.cnn.com/2017/05/15/us/2017-atlantic-hurricane-season-fast-facts/index.html>
- Demetriou, D., Nikitas, N., and Tsavdaridis, K.D. (2014). Performance of proportional-integral-derivative controllers on structures with variable damping active tuned mass dampers. *The 6th World Conference on Structural Control and Monitoring - Special Session 12: Advanced Modeling for Structural Control*, 15-17 July 2014, Barcelona, Spain. 6WCSCM.
<http://eprints.whiterose.ac.uk/80998/>
- Dyke, S. J., Spencer Jr, B. F., Sain, M. K., & Carlson, J. D. (1998). An Experimental Study of MR Dampers for Seismic Protection. *Smart materials and structures*, 7(5), 693.
- Ealangi, I. (2010). Earthquake Protection of Buildings by Seismic Isolation: Devices and Concepts. In *Young Researchers Conference*.

- Ein-Mozaffari, F. & Upreti, S. R. (2010). Investigation of Mixing in Shear Thinning Fluids Using Computational Fluid Dynamics. In OH H. W. (Ed). (2010). *Computational Fluid Dynamics*, 420. INTECH, Croatia. www.sciyo.com
- Ellis, R. (2017, September 25). Mexico earthquake: Crews keep searching for victims. *CNN*. Retrieved Feb 4th, 2018 from <http://www.cnn.com/2017/09/25/americas/mexico-earthquake/index.html>
- Engineering360. (2018). *Polyalphaolefin Oil Molykote ® L – 1268 Synthetic Compressor Oil*. Engineering360 powered by IEEE GlobalSpec. Retrieved April 3rd, 2018 from https://www.globalspec.com/industrial-directory/polyalphaolefin_oil
- Erdbrink, T. (2017, November 13). Iran-Iraq Earthquake Kills More Than 500. *The New York Times*. Retrieved Feb 4th, 2018 from <https://www.nytimes.com/2017/11/13/world/middleeast/iran-iraq-earthquake.html>
- Fan, L., Mao, Z. S., Yang, C., & Wang, Y. (2007). Numerical simulation of laminar solid-liquid two-phase flow in stirred tanks. *Chemical Engineering Communications*, 194(3), 291–308.
<https://doi.org/10.1080/00986440600829861>
- GFDL (2017). Global Warming and Hurricanes. Geophysical Fluid Dynamics Laboratory, *National Oceanic and Atmospheric Administration*. Retrieved March 3rd, 2018 from <https://www.gfdl.noaa.gov/global-warming-and-hurricanes/>

- Gołdasz, J., & Sapiński, B. (2017). Magnetostatic Analysis of a Pinch Mode Magnetorheological Valve. *Acta Mechanica et Automatica*, 11(3), 229–232. <https://doi.org/10.1515/ama-2017-0035>
- Goncalves, F. D. (2005). *Characterizing the Behavior of Magnetorheological Fluids at High Velocities and High Shear Rates* (Doctoral dissertation), Virginia Polytechnic Institute and State University.
- Goncalves, F. D., & Carlson, J. D. (2009). An alternate operation mode for MR fluids—magnetic gradient pinch. *Journal of Physics: Conference Series*, 149, 12050. <https://doi.org/10.1088/1742-6596/149/1/012050>
- Guazzelli, É. (2006). Sedimentation of small particles: how can such a simple problem be so difficult? *Comptes Rendus - Mecanique*, 334(8–9), 539–544. <https://doi.org/10.1016/j.crme.2006.07.009>
- Heydari, A. S. (2014). *A Study of Integrated Structural Control Systems for Multi-Hazard Response Mitigation*. (M.A.Sc. Thesis) McMaster University.
- History.com (2009). 2005 Kashmir Earthquake. *History.com*. Retrieved Feb 4th, 2018 from <http://www.history.com/topics/kashmir-earthquake>
- Hosseini, S., & Patel, D. (2010). Study of Solid– Liquid Mixing in Agitated Tanks through Computational Fluid Dynamics Modeling. *Ind. Eng. Chem. Res.*, (49), 4426–4435. American Chemical Society <https://doi.org/10.1021/ie901130z>
- Housner, G. W., Bergman, L. A., Caughey, T. K., Chassiakos, A. G., Claus, R. O., Masri, S. F., ... Yao, J. T. P. (1997). STRUCTURAL CONTROL : PAST , PRESENT , AND FUTURE. *Journal of Engineering Mechanics*, 123 (September), 897–971.

- Jansen, L. M., & Dyke, S. J. (2000). Semiactive Control Strategies for MR Dampers: Comparative Study. *Journal of Engineering Mechanics*, 126(8), 795–803.
[https://doi.org/10.1061/\(ASCE\)0733-9399\(2000\)126:8\(795\)](https://doi.org/10.1061/(ASCE)0733-9399(2000)126:8(795))
- Jiang, Z., Mantoni, D., Christenson, R., Chae, Y., Ricles, J., Friedman, A., ... & Spencer, B. F. (2010). Comparison of 200 KN MR Damper Models for Use in Real-Time Hybrid Simulation. In *Fifth World Conference on Structural Control and Monitoring*.
- Jiang, Z. & Christenson, R. (2011). A comparison of 200 kN magneto-rheological damper models for use in real-time hybrid simulation pretesting. *Smart Materials and Structures* 20(6). <http://dx.doi.org/10.1088/0964-1726/20/6/065011>
- Jiang, Z. & Christenson, R. (2012). A fully dynamic magneto-rheological fluid damper model. *Smart Materials and Structures* 21(6).
<http://dx.doi.org/10.1088/0964-1726/21/6/065002>
- Jolly, M. R., Carlson, J. D., & Munoz, B. C. (1996). A model of the behaviour of magnetorheological materials. *Smart Materials and Structures*, 5(5), 607.
- Jolly, M. R., Bender, J. W., & Carlson, J. D. (1998). Properties and Applications of Commercial Magnetorheological Fluids. In *SPIE 5th Annual Int. Symposium on Smart Structures and Materials*. San Diego, CA.
- Jolly, M. R., Bender, J. W., & Carlson, J. D. (1999). Properties and Applications of Commercial Magnetorheological Fluids. *Journal of Intelligent Material*

Systems and Structures, 10(1), 5–13.

<https://doi.org/10.1177/1045389X9901000102>

Kciuk, M., & Turczyn, R. (2006). Properties and Application of Magnetorheological Fluids. *Journal of Achievements in Materials and Manufacturing Engineering*, 18(1–2), 127–130. <https://doi.org/10.1177/1045389X9901000102>

Keivan, A., Phillips, B. M., Ikenaga, M., & Ikago, K. (2017). Causal Realization of Rate-Independent Linear Damping for the Protection of Low-Frequency Structures. *Journal of Engineering Mechanics*, 143(9), 04017058.

Khansefid, A. & Ahmadizadeh, M. (2016). An investigation of the effects of structural nonlinearity on the seismic performance degradation of active and passive control systems used for supplemental energy dissipation. *Journal of Vibration and Control* 22(16), 3544–3554. doi:10.1177/1077546314563969

Laird-Signal Integrity Products. <https://www.lairdtech.com/products/28b2000-100>

Lavan, O. & Dargush, G.F. (2009). Multi-objective evolutionary seismic design with passive energy dissipation systems. *Journal of Earthquake Engineering* 13(6), 758-790. <https://doi-org.proxy-um.researchport.umd.edu/10.1080/13632460802598545>

Li, W. H., Chen, G., & Yeo, S. H. (1999). Viscoelastic properties of MR fluid. *Smart Materials and Structures*, 8, 460–468.

Lord Corporation (2018). Retrieved April 3rd, 2018 from <https://www.lord.com/>

Mak, A. T.-C. (1992). Solid–liquid mixing In Mechanically Agitated Vessels.

THESIS in Doctor of Philosophy in the University of London, (June), 248.

<http://onlinelibrary.wiley.com/doi/10.1002/0471451452.ch10/summary>

Maleki-Jirsaraei, N., Ghane-Motlagh, B., Ghane-golmohamadi, F., Ghane-Motlagh, R., & Rouhani, S. (2010). Synthesis and analysis of the properties of ferrofluids. In *2010 International Conference on Nanoscience and Nanotechnology* (pp. 91–93). IEEE. <https://doi.org/10.1109/ICONN.2010.6045188>

Mann, R., Williams, R. a., Dyakowski, T., Dickin, F. J., & Edwards, R. B. (1997). Development of mixing models using electrical resistance tomography. *Chemical Engineering Science*, 52(13), 2073–2085. [https://doi.org/10.1016/S0009-2509\(97\)00035-3](https://doi.org/10.1016/S0009-2509(97)00035-3)

MathWorks (2018). MATLAB and Simulink. Retrieved April 3rd, 2018 from <https://www.mathworks.com/products/matlab.html>

McKee, S. L., Williams, R. A., & Boxman, A. (1995). Development of solid-liquid mixing models using tomographic techniques. *The Chemical Engineering Journal* (56) 101-107.

MTS (2018). Retrieved April 3rd, 2018 from <https://www.mts.com>

Murty, C.V.R. (2005). IITK-BMTPC Earthquake Tips: Learning Seismic Design and Construction. *National Information Centre of Earthquake Engineering*. <http://www.nicee.org/EQTips.php>

Nauman B. & Nigam A. (2005). On Axial Diffusion in Laminar-Flow Reactors. *Ind. Eng. Chem. Res.*, (44), 5031-5035. American Chemical Society
10.1021/ie049677b

- Ngatu, G. T., & Wereley, N. M. (2007). Viscometric and sedimentation characterization of bidisperse magnetorheological fluids. *IEEE Transactions on Magnetics*, 43(6), 2474–2476. <https://doi.org/10.1109/TMAG.2007.893867>
- Nienow, A. W. (1985) The Dispersion of Solids in Liquids. In Ulbrecht, J. J., & Patterson, G. K. (Eds.). (1985). *Mixing of liquids by mechanical agitation* (1) 273-307. Taylor & Francis.
- Ocean Networks Canada (2017). Are Earthquakes On The Rise?. *Ocean Networks Canada*. <http://www.oceannetworks.ca/are-earthquakes-rise>
- Ohtori, Y., Christenson, R. E., Spencer, B. F. Jr., and Dyke, S. J. (2004). “Benchmark control problems for seismically excited nonlinear buildings.” *J. Eng. Mech.* 4(366), 366–385. 10.1061/(ASCE)0733-9399(2004)130.
- Omega (2018). Retrieved April 3rd, 2018 from <https://www.omega.com/>
- Peng, Y.B., Feng, Y., Chen, J.B., & Li, J. (2013). Molecular Dynamics Simulations Based Magnetic Pulse Regulation on Suspension Settlement of Magneto-Rheological Fluids. In Deodatis, G., Ellingwood, B. R., & Frangopol, D. M. (Eds.), *Safety, Reliability, Risk and Life-Cycle Performance of Structures and Infrastructures*, 853-858. CRC Press.
- Phillips, B. M., Jiang, Z., Ricles, J. M., Dyke, S. J., Chae, Y., Spencer, B. F., ... & Agrawal, A. (2010). Real-Time Hybrid Simulation Benchmark Study with a Large-Scale MR Damper. *Proc. of the 5th WCSCM*, 12-14.
- Phillips, B. M. & Spencer, B. F. (2012). Model-Based Feedforward-Feedback Tracking Control for Real-Time Hybrid Simulation. *NSEL Report Series* (31).

https://www.ideals.illinois.edu/bitstream/handle/2142/33794/NSEL_31.pdf?..5

Pope, S. B. (2000). *Turbulent Flows*. Cambridge: Cambridge University Press.

<https://doi.org/10.1017/CBO9780511840531>

Premalatha, S. E., Chokkalingam, R., & Mahendran, M. (2012). Magneto Mechanical Properties of Iron Based MR Fluids. *American Journal of Polymer Science*, 2(4), 50–55. <https://doi.org/10.5923/j.ajps.20120204.01>

Rai, N.K., Reddy, G.R., Ramanujam, S., Venkatraj, V., & Agrawal, P. (2009).

Seismic Response Control Systems for Structures. *Defence Science Journal* 59(3), 239-251.

Riley, M. A. & Reinhorn, A. M. (1998). Implementation issues and testing of a hybrid sliding isolation system. *Engineering Structures*, 20(3), 144-154.

Royal Society of Chemistry RSC. (2014). *Magnetorheology: Advances and Applications*. The Royal Society of Chemistry. Wereley, N. (Ed.). 232.

doi:10.1039/9781849737548-00229

Schaffner (2018). Retrieved April 3rd, 2018 from

<https://www.schaffner.com/products/download/product/datasheet/fn-2080-multi-stage-high-performance-emcemi-filter/>

Sigma-Aldrich (2018). Mineral Oil, light. Sigma-Aldrich. Retrieved April 3rd, 2018 from

<https://www.sigmaaldrich.com/catalog/product/sial/330779?lang=en®ion=US>

- Soong, T.T. & Spencer, B.F. (2000). Active, Semi-Active and Hybrid Control of Structures. *Bulletin of the New Zealand National Society for Earthquake Engineering*, 33(3), 387-402.
- Spaggiari, A. (2013). Properties and Applications of Magnetorheological Fluids. *Frattura ed Integrità Strutturale*, (23), 48.
- Spencer, B.F. (2008). Structural Control in Honor of Takuji Kobori. *The 14th World Conference on Earthquake Engineering, Beijing, China*.
www.iitk.ac.in/nicee/wcee/article/14_S24-014.pdf
- Spencer Jr, B. F., Dyke, S. J., Sain, M. K., & Carlson, J. (1997). Phenomenological Model for Magnetorheological Dampers. *Journal of engineering mechanics*, 123(3), 230-238.
- Spencer Jr, B. F., Yang, G., Carlson, J. D., & Sain, M. K. (1998, June). Smart dampers for seismic protection of structures: a full-scale study. In *Second World Conference on Structural Control, Kyoto* (pp. 417-426).
- Stanway, R. Sproston, J.L. and Stevens, N.G. (1985). Non-linear Identification of an Electro-Rheological Vibration Damper. *IFAC Identification and System Parameter Estimation Proceedings Volumes*, 18(5), 195-200.
doi:10.1016/S1474-6670(17)60558-5
- Sugiyama, S., Sakurai, T., & Morishita, S. (2013). Vibration control of a structure using Magneto-Rheological grease damper. *Frontiers of Mechanical Engineering*, 8(3), 261–267. <https://doi.org/10.1007/s11465-013-0268-4>
- Sullivan, B.K. (2017, November 26). The Most Expensive U.S. Hurricane Season Ever: By the Numbers. *Bloomberg*. Retrieved Feb 4th, 2018 from

<https://www.bloomberg.com/news/articles/2017-11-26/the-most-expensive-u-s-hurricane-season-ever-by-the-numbers>

Taipei-101 (2014). Wind Damper. *Taipei 101.com.tw*. Retrieved March 21st, 2018 from <https://www.taipei-101.com.tw/en/observatory-damper.aspx>

Taywade, P. W. & Savale, M. N. (2015). Sustainability of Structure Using Base Isolation Techniques for Seismic Protection. *International Journal of Innovative Research in Science, Engineering and Technology* 4(3), 1215 – 1228. doi: 10.15680/IJIRSET.2015.0403032

USGS (2018). Earthquake Facts & Earthquake Fantasy. *USGS Earthquake Hazards Program*. https://earthquake.usgs.gov/learn/topics/megaqk_facts_fantasy.php

Wahid, S. A., Ismail, I., Aid, S., & Rahim, M. S. A. (2016). Magneto-rheological defects and failures: A review. *IOP Conference Series: Materials Science and Engineering*, 114(1). <https://doi.org/10.1088/1757-899X/114/1/012101>

Weaver, M. & Gabbatt, A. (2017, September 21). Mexico Earthquake: Military criticized over search and rescue missions – as it happened. *The Guardian*. Retrieved Feb 4th, 2018 from <https://www.theguardian.com/world/live/2017/sep/21/mexico-earthquake-search-for-survivors-live-frida-sofia-updates>

Weisstein, Eric W. "Horizontal Cylindrical Segment." From MathWorld--A Wolfram Web <http://mathworld.wolfram.com/HorizontalCylindricalSegment.html>

Xie, L., Choi, Y., Liao, C. & Wereley, N. (2016). Long term stability of magnetorheological fluids using high viscosity linear polysiloxane carrier

fluids. *Smart Mater. Struct.* 25. <http://dx.doi.org/10.1088/0964-1726/25/7/075006>

Yamaguchi, N., Narafu, T., Turer, A., Iiba, M., Imai, H. (2008). Shaking Table Test of Simple and Affordable Seismic Isolation. *The 14th World Conference on Earthquake Engineering, Beijing, China.*

www.iitk.ac.in/nicee/wcee/article/14_S18-028.PDF

Yang, G. (2001). *Large-Scale Magnetorheological Fluid Damper for Vibration Mitigation: Modeling, Testing and Control.* (Doctoral dissertation) University of Notre Dame.

Yang, G., Spencer, B. F., Carlson, J. D., & Sain, M. K. (2002). Large-scale MR fluid dampers: modeling and dynamic performance considerations. *Engineering structures*, 24(3), 309-323.

Yang, G., Spencer Jr, B. F., Jung, H. J., & Carlson, J. D. (2004). Dynamic Modeling of Large-Scale Magnetorheological Damper Systems for Civil Engineering Applications. *Journal of Engineering Mechanics*, 130(9), 1107-1114.

Zhang, X. Li, W. & Gong, X (2010). Thixotropy of MR shear-thickening fluids. *Smart Mater. Struct.* 19. <http://dx.doi.org/10.1088/0964-1726/19/12/125012>

Zhang, R. & Phillips, B. (2016). *J. Eng. Mech.* 142(1)